USDOT Tier 1
University Transportation Center
on Improving Rail Transportation
Infrastructure Sustainability and Durability

Final Report VT-7

Energy Harvester Tie for Serving the Needs of the Railroad Industry to Access Electric Power in Remote Locations

By

Mehdi Ahmadian, J. Bernard Jones Chair and Director

and

Yu Pan, Graduate Research Assistant

Center for Vehicle Systems and Safety
Railway Technologies Laboratory
Virginia Tech
3103 Commerce Street
Blacksburg, VA 24060

May 2024

Grant Number: 69A3551747132

DISCLAIMER

The contents of this report reflect the views of the authors, who are responsible for the facts and the accuracy of the information presented herein. This document is disseminated in the interest of information exchange. The report is funded, partially or entirely, by a grant from the U.S. Department of Transportation's University Transportation Centers Program. However, the U.S. Government assumes no liability for the contents or use thereof.

ABSTRACT

This study proposes various methods to harvest the mechanical energy present in railcar suspensions and railroad tracks to generate low-power electricity that is suitable for onboard or trackside electronics, using electromagnetic generators. A compact electromagnetic energy harvester that can be installed onboard railcars or wayside on railroad tracks is designed, fabricated, and tested. The design integrates a mechanical motion rectifier (MMR) with an embedded one-way clutch in the bevel gears, to convert the bi-directional mechanical energy that commonly exist in the form of vibrations into a unidirectional rotation of the generator. The ball-screw mechanism is configured such that it has reduced backlash and thus can more efficiently harvest energy from low-amplitude vibrations.

A porotype harvester is fabricated and tested expensively in the laboratory using a suspension dynamometer and, in the field, onboard a railcar and on a test track. The laboratory evaluation indicate that the harvester is capable of harvesting power with sufficient current and voltage for successfully powering light electronics or charging a low demand battery pack. The harvested power varies widely from a few to tens of Watts, depending on the resistive load across the harvester and the amplitude and frequency of the mechanical motion. The laboratory test results are verified through field testing. The harvester is tested onboard a passenger railcar, placing it across the axle suspension, to use the small amount of relative displacement at the axle to harvest energy. It is also placed on a test track to use the vertical motion that happens due to passing wheel for wayside energy harvesting. Both onboard and wayside tests confirm the laboratory test results in terms of the success of the design concept in providing low-power electrical power.

The harvester design is further integrated into a conventional railroad tie for ease of field installation and improving the efficiency of harvesting the mechanical energy at the rail. The integrated design, referred to as the “smart tie,” not only protects the energy harvester, the wiring harness, and supporting electronics from the maintenance-of-the-way equipment but also positions the harvester in a mechanically advantageous position that can maximize the track-induced motion, and hence the harvested power. Although for testing purposes, the smart tie uses a modified composite tie, it can be integrated into other track tie arrangements that used for revenue service track, including concrete and wooden ties.

A prototype smart tie is fabricated for laboratory testing, including a power management system with an energy storage circuit. The laboratory test results nearly duplicate the results obtained earlier from the wayside harvester. The smart tie is currently being considered for revenue service field testing over an extended length of time, potentially at a railroad mega site or similarly suitable location.

CONTENT

LIST OF FIGURES

LIST OF TABLES

Chapter 1 Introduction

1.1 Motivation

The significance of railroad transportation in people's life cannot be underestimated. Compared with road vehicles, rolling stock generally encounters lower frictional resistance, so passenger and freight cars could be coupled into longer trains, being a great choice for traveling and goods transporting. With the rapid development of electrification, passenger trains could usually obtain the electrical power from the pantograph or third rail for train traction as well as different electrical equipment. However, for the most freight trains, there are few electrical grids along the track, resulting in few reliable cost-effective onboard or trackside electrical energy sources to power the advanced electronic devices. Without dependable electrical supplies, modern smart devices and technologies, such as GPS, train condition real-time monitoring system, positive train control, and well as wireless communications, cannot be applied to improve the operational safety and efficiency. Besides, to achieve a safe and reliable transportation operation, many trackside electrical devices or smart technologies, such as signal lights, track switches, hotbox detectors, rail health monitoring systems, and wireless communication modules, have been applied to the rail system. However, cost-effective stable power supplies for freight train track electrical devices and subway tunnel lights are very limited. Therefore, seeking alternative railroad trackside and onboard cost-effective power sources for the railway safety electrical devices attracts more attention and has been an appealing research topic recently.

1.2 Objectives

The primary objectives of this report are listed below:

- Develop a novel electromagnetic energy harvester as an alternative power source for powering railroad trackside electrical devices. Apply it in a real railroad system.
- Develop a smart railroad tie for energy harvesting to supply trackside electrical devices and resolve the preload and installation challenges of bidirectional harvesting.
- Develop an electromagnetic energy harvester for railcar suspensions to power onboard electrical devices. Apply it in a real railcar suspension system.
- Develop a power management system for railcar suspension energy harvester to store the energy and supply for different electrical applications.
- Investigate the dynamic influence of the railcar suspension energy harvester (energy harvesting shock absorber) to the railcar ride comfort.

1.3 Challenges

The following challenges are faced in the study:

- Difficulty in developing compact and reliable mechanical structures to transfer the small railroad track vibration energy into electricity

- Difficult to install the track energy harvester in such limited allowable space between the track and the rail foundation.
- Harvest enough energy from the small-amplitude track vibration, especially from the rapid transit track, is a challenge.
- Traditional method to harvest energy bi-directionally has high impact force, which is not reliable.
- Difficult to investigate/evaluate the influence of track energy harvester to the rail-train system.

- Difficulty in developing suspension energy harvester to transfer the reciprocating railcar suspension vibration energy into electricity

    - Difficult to install the railcar suspension energy harvester in a limited allowable space in railcar suspension
    - Harvesting enough energy from the small and low frequency random suspension vibration is challenging.
    - Traditional method to harvest energy bi-directionally has high impact force, which is not reliable.
    - Difficult to develop a power management system to store and properly manage the power for different electrical applications.
    - Hard to determine best parameters to improve the railcar ride comfort due to the nonlinearity of the overall coupled system.

1.4 Approaches

The following approaches are employed to overcome the challenges in this dissertation:

- The mechanical motion rectifier (MMR) mechanism, which is realized by the embedded one-way clutches in the two bevel gears, converts the bi-directional vibration into the unidirectional rotation of the generator. This special mechanism eliminates the impact forces during transmission and results in high energy harvesting performance.
- Utilizing ball-screw mechanism to transmit the bidirectional track linear vibration into unidirectional rotation of the generator can reduce backlash during transmission and thus can harvest energy from a small input of the track deflection induced by the moving train
- A comprehensive model considering the train-rail-harvester interaction is developed to analyze the dynamic characteristics of the coupled system and predict the energy harvesting performance of the harvesters at different train speeds.
- The proposed smart energy harvesting tie, as an upgraded development of the compact track harvester, only harvests the kinetic energy of the track when the wheels push it downwards, which resolves the preload and installation challenges of bidirectional harvesting and increases the overall system reliability.
- A rack-pinion based suspension energy harvester with a simplified structure is designed to fit into the railcar suspension. Facing the severe vibration and huge load conditions during the operation of the freight cars, an enclosed lubricated gearbox and a unique two guide-rail mechanism are specifically designed for the harvester to reduce the friction loss and increase transmission reliability and durability.

- AC-DC and buck-boost (DC-DC) converters are employed in the railcar energy storage circuit to convert the AC voltage to DC voltage and set an effective resistance (equivalent damping) to the transducers. The oscillator circuit in the self-designed buck-boost converter controls the switching frequency and duty cycle of the power MOSFET. A modified commercial battery charging circuit is located at the output side of the buck-boost converter to maximally store the electrical energy into the lead-acid battery.
- A 6 degree of freedom railcar-harvester model is established, and parameter simulation study is performed to determine the best pair of damping and equivalent inertance for improving the ride comfort.

1.5 Contributions

The primary contributions of this research include:

1. A novel ball-screw based railway track energy harvester with mechanical motion rectifier mechanism was designed, modeled and tested.

    - Due to the nonlinear characteristics induced by the one-way clutches in the mechanical motion rectifier (MMR) mechanism, the proposed energy harvester could convert the bi-directional track vibration into unidirectional rotation of the generator, which significantly improves the motion transmission by reducing the impact forces.
    - A comprehensive model considering the coupled dynamic behaviors of the train, railway track and harvester was developed and validated. It is shown that the proposed ball-screw based energy harvester acts as a fixed inerter in parallel with pre-compressed springs and an adjustable damper tuned by external resistive load of the generator, when the one-way clutch is in engagement. When both one-way clutches disengage from the bevel gears, the energy harvester behaves as pre-compressed springs only, and the inertia of the generator drives the generator itself continuously to produce electricity. This piece-wise mass-spring-damper of the single freedom harvester is integrated into the train-track model and the performance of the harvester at different train speeds can be predicted by the model.
    - The in-lab and field tests were conducted to further validate the dynamic characteristics and evaluate the performance of the proposed energy harvester. The harvester could effectively work under a very small input with the amplitude of ±0.2 mm, which shows that the proposed harvester has an improved sensitivity to the environment vibrations. Field test results showed that an average power of 1.12 and 2.24W were achieved for prototype 1 and 2 respectively at 30 km/hr rapid transit speed. More power could be obtained by choosing a higher limit one-way clutch, increasing the reset spring stiffness and refining the installation condition.

2. A smart energy harvesting railroad tie to power the trackside electrical device has been proposed, designed, modeled and tested for potentially improving the train operational efficiency and safety.

    - The smart tie, which is designed to have similar dimensions to a conventional railroad tie, can be installed in the same manner as a standard tie on the track.
    - Through a ball-screw, a pair of bevel gear and an output shaft with a single one-way clutch, the generator can be driven to generate electricity. Different from bidirectional energy harvesters, the proposed smart tie only harvests the kinetic energy of the railroad tie when the tie moves

downwards due to the approaching wheel, which resolves the preload and installation challenges and increases the overall system reliability.

- An analytical model is developed, and the dynamic simulation is conducted to better understand the system nonlinearity and predict the performance.
- During the bench tests, the smart tie demonstrates great sensitivity to the environment vibration due to its small backlash (less than 0.1 mm). In-lab test results show that an average power of 26.1 and 42.2W for 4 and 2 Ohms external loads are obtained, respectively, under simulated tie movement conditions. This indicates that the proposed smart tie is capable of powering most wayside electrical devices, with a great potential to improve the train operational safety.

3. A rack-pinion based freight railcar energy harvester with a mechanical motion rectifier (MMR) mechanism was designed, modeled, and tested both in the lab and in the field.

    - The proposed energy harvester could translate the bidirectional freight railcar suspension vertical vibration into unidirectional rotation of the electromagnetic generator by utilizing two one-way clutches embedded in transmission bevel gears. An enclosed MMR gearbox with lubricant inside was designed to increase the transmission durability and decrease the friction loss.
    - A coupled model for the freight railcar integrated with the proposed energy harvesters at the secondary suspensions was developed. A simulation study was performed with the Association of American Railroad (AAR) Class 5 and 6 track irregularities as the system input, showing that the generated power from the harvester and the suspension vibration RMS velocity increase with the train speeds. Energy harvesting performances at different train speeds for the proposed harvester were also predicted through modeling and numerical simulations.
    - The in-lab and onboard field tests were carried out to evaluate the performance of the proposed train suspension energy harvester. In-lab test results showed that an average power of 14.5 and 9.2W were achieved with the typical recorded suspension displacement (vibration RMS velocity is 0.030 m/s) at 90 km/hr on an operational track for the prototype harvesters with 66:1 and 43:1transmission ratios, respectively. The model was validated through bench tests using both the sinusoidal inputs and the recorded displacement inputs.
    - An onboard test was also carried out on a test track in CRRC Yangtze, Co., Ltd., and test results showed a peak of 73.2W phase power and an average of 1.3W were achieved at a train speed of 30 km/hr (vibration RMS velocity is 0.017 m/s) for the harvester with 43:1 transmission ratio. Both the in-lab and onboard test results indicate that the proposed train suspension energy harvester could continuously generate an amount of power (watts to tens of watts level) useful for powering onboard auxiliary electrical devices, which can potentially improve the freight railcar operational safety.

4. A power management system with an energy storage circuit is designed, prototyped and tested.

    - AC-DC and buck-boost (DC-DC) converters are employed in the energy storage circuit to convert the AC voltage to DC voltage and set an effective resistance (equivalent damping) to the transducers. The oscillator circuit in the self-designed buck-boost converter controls the switching frequency and duty cycle of the power MOSFET.
    - A modified commercial battery charging circuit is located at the output side of the buck-boost converter to maximally store the electrical energy into the lead-acid battery. Power management system is also integrated with the self-designed energy storage circuit, battery indicator circuits and two boost converters.

- Tests were conducted and results showed that an around 7-Ohm resistance and a maximum 77% efficiency could be achieved for the buck-boost converter. The overall power management system could perform well in the bench test conditions.

5. The MMR energy harvester on railcar dynamics has been also investigated.

    - A nonlinear railway vehicle model integrating EHSAs at the primary suspension with six degrees of freedom is built and simulations with analysis are presented.
    - Results shows that compared with vehicle with traditional shock absorbers, railcars with MMR energy harvester as new-type shock absorber could perform better for ride comfort when the equivalent inertia mass and damping coefficient is properly designed.

1.6 Outline

- Chapter 1 introduces the study and provides the objectives, challenges, approaches and contributions from the research, and outlines the dissertation.
- Chapter 2 gives background knowledge and an overview of existing energy harvesting technologies for railroad track and railcars.
- Chapter 3 presents the design, modeling and field-test of a compact ball-screw based electromagnetic energy harvester for railroad transportation
- Chapter 4 presents the design, modeling and tests of a smart energy harvesting railroad tie
- Chapter 5 presents the design, modeling and onboard test of an electromagnetic energy harvester for railway cars
- Chapter 6 presents the power management system of energy harvester for railcar suspension and performance evaluation of energy harvesting shock absorber on railway vehicle dynamics
- Chapter 7 provides the confusions for the investigation and discusses the future work.

Chapter 2 Background and Literature Review

This chapter provides background information about the urgent need of alternative power sources and the energy harvesting technologies that have been employed in railroad. Firstly, the background for the railroad track energy harvesting is introduced in Chapter 2.1, and subsequently, the background for railcar energy harvesting is presented in Chapter 2.2.

2.1 Background for railroad track energy harvesting

In the past decade, energy harvesting techniques which could be used for powering smart electronic devices have received increasing attention. Based on piezoelectric and electromagnetic method via linear and nonlinear [1, 2] mechanism, researchers have investigated energy harvesting in many different modes including ocean waves [3, 4], wind flow [5], vibrations in automobile suspension [6, 7] and transportation infrastructure [8, 9].

For transporting passengers living inner city, the rapid transit system has become one significant option in recent decades. Often seen along urban growth in congested cities, rapid transit systems are an appealing solution for reducing vehicle traffic. Interconnected metro lines cross, merge, and mingle with others beneath the crowded cities, leaving the safety consideration for the rapid transit system to be the highest priority. To achieve a safe and reliable transportation operation, many trackside electrical devices or smart technologies, such as signal lights, track switches, hotbox detectors, rail health monitoring systems, and wireless communication modules, have been applied to the rail system. Let alone the sophisticated operation auxiliaries, the tunnel lights themselves consume a lot of electricity. However, cost-effective stable power supplies for tunnel lights are very limited. Seeking an alternative cost-effective power source for the railway safety electrical devices has been an appealing research topic for the industry.

There is a vast energy potential in the railway track deflection induced by wheel-rail vertical contact force. The amplitude and frequency of railway track deflection can vary from 1-12 mm and 1-4 Hz, respectively, depending on the types of trains, track structures and carrying loads [10, 11]. Aiming at utilizing a relatively small fraction of the energy stored in the railroad tracks to power the electronic safety devices, many energy harvesting technologies, such as those using piezoelectric[12-16], hydraulic[14, 17] and electromagnetic [14, 18-29], have been widely studied. For example, *Wischke et al.*[12] developed a piezoelectric vibration harvester equipped with a power interface circuit to power wireless sensor nodes in railway tunnels, and an average energy of 395μJ per train was achieved during the in-field test. *Nelson et al.*[13] and *Pourghodrat et al.*[14] developed a piezoelectric energy harvester which can be mounted on the bottom of the rail track, exposing it to longitudinal strain during the passing of trains. Figure 2-1(a) shows the piezoelectric energy harvester. Numerical simulation indicated a maximum average power output of 1.1 mW and an average power of 53 μW were obtained in the field test when an unloaded train traveled at approximately 24 km/hr (15 mph). *Yuan et al.*[15] established a model of piezoelectric drum harvester with 100 mW in the simulation analysis. An experiment was conducted in lab using a 1:10 track test rig with a single wheel and an average 0.1 mW was achieved when the speed of the wheel ran at 0.5 km/hr. *Wang et al.*[16] established a detailed model for a piezoelectric stack in the railway track model under moving multi-loads and an average power of 0.19 mW was obtained in the simulation. Overall, due to low power output and high impedance of piezoelectric

material, the harvested power could only supply sensors for health monitoring purpose. This suggests that it is inadequate for most safety electronic devices such as signal lights, track switches and hotbox detectors. Hydraulic energy harvester for railway track has also been studied. *Pourghodrat, Nelson and co-workers*[14, 17] designed a hydraulic energy harvester with hydraulic motor, planetary gearbox and a generator, shown in Figure 2.1(b). An average power of 11W was obtained in the lab bench test under 3.75 mm and 0.375 Hz harmonic excitation. However, there is no field test to validate its energy harvesting performance under real track vibrations.

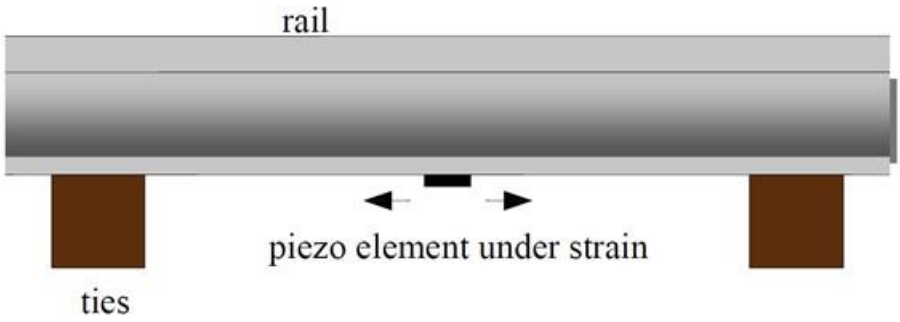

(a)

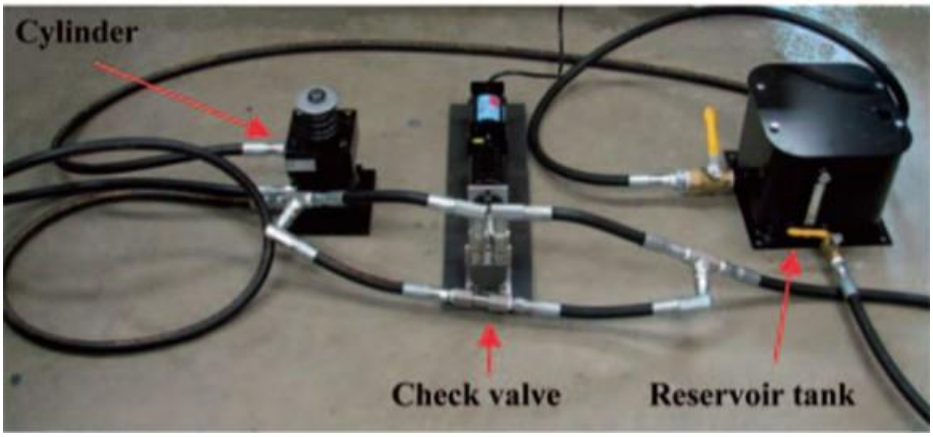

(b)

Figure 2-1. Piezoelectric energy harvester [13] and hydraulic energy harvester [14] for railway track

Other than piezoelectric and hydraulic harvesters, mechanical based electromagnetic energy harvesters have been gaining more popularity in the past decade. *Nelson et al.*[13] and *Pourghodrat et al*. [14] designed an inductive voice coil energy harvester with the coil rigidly attached to the rail track and a permanent magnet with a radial magnetic field fixed on the ground, shown in Figure 2-2. A maximum average power of 0.146 mW was derived under a low-amplitude, 10-Hz sinusoidal excitation in the lab bench test. However, field tests provided different results including an average power of 4 mW when a train consisting of empty cars traveled at 18 km/hr (11 mph) and an average power of 12 mW when a loaded train ran at 21 km/hr (13 mph). *Gao et al.*[18] also developed a linear electromagnetic energy harvester with an inductive coil and an average power of 119 mW was attained with a simulated rail displacement of 1.2 mm in the lab bench test. *Gatti et al.* [19] researched on harvesting energy from the vibration of a passing train using a single-degree-of-freedom mechanical oscillator, and the optimal amount of energy

harvested per unit mass is found to be proportional to the product of the square of the input duration and acceleration amplitude. *Brennan et al.* [20] presented an investigation about the upper bound of the scavenged energy on mechanical oscillators, which can be used for harvesting energy from track deflections, and conducted a fundamental study to determine the optimal set of mechanical design parameters of a linear single degree of freedom spring-mass-damper system.

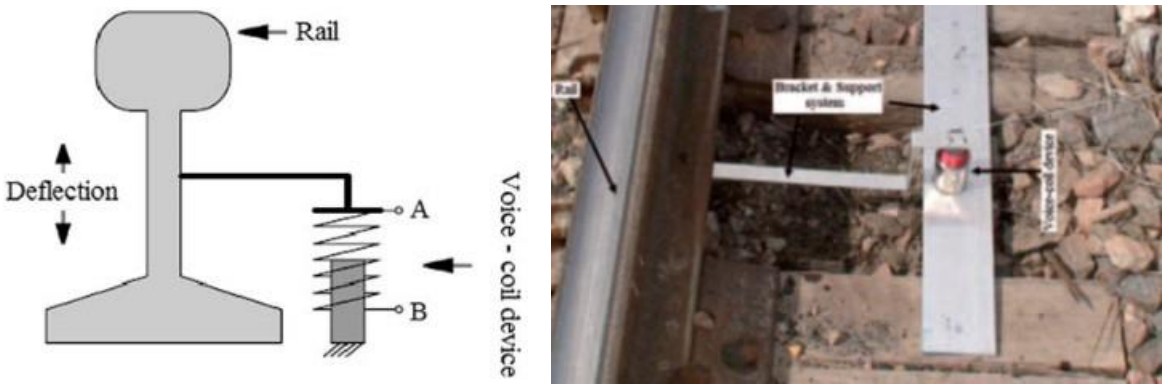

(a) (b)

Figure 2-2. Inductive voice coil energy harvester: (a) voice-coil device; (b) in field test [14]

Besides linear electromagnetic harvesters, many researchers have designed rotary harvesters which could have a higher power density than linear harvesters and can convert the bi-directional track vibration into rotation of an electromagnetic generator. *Pourghodrat et al.* [14, 21, 22] proposed a mechanical energy harvester using rack and pinion mechanism (shown in Figure 2-3(a)) with a clutch bearing to harvest the track vibration energy when the track moves down, while generator freewheels when the track moves up. The in-field test results showed an average power of 0.22W was obtained with 12.7 mm (0.5 in) track deflection when a loaded train traveled at 18.5 km/hr (11.5 mph). They also provided another updated design, which can harvest energy when the track vibrates in both directions, and simulation results showed a significant improvement in performance. *Wang et al.* [23] proposed a design to convert the bi-directional vibration into unidirectional rotation by using three shafts, three spur gears, a pair of rack and pinion, and two roller clutches which is shown in Figure 2-3(b). Lab test results indicated a maximum average power of 1.4W was obtained with a 10-25% mechanical efficiency. Much of its low efficiency was attributed to the design complexity and backlash between the rack and pinion gears. *Zhang et al.* [24, 25] proposed two different kinds of track energy harvester design and lab tests illustrated that a 55.5% mechanical efficiency and a peak voltage of 58 V at 1Hz with a displacement of 2.5 mm were achieved, respectively. *Wang and Lin et al.* [26, 27] proposed a simplified single shaft rack-pinion design and then *Lin et al.* [28, 29] implemented an anchorless mounting in an updated design using MMR, converting the bi-directional track vibration into unidirectional rotation of the generator and increasing the energy harvesting performance. The single shaft design (shown in Figure 2-3(c))achieved a 74% mechanical efficiency [27] because of less friction loss, and the anchorless prototype [28, 29], with 60 cm length, 15 cm height and 40 kg weight, can be installed in-field without any physical anchor, avoiding damages to the railroad subgrade. An average power of 6.9W was obtained by the anchorless prototype under a 5.7 mm freight train track deflection infield when the train traveled at 64 km/hr (40 mph).

(a)

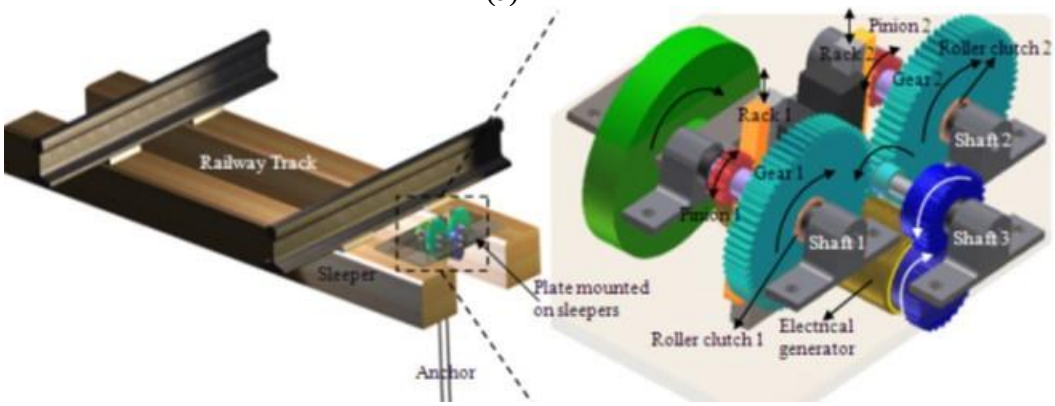

(b)

(c)

Figure 2-3 Electromagnetic energy harvesters: (a) rack-pinion based design with anchor [21]; (b) rack-pinion based design with MMR mechanism [26]; (c) rack-pinion based design with anchorless mounting [28].

2.2 Background for railway car energy harvesting

Compared with road vehicles, rolling stock generally encounters lower frictional resistance, so railcars could be coupled into longer trains, being a cost-effective choice for passenger travel and

goods transportation. For the safe operation and efficient management of rail transportation, electrical devices are installed both on the trackside and on board. Researchers have investigated the energy harvesting technologies, such as piezoelectric [14] and electromagnetic [25] methods, to power trackside electronics, such as signal lights, track switches, and rail health monitors, etc. Besides trackside devices, onboard smart technologies, such as GPS and real-time train condition monitoring system, are also essential for trains [30, 31]. However, unlike the passenger railcars, which can obtain the electrical power from the electrical grid or the locomotives, for freight trains with up to 200 trailers, it is difficult for the freight trailers to obtain electricity from the locomotive for these electronic devices due to the overall length. Batteries or onboard diesel generators might be a choice for the trailers; however, the frequent replacement/recharging of batteries or refueling of the diesel generators will increase the maintenance cost and inevitably interrupt the transportation. Without dependable electrical supplies, these modern "smart" technologies would not be applied to the freight vehicles to improve operational safety and efficiency.

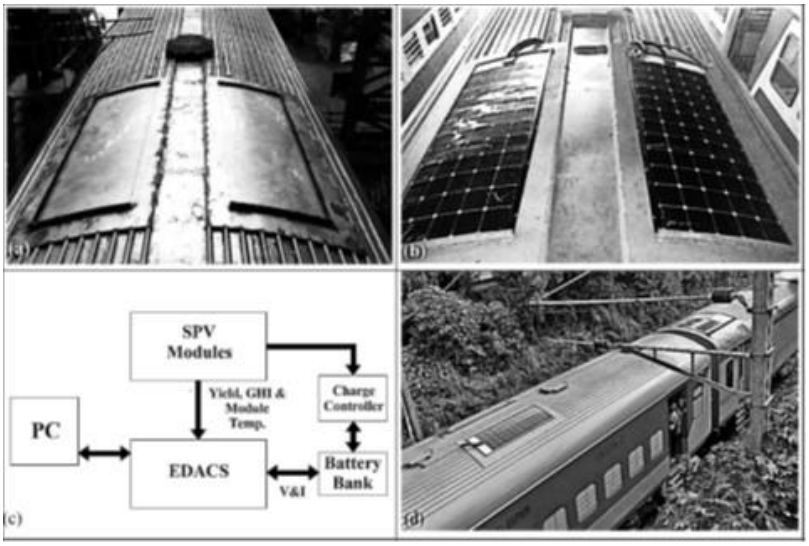

Figure 2-4 Trial SPV Coach and Online Monitoring System (OMS) [32]: (a) MMS without SPV modules. (b) SPV modules mounted on the coach. (c) Line diagram of OMS. (d) Trial SPV Coach on Trials.

Onboard energy harvesting solutions have been developed in academia to convert the ambient solar, heat, and vibration into electricity. *Vasisht et al.* [32] and *Rohollahi et al.* [33] conducted case studies using photovoltaic (PV) cells mounted on the roof of a passenger coach to harvest reasonably large power. Figure 2-4 shows the work from [32]. However, photovoltaic panels might not be a feasible choice for freight cars since many freight cars, such as gondolas, are open-topped vehicles for transporting loose bulk materials and there is no roof to mount the PV panels. *Nagode et al.* [34] designed and tested an axle generator (shown in Figure 2-5(b)), which can be clamped on the train axle and produced average 300W power on the test bench at simulated 88.5 km/hr (55 mph). *Ahn et al.* [35] developed a thermoelectric energy harvester using the temperature difference between the axle bearing housing and ambient air during the train traveling and it yielded up 19.3 mW average power during the onboard test for some low-power sensors. When the railway vehicles are operating, vibration usually occurs on the car bodies, wheelsets, and suspensions. *Pasquale et al.* [36] designed a piezoelectric energy harvester (shown in Figure 2-6(a))which produced 12 mW average power at a vibration acceleration of 1.53 *g* on a 1:4 scaled bogie. *Cho*

et al. [37] designed a piezoelectric energy harvesting system with magnetic pendulum movement for trains and achieved a maximum average power density of 40.24 $\mu W/cm^3$ in the optimized conditions. Although the broadband [38, 39] or asymmetric tristable [2] piezoelectric vibration harvesters have been investigated to enhance the performance, the power output is still too small for onboard devices. *Ung et al.* [40] designed a two degree of freedom energy harvester using a magnet and a conductive coil and achieved peak power 0.35 and 0.23W at two resonances of 6 Hz and 14.6 Hz at 0.5g vibration acceleration. *Pasquale et al.* [41] developed an energy harvester with a magnetic suspended proof mass and obtained an average output power of 0.1W on a scaled roller rig test corresponding to 80 km/hr train speed.

(a) (b)

Figure 2-5 Axle generator: (a) FAG Axlebox generator [42]; (b) axle generator with friction wheels [34].

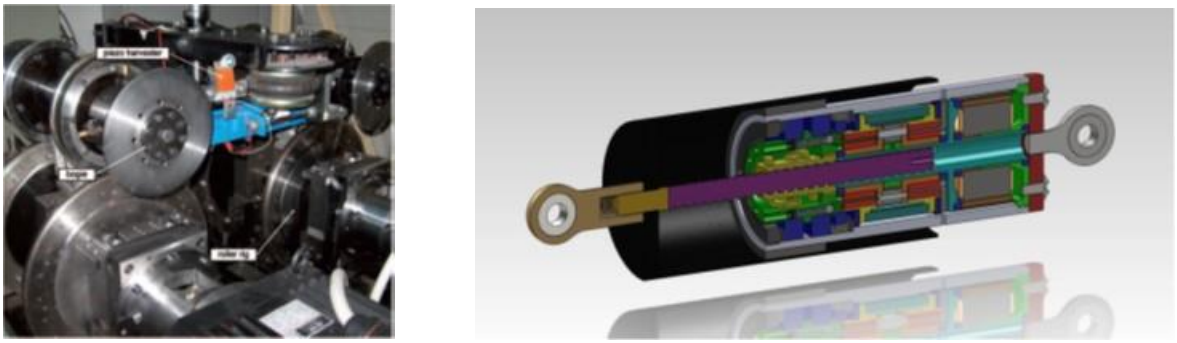

(a) (b)

Figure 2-7 Vibration energy harvesters for railway vehicles: (a) piezoelectric energy harvester [36]; (b) electromagnetic rotary energy harvester for train suspensions [43].

There is a vast amount of kinetic energy in railway vehicle suspensions, which is usually dissipated into heat by wedge friction or oil shock absorbers. *Matamoros-Sanchez* [44] and *Wang et al.* [45] investigated the energy dissipated in the train suspension and showed a large amount of dissipated energy. *Wang et al.* [46] and *Abdelkareem et al.* [47] indicated a huge energy potential in the railcar suspensions. Mechanical based electromagnetic energy harvesting can be used to convert a small portion of this large-power vibration energy that is otherwise dissipated into heat, into useable electricity, which is a more promising solution to power onboard electrical devices than the

piezoelectric and other electromagnetic energy harvesting technologies. *Nagode* [43] and his co-workers designed and tested three types of mechanical based electromagnetic railcar suspension energy harvesters, including a linear motion energy harvester in which the magnets move linearly with the train suspension inside coils, and two ball-screw based rotary electromagnetic energy harvesters with two customized planetary gearboxes, converting the bidirectional linear motion of the suspension into bidirectional rotation [48, 49] or unidirectional rotation (shown in Figure 2-6(b)), [43] of the generator. The in-lab bench test results showed the linear harvester produced average output power 0.545W under 19.05 mm (0.75 inch) and 1.5 Hz harmonic vibration, and the ball-screw based energy harvester achieved an average power of 65W under 25.4 mm (1 inch) 1.5 Hz harmonic excitation. The onboard tests in *Transportation Technology Center, Inc.* (TTCI) facilities demonstrated an average power of 0.35-0.55W on the freight railcars.

Chapter 3 Design, Modeling and Field-test of a Compact Ball-screw Based Electromagnetic Energy Harvester for Railroad Transportation

To enable the smart technologies and safe operation of transit and rail transportation, such as hotbox detector, track health monitoring and wireless communication on the railroad side, a cost-effective energy source is in need. This chapter presents the design, modeling, in-lab experiment and field-test results of a compact ball-screw based electromagnetic energy harvester with a mechanical motion rectifier (MMR) mechanism for smart railway transportation. The MMR mechanism is realized by the embedded one-way clutches in the bevel gears, which converts the bi-directional track vibration into the unidirectional rotation of the generator. Compared to previous designs, the proposed harvester has reduced backlash and thus can harvest energy from a small input of the track deflection induced by the moving train. Two prototypes with different key design parameters were built and tested. A comprehensive model considering the train-rail-harvester interaction was developed to analyze the dynamic characteristics of the coupled system and predict the energy harvesting performance of the harvesters at different train speeds. Both in-lab and field tests were carried out to examine the energy harvesting performance of the harvester and validate the model. Field test results illustrated that an average power of 1.12 and 2.24W were achieved for two prototypes respectively when a Type A rapid transit passed by with a 30 km/hr vehicle speed.

3.1 Chapter Introduction

As discussed in Chapter 2.1, among the energy harvesting technologies in railway, the rack pinion based electromagnetic energy harvesters, especially those with MMR mechanism, have proven to have reasonable performance for powering trackside electronics. However, three main challenges remain in the existing technologies: (i) almost all the current rotary track energy harvesters are relatively cumbersome or not easy to install; (ii) the backlash between the rack teeth and pinion teeth in rack-pinion based harvesters can be large and lead to relatively low energy harvesting performance when the excitation is small [50, 51]; (iii) a coupled model consists of the train, harvester and track system is needed for predicting the energy harvesting performance at different train speeds.

In this chapter, a compact design with an MMR mechanism is proposed for harvesting energy from rapid transit track deflection in the tunnels or freight track deflection. The energy could be stored in a battery through self-designed or commercial battery charging circuits and used to power different trackside electrical devices, such as signal lights, track switches, hotbox detectors, rail health monitoring systems, and wireless communication modules, which could potentially increase the safety of train operation. Two prototypes are fabricated using the ball-screw mechanism with less backlash during transmission and high sensitivity to the vibration environment. A systematic model considering the train-track-harvester interaction is developed to analyze the dynamic characteristics of the coupled system and predict the energy harvesting performance of the harvesters at different train speeds. In-lab and field tests have been carried out to examine the performance of the harvester and validate the model. Field test results show that an average power of 1.12 and 2.24W are achieved for prototype 1 and 2 at 30 km/hr, respectively.

This chapter is organized as follows. Chapter 3.2 introduces the detailed design and working principle of the two prototypes with different parameters. Chapter 3.3 is the systematic modeling for the proposed energy harvester coupled with the rail system. Chapter 3.4 is the in-lab test of the proposed energy harvesters and Chapter 3.5 is the harvester in-filed test. Chapter 3.6 provides the concluding remarks.

3.2 Design and Working Principle

The proposed based track energy harvester is comprised of a ball-screw, an enclosed MMR gearbox, an electromagnetic generator with a gearhead and anchorless mounting parts, as shown in Figure 3-1(a). Compared with previous rack pinion based designs[27, 29], the ball-screw mechanism can significantly reduce the backlash during the process of converting the bi-directional linear motion to rotation [51]. Therefore, it can provide a higher energy harvesting performance when the excitation displacement is small. The harvester is designed to be installed under the track between two adjacent sleepers, and the input plate could be considered as rigidly connected to the railway track by two clamping blocks with bolts. The bending stiffness of the input plate (made of steel) is large enough so that the deformation of the input plate can be ignored. To quickly install the harvester on site and prevent the potential risk of the physical anchor from changing the property of ballast and subgrade, two reset springs are pre-loaded and positioned between the input plate and ground plate, providing enough spring force to keep the ground plate stationary on the rail foundation. When the train passes by, the track deflects due to the wheel-rail vertical contact forces and the input plate of the harvester vibrates together with the track vertically. The ball nut is embedded near one end of the input plate and the ball-screw is used in the back-driven mode, which can convert the low-speed reciprocal linear motion of the track vibrations into bi-directional rotation of the screw at a higher speed. A mechanical coupler is employed to connect the screw shaft and the input shaft of the enclosed MMR gearbox so that the input shaft can also rotate bi-directionally.

The enclosed MMR gearbox consists of a pair of large bevel gears embedded with one-way sprag clutches, a small bevel gear connected to the gearhead shaft and five angular contact bearings. The rotational motion could be transmitted from the large bevel gear pair to the small bevel gear, and consequently, the gearhead and electromagnetic generator could rotate as well. Angular contact bearings are applied to provide shaft and gears with both the radial and thrust forces so that the overall transmission could be smooth and steady. Meanwhile, shaft seals and O-rings are used in the gearbox design, so, by adding the lubricant oil or grease inside the enclosed gearbox, the transmission reliability and efficiency could be improved.

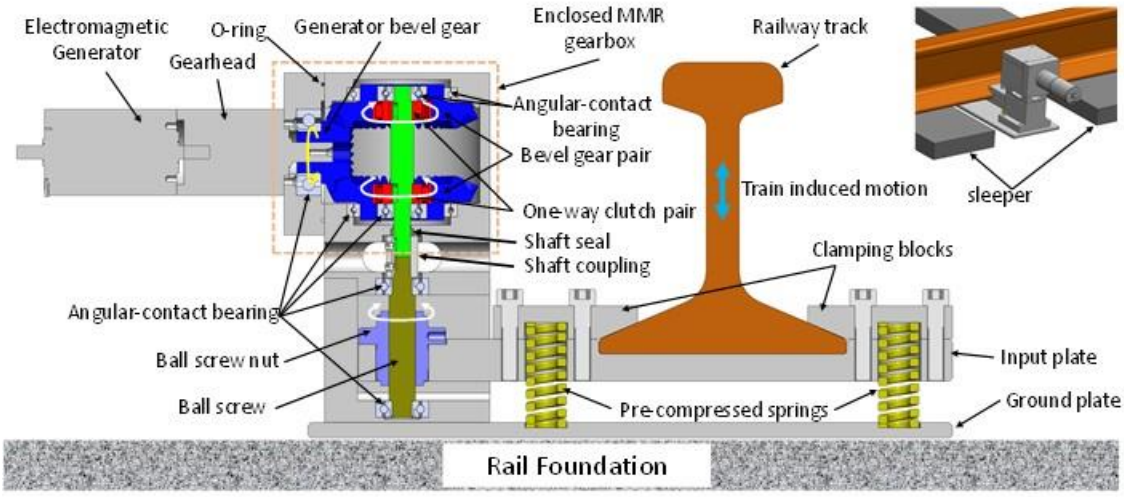

(a)

(b)

Figure 3-1. Design of a ball-screw based railway track energy harvester with MMR mechanism: (a) Design details (b) Prototype

Figure 3-2 illustrates the working principle of the ball-screw based MMR railway track energy harvester. For instance, in Figure 3-2, if the track moves down when the train wheel approaches, the ball-screw will spin counterclockwise from the bottom view, and at this moment, the upper bevel gear can be engaged with the embedded clutch and become the driving gear, while the lower bevel gear is disengaged with the embedded clutch and becomes an idle gear. In this way, the small bevel gear is driven by the upper driving gear and will spin counter-clockwise (from the left view). If the track moves up when the train wheels move away, the ball-screw will spin clockwise from the bottom view, and at this moment, the lower bevel gear is engaged with the embedded clutch and becomes the driving gear, while the upper bevel gear is disengaged from the embedded

clutch and becomes an idle gear. In this way, the small bevel gear and thus the generator will continuously spin counter-clockwise (from the left view). In other words, no matter if the railway track moves upwards or downwards, the electromagnetic generator always rotates unidirectionally, resulting in high energy harvesting performance and low impact force during transmission [27]. This special mechanism, converting the reciprocating vibration into unidirectional rotation of the generator, is referred to as mechanical motion rectifier (MMR) [52]. Two prototypes are fabricated with the same design but different ball-screw leads, reset springs, gearheads, and generators. The main parameters of these two prototypes are listed in Table 3-1.

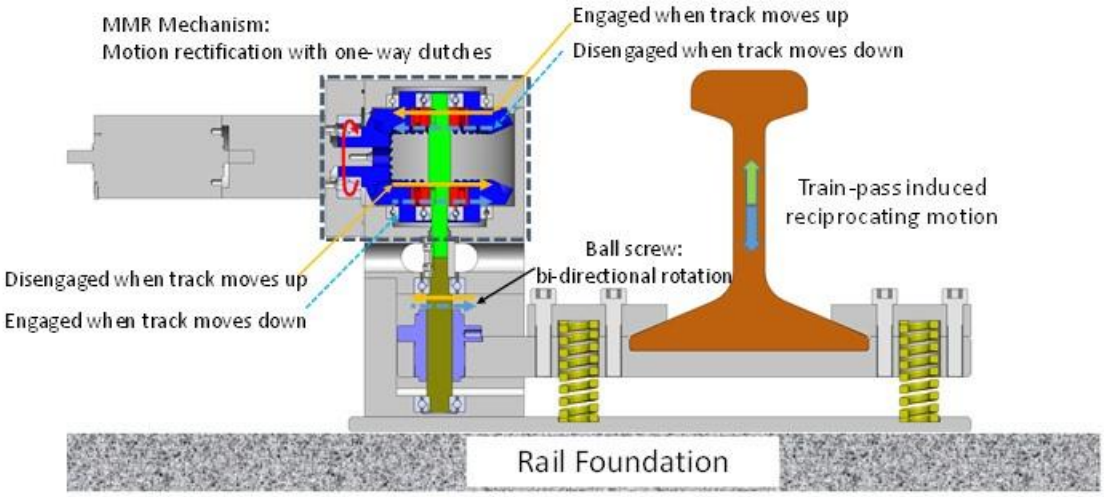

Figure 3-2. Bidirectional vertical track motion induced by wheel-rail vertical contact force will drive the generator to rotate in one direction using the proposed ball-screw MMR mechanism: green lines represent the case that track moves up and blue lines represent the case that the track moves down.

Table 3-1. Parameters of the proposed energy harvesters

Parameters	Value	Discription	Parameters	Value	Description
d_m	15.75 mm	Screw diameter	r_b	2	Bevel gear transmission ratio
l_1	20 mm	Screw lead in Prototype 1	r_{1g}	4.3	Generator 1 gearhead ratio
l_2	16 mm	Screw lead in Prototype 2	r_{2g}	12	Generator 2 gearhead ratio
J_{1m}	3.06 kgcm^2	Generator inertia of Prototype 1	k_{1e}	0.163 V/rads	Generator 1 voltage constant
J_{2m}	0.17 kgcm^2	Generator inertia of Prototype 2	k_{2e}	0.054 V/rads	Generator 2 voltage constant
J_{lg}	30 kgcm^2	Large gear inertia	k_{1t}	0.163 Nm/A	Generator 1 torque constant
J_{sg}	3 kgcm^2	Small gear inertia	k_{2t}	0.054 Nm/A	Generator 2 torque constant
J_{bs}	0.038 kgcm^2	Screw inertia	L_1	2.5 mH	Generator 1 phase to phase inductance
R_{1i}	2.28 Ω	Terminal resistance phase to phase of Generator 1	L_2	0.443 mH	Generator 2 phase to phase inductance
R_{2i}	0.284 Ω	Terminal resistance phase to phase of Generator 1	k_1	26269N/m	Spring constant of Prototype 1
$Stroke$	15 mm	Harvester stroke	k_2	95269N/m	Spring constant of Prototype 2
$Weight$	15 kg	Harvester weight	$Height$	20 cm	Harvester overall height

Note: Generator 1 and Generator 2 represent the generator inside the harvester prototype 1 and harvester prototype 2, respectively.

3.3 Modeling and System Dynamics

3.3.1 Dynamics of three-phase AC generator

A three-phase AC generator is applied in the proposed railway track energy harvester and a star shape tunable resistive load is employed in the energy harvesting circuit model. Fig. 3 shows the dynamic model of the three-phase AC generator. V_1, V_2, V_3 are the back electromotive force (EMF) of the generator, and i_1, i_2, i_3 are induced current in each phase, respectively. L is the inductance of coils per phase, which has a negligibly small value, and R_i , R_e are internal and external resistance, respectively.

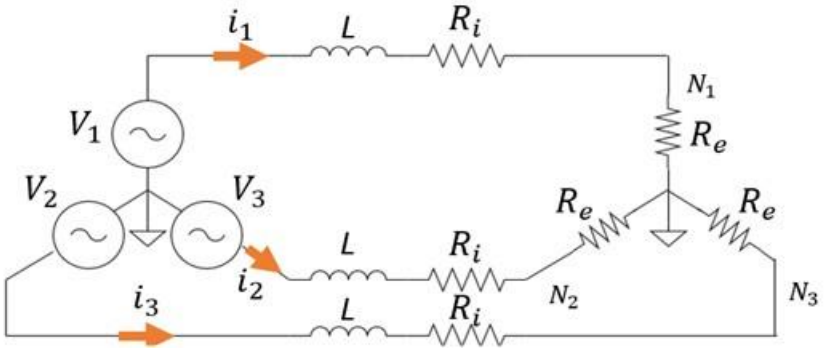

Figure 3-3. Modeling of star shape three-phase generator with star shape resistive load [29].

The dynamics and the electrical damping characteristics of the generator have been analyzed in [29]. By ignoring the inductance, the resistive torque T_{ge} induced by the electrical damping of a three-phase generator can be expressed as

$$T_{ge} = \frac{3k_t k_e}{2(R_i + R_e)} \omega_{ge} \tag{3.1}$$

where k_t and k_e are the speed and torque constants, and ω_{ge} is the angular velocity of the three-phase AC generator.

According to Newton's second law, the equation of motion of the generator can be expressed as

$$T_m - T_{ge} = J_m \dot{\omega}_{ge} \tag{3.2}$$

where T_m is the input torque. Substituting (1) into (2), the driving torque T_m for the generator can be written as

$$T_m = J_m \dot{\omega}_{ge} + \frac{3k_t k_e}{2(R_i + R_e)} \omega_{ge} \tag{3.3}$$

3.3.2 Dynamic model of the proposed ball-screw based track energy harvester

Figure 3-4 illustrates the dynamic model of the proposed ball-screw based energy harvester for railway track. Different from the linear harvesters and some rotary harvesters, ball-screw based MMR harvester can convert the bi-directional linear vibration into the unidirectional rotation of generator by utilizing the one-way clutches embedded in the large bevel gears, producing nonlinear dynamic characteristics within the harvester. Specifically, when the ball-screw angular velocity equals that of one of the large bevel gear, the one-way clutch embedded in that bevel gear is engaged to the shaft, so that the torque could be transmitted from the input shaft to the bevel gears and the generator is driven by small bevel gears to rotate. Instead, when the ball-screw angular velocity is smaller than that of the large bevel gears, both one-way clutches embedded in the bevel gears are disengaged from the shaft, indicating that there is no motion transmission from the shaft to the bevel gears so that gears and generator will rotate freely due to their inertia.

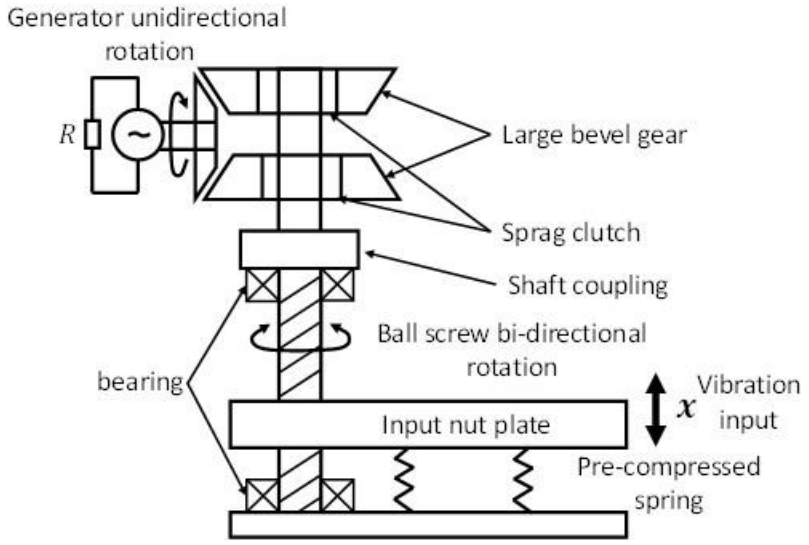

Figure 3-4. Dynamic model of the proposed railway track energy harvester

Assuming the track deflection is x, velocity is $\dot{x}$, the ball-screw lead is l , the gear ratio of the gearbox and MMR gearbox together is n_g, the rotational speed of the generator ω_{ge} at engagement period can be obtained as

$$\omega_{ge} = \frac{2\pi n_g}{l}\dot{x} \tag{3.4}$$

The resisting force on the ball-screw nut due to the electrical damping of the generator, which can be obtained as

$$F_d = \frac{2\pi n_g}{l}T_{ge} = \frac{6\pi^2 {n_g}^2 k_t k_e}{l^2(R_i + R_e)}\dot{x} = c_e\dot{x} \tag{3.5}$$

where $c_e = \frac{6\pi^2 {n_g}^2 k_t k_e}{l^2(R_i+R_e)}$, which can be regarded as the equivalent damping coefficient of the proposed energy harvester during the engagement period.

Using the energy method, the kinetic energy of the system could be obtained as follows

$$\sum_1^n T_{kinetic} = \frac{1}{2}m_e{\dot{x}}^2 \tag{3.6}$$

$$\sum_1^n T_{kinetic} = \frac{1}{2}m_{ip}{\dot{x}}^2 + \frac{1}{2}J_{bs}\omega_{bs}^2 + \frac{1}{2}J_s\omega_s^2 + \frac{1}{2}J_{lb}\omega_{lb}^2 + \frac{1}{2}J_{sb}\omega_{sb}^2 + \frac{1}{2}J_{gh}\omega_{gh}^2 + \frac{1}{2}J_{ge}\omega_{ge}^2 \tag{3.7}$$

$$\omega_{bs} = \omega_s = \omega_{lb} = 2\pi\frac{\dot{x}}{l} \tag{3.8}$$

$$\omega_{sb} = 2\omega_{lb} \tag{3.9}$$

$$\omega_{gh} = \omega_{ge} = 2\pi n_g\frac{\dot{x}}{l} \tag{3.10}$$

where m_e and $T_{kinetic}$ represent the equivalent mass and the kinetic energy of the engaged system, ω_{bs}, ω_s, ω_{lb}, ω_{sb}, ω_{gh}, and ω_{ge} are the angular velocity of the ball-screw, shaft, large bevel gear, small bevel gear, gearhead and the generator respectively. $J_{bs}, J_s, J_{lb}, J_{sb}, J_{gh},$ and J_{ge} represent the moment of inertia of the ball-screw, shaft, large bevel gear, small bevel gear, gearhead and the generator, respectively. m_{ip} is the mass of the input plate.

Substitute (3.7) - (3.10) into (3.6), the equivalent mass of the engaged system can be derived as

$$m_e = m_{ip} + \frac{4\pi^2}{l^2}(J_{bs} + J_{bs} + J_{lb} + 4J_{sb}) + \frac{4\pi^2}{l^2}{n_g}^2 J_{ge} \approx \frac{4\pi^2}{l^2}{n_g}^2 J_{ge} \tag{3.11}$$

In Equation (3.11), the contribution of the inertia of the input plate, the gears, and the screws, $m_{ip} + \frac{4\pi^2}{l^2}(J_{bs} + J_{bs} + J_{lb} + 4J_{sb})$, is much smaller than that of the generator $\frac{4\pi^2}{l^2} {n_g}^2 J_{ge}$, especially when the gear amplification ratio is large. Therefore, the equivalent inertance of the proposed track energy harvester is mainly dominated by the rotational inertia of the electromagnetic generator. The inertia of other mechanical components could be negligible.
Hence, during the engagement period, the dynamic model of the proposed energy harvester can be simplified as a single degree of freedom spring-mass-damper system under a force excitation from the railway track. The total force the energy harvester gives to the railway track can be expressed as

$$F_e = m_e\ddot{x} + c_e\dot{x} + 2k(x + \delta_0) = \frac{4\pi^2}{l^2} {n_g}^2 J_{ge}\ddot{x} + \frac{6\pi^2 {n_g}^2 k_t k_e}{l^2(R_i + R_e)}\dot{x} + 2k(x + \delta_0) \qquad (3.12)$$

where δ_0 is the original compression length of the pre-loaded springs. The above equation indicates that the energy harvester could be regarded as a fixed inerter in parallel with two pre-loaded springs and a tunable damper.

During the disengagement, the bevel gear disengages with the shaft, and therefore, there is no transmission from the shaft to the bevel gears. The only force from the energy harvester to the railway track is the spring force coming from the two reset springs, and at this time, the generator will rotate freely only with viscous damping from the generator.

In summary, the dynamics equation and the induced single-phase voltage of the proposed railway energy harvester could be obtained as

$$\begin{cases} F_e = \frac{4\pi^2}{l^2} {n_g}^2 J_{ge}\ddot{x} + \frac{6\pi^2 {n_g}^2 k_t k_e}{l^2(R_i + R_e)}\dot{x} + 2k(x + \delta_0) & Engagement \\ F_e = 2k(x + \delta_0) & Disengagement \end{cases} \qquad (3.13)$$

$$\begin{cases} V_{ge} = 2\pi k_e n_g \sin\left(\int_0^t \omega_e dt + \frac{2k}{3}\pi\right)\frac{\dot{x}}{l} & Engagement \\ V_{ge} = \dot{\theta}_s(t) = e^{-\frac{c_e}{m_e}(t-t_0)}\dot{\theta_{s0}} \sin\left(\int_0^t \omega_e dt + \frac{2k}{3}\pi\right) & Disengagement \end{cases} \qquad (3.14)$$

where t_0 and $\dot{\theta}_{s0}$ are the time and angular velocity when disengagement occurs, and ω_e is the angular frequency of the induced voltage of the generator, which will be ω_{ge} multiplied by the total number of generator pole pairs. $k = 0, 1, 2$, representing the 1st, 2nd and 3rd phase of the generator.

3.3.3 System dynamics

To further understand the dynamic interaction among the train, rail and track harvester and to predict the energy harvesting performance at different train speeds, a comprehensive model is established and presented in Figure 3-5. A two-unit rapid transit train model is employed with four wheelsets per train. The wheel-rail vertical contact forces behave as the force input to the track-

harvester system and can be considered as moving loads $f_1 \sim f_8$ with vehicle speed V_0. It has been investigated that railway track can be modeled as a simply supported beam if the rail length is longer than 100 m [53]. Neglecting the shear deformation and rotational inertia of the railway track, a uniform Euler-Bernoulli beam of mass m_r per unit length and flexural rigidity EI, with individual sleepers supported beneath, is applied in this model. Rail pads are positioned between the rail and sleepers to provide stiffness and damping, and sleepers are supported by the ballast bed. The proposed energy harvester, which can be considered as a fixed inertia mass in parallel with a tunable damper and pre-loaded springs, is installed between two adjacent sleepers, as shown in the red dash box in Figure 3-5.

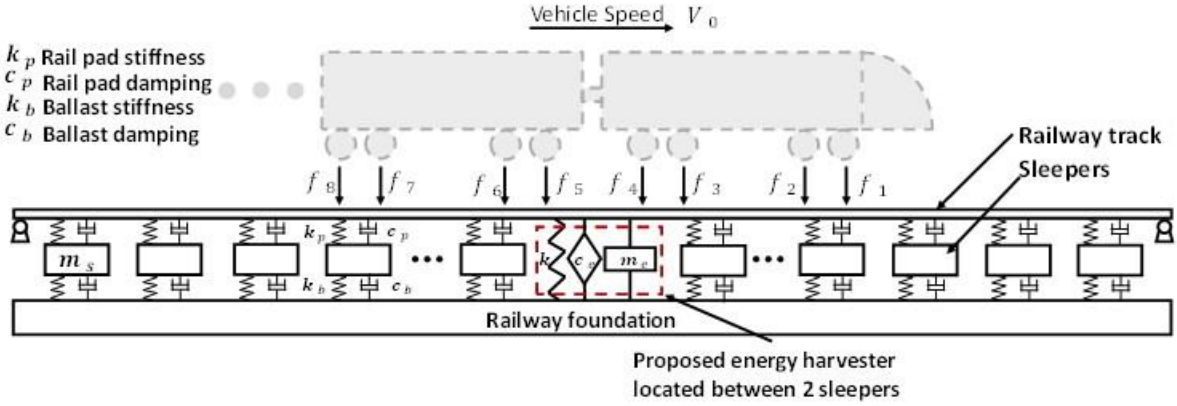

Figure 3-5. Dynamic model of Train-track-harvester system

$$EI\frac{\partial^4 Z_r}{\partial x^4}(x,t) + m_r\frac{\partial^2 Z_r}{\partial t^2}(x,t) = f(x,t) \tag{3.15}$$

where Z_r is the rail deflection (subscript r means rail) and $f(x,t)$ is the total external forces applied on the rail, including the supporting forces $F_{rsk}(t)$ from the $1 \sim k$ sleepers (subscript rs means the force between the rail and sleeper, and k means the kth sleeper), eight wheel-rail vertical contact forces $P_l(t)$ (subscript l means the lth load) from the train wheels and supporting force $F_h(t)$ from the proposed harvester (subscript h means the harvester). This three forces could be expressed as follows

$$F_{rsk}(t) = K_{pk}[Z_r(x_k,t) - Z_{sk}(t)] + C_{pk}\left[\dot{Z}_r(x_k,t) - \dot{Z}_{sk}(t)\right] \tag{3.16}$$

$$P_l(t) = f_0 \tag{3.17}$$

$$F_h(t) = \begin{cases} m_e\ddot{Z}_r(x_h,t) + c_e\dot{Z}_r(x_h,t) + 2k_{spring}(Z_r(x_h,t) + \delta_0) & engage \\ 2k_{spring}(Z_r(x_h,t) + \delta_0) & disengage \end{cases} \tag{3.18}$$

where K_{pk}, C_{pk} are stiffness and damping of the rail pad; x_h, x_k are the horizontal coordinates of the harvester and kth sleeper; $Z_{sk}(t)$, $\dot{Z}_{sk}(t)$ are vertical displacement and velocity of kth sleeper; k_{spring} and δ_0 are the stiffness and pre-compressed length of the pre-loaded springs. The engagement happens when the rotational speed of one large bevel gear equals that of the input shaft, while the disengagement happens when the rotation of large bevel gears is larger than that of the input shaft and no torque transmision exists between the shaft and gears. The force $F_h(t)$ from the energy harvester is a piecewise linear function during engagement and disengagement,

which endues the nonlinear characteristics to the system. The overall external force on the rail can be written as

$$f(x,t) = -\sum_{k=1}^{N} F_{rsk}(t)\delta(x - x_k) + \sum_{l=1}^{8} P_l(t)\delta(x - x_{wl}) - F_h(t)\delta(x - x_h) \tag{3.19}$$

where N is the number of sleepers, $\delta(x)$ is the Dirac delta function and x_{wl}, ($l = 1{\sim}8$) is the horizontal coordinate of the eight moving loads.

By using the method of separation of variables, the deflection of the rail can be written as:

$$Z_r(x,t) = \sum_{i=1}^{M} \phi_i(x) q_i(t) \tag{3.20}$$

where $q_i(t)$ is the ith modal time coordinate and M is the total number of modes considered in the model. It has been investigated that a good convergence of the solution could be obtained if M is larger than half of the system degrees of freedom [53]. For simply supported Euler-Bernoulli beam, the mode shape function could be written as

$$\phi_i(x) = \sin\left(i\frac{\pi}{l}x\right) \tag{3.21}$$

For ith mode, the dynamic equation of the railway track is given by

$$EI\frac{\partial^4 Z_{ri}}{\partial x^4}(x,t) + m_r\frac{\partial^2 Z_{ri}}{\partial t^2}(x,t) = f(x,t) \tag{3.22}$$

After substituting Equation (3.21) into (3.22) and performing some manipulation, we can get

$$EI\beta^4\phi_i(x)q_i(t) + m_r\phi_i(x)\frac{\partial^2 q_i(t)}{\partial t^2} = f(x,t) \tag{3.23}$$

where $\beta^4 = \frac{\omega^2}{c^2} = \frac{\rho A\omega^2}{EI}$. Using the orthogonality of the mode shapes, the above equation can be expressed as

$$EI\beta^4 q_i(t)\int_0^l \phi_i(x)\phi_j(x)dx + m_r\ddot{q}_i(t)\int_0^l \phi_i(x)\phi_j(x)dx = \int_0^l f(x,t)\phi_j(x)dx \tag{3.24}$$

where

$$\int_0^l \phi_i(x)\phi_j(x)dx = \begin{cases} 0 & i \neq j \\ \dfrac{l}{2} & i = j \end{cases} \tag{3.25}$$

Therefore, the final equation of motion for the rail is given by

$$EI\beta^4\frac{l}{2}q(t)+m_r\frac{l}{2}\ddot{q}(t)=\int_0^l f(x,t)\phi_i(x)dx \tag{3.26}$$

During the engagement period, the governing equation of the rail track could be expressed as

$$\begin{aligned}\left[m_r\frac{l}{2}+m_e{\phi_i}^2(x_h)\right]\ddot{q}_i(t)+\left[c_e{\phi_i}^2(x_h)+C_{pk}\sum_{k=1}^{N}{\phi_i}^2(x_k)\right]\dot{q}_i(t)-C_{pk}\sum_{k=1}^{N}\phi_i(x_k)\,\dot{Z}_{sk}(t)\\+\left[EI\beta^4\frac{l}{2}+2k_{spring}{\phi_i}^2(x_h)+K_{pk}\sum_{k=1}^{N}{\phi_i}^2(x_k)\right]q_i(t)-K_{pk}\sum_{k=1}^{N}\phi_i(x_k)Z_{sk}(t)\\=\int_0^l\sum_{l=1}^{8}P_l(t)\delta(x-x_{wl})\,\phi_i(x)dx-\int_0^l 2k\delta_0\phi_i(x_h)\delta(x-x_h)dx\end{aligned} \tag{3.27}$$

During the disengagement period, the governing equation of the rail track could be expressed as

$$\begin{aligned}m_r\frac{l}{2}\ddot{q}_i(t)+\left[C_p\sum_{k=1}^{N}{\phi_i}^2(x_k)\right]\dot{q}_i(t)-C_{pk}\sum_{k=1}^{N}\phi_i(x_k)\,\dot{Z}_{sk}(t)\\+\left[EI\beta^4\frac{l}{2}+2k_{spring}{\phi_i}^2(x_h)+K_p\sum_{k=1}^{N}{\phi_i}^2(x_k)\right]q_i(t)-K_p\sum_{k=1}^{N}\phi_i(x_k)Z_{sk}(t)\\=\int_0^l\sum_{l=1}^{8}P_l(t)\delta(x-x_{wl})\,\phi_i(x)dx-\int_0^l 2k\delta_0\phi_i(x_h)\delta(x-x_h)dx\end{aligned} \tag{3.28}$$

The equation of motion for the kth sleeper is given by

$$\begin{aligned}m_{sk}\ddot{Z}_{sk}(t)+\left(C_{pk}+C_{bk}\right)\dot{Z}_{sk}(t)+\left(K_{pk}+K_{bk}\right)Z_{sk}(t)-C_{pk}\sum_{i=1}^{N}\phi_i(x_k)\dot{q}_k(t)\\-K_{pk}\sum_{i=1}^{N}\phi_i(x_k)q_k(t)=0\end{aligned} \tag{3.29}$$

where K_{bk}, C_{bk} are the ballast stiffness and damping, respectively.

By combining all the equations above, a standard matrix form of the governing equations of the system can be formulated and expressed as follows

$$\begin{cases}\mathbf{M_{engage}}\ddot{X}(t)+\mathbf{C_{engage}}\dot{X}(t)+\mathbf{K}X(t)=\mathbf{F(t)} & engage\\ \mathbf{M_{disengage}}\ddot{X}(t)+\mathbf{C_{disengage}}\dot{X}(t)+\mathbf{K}X(t)=\mathbf{F(t)} & disengage\end{cases} \tag{3.30}$$

where $\ddot{X}(t)$, $\dot{X}(t)$, and $X(t)$ are the generalized acceleration, velocity and displacement vectors, respectively; $\mathbf{M_{engage}}$ and $\mathbf{M_{disengage}}$ are generalized mass matrices during engagement and disengagement, respectively; $\mathbf{C_{engage}}$ and $\mathbf{C_{disengage}}$ are generalized damping matrices during engagement and disengagement, respectively; $\mathbf{K}$ is generalized stiffness matrices, which keeps unchanged during the switching of engagement and disengagement and $\mathbf{F(t)}$ is the corresponding force, which contains the eight moving load $f_1 \sim f_8$ and the generalized modal forces.

3.3.4 Simulation of energy harvesting performance

Simulation has been conducted using the developed comprehensive train-track-harvester model. Since the formulated matrices have a very large size and equations are coupled with the nonlinearity of the engagement and disengagement characteristics, the conventional direct time integration method is inefficient and computationally expensive. An improved fast explicit integration algorithm, proposed by *Zhai* [53, 54], has been adopted in this paper to solve the governing equations, which can be expressed as follows

$$\{X\}_{n+1} = \{X\}_n + \{V\}_n \Delta t + \left(\frac{1}{2} + \psi\right)\{A\}_n \Delta t^2 - \psi\{A\}_{n-1}\Delta t^2 \tag{3.31}$$

$$\{V\}_{n+1} = \{V\}_n + (1+\varphi)\{A\}_n \Delta t - \varphi\{A\}_{n-1}\Delta t \tag{3.32}$$

where Δt is the time step. The maximum time step size for the freight train-track system is found to be $5 \times 10^{-5} s$ [53, 54]. X, V and A are modal displacement, velocity and acceleration, respectively. $n+1$, n and $n-1$ represent every three adjacent time step. φ and ψ are integration parameters, which are both chosen as 0.5 in the simulation.

Table 3-2. Simulation parameters

Parameters	Description	Value
f_0	Static moving load	105 kN (@30 km/hr)
m_r	Rail mass per meter	51.5 kg/m
EI	Elastic modulus of rail	4×10^6
K_{pk}	Rail-pad stiffness	20MN/m
C_{pk}	Rail-pad damping	21.8 KNs/m
K_{bk}	Ballast stiffness	10 MN/m
C_{pk}	Ballast damping	21.8 KNs/m
m_{sk}	Sleeper mass	125.5 kg
l_s	Sleeper spacing	0.545 m
l	Rail length	139.52 m
V_0	Velocity of the wheel	20~80 km/hr

The parameters of the simulation are listed in Table 3-2. A two-unit rapid transit train with 4 wheelsets per unit was selected in the simulation, and the results of the two prototypes are shown in Figure 3-6. Figure 3-6(a) illustrates the simulated track displacement (at the harvester

installation point) at 20 km/hr train speed, single-phase voltage and single-phase power with an 8 Ohm resistive load. It should be noted that while the train passes by the track deflects down and up when every wheelset approaches and leaves, exciting the harvester to produce energy twice for a single wheel. The first four wheelsets of the first rapid transit unit contribute the first four displacement valleys, while the last four displacement valleys come from the four wheelsets of the second rapid transit unit as shown in Figure 3-6(a). Results with similar shapes are also expected for the freight trains cases, but since freight train track deflection will have larger amplitudes and frequencies due to higher train speed and load, higher power output will be achieved.

Figure 3-6(b) and 3-6(c) show the simulated average power versus different train speeds and external resistive loads for two different prototypes. The dash lines represent the results that consider the moving loads as constants, which means that the wheel-rail force remains unchanged when the train moves at different speeds. The solid lines represent the results that consider the moving loads as speed-dependent ones, in other words, the wheel-rail vertical contact force will be larger when the train runs faster due to the rail irregularity and train dynamics [55, 56], which is much closer to the real case. As the train speed increases, the simulated power could be larger and the average power is 5-10W for prototype 1 and 20-30W for prototype 2 at 60 km/hr, which could be an adequate energy source for most of the smart electronic devices.

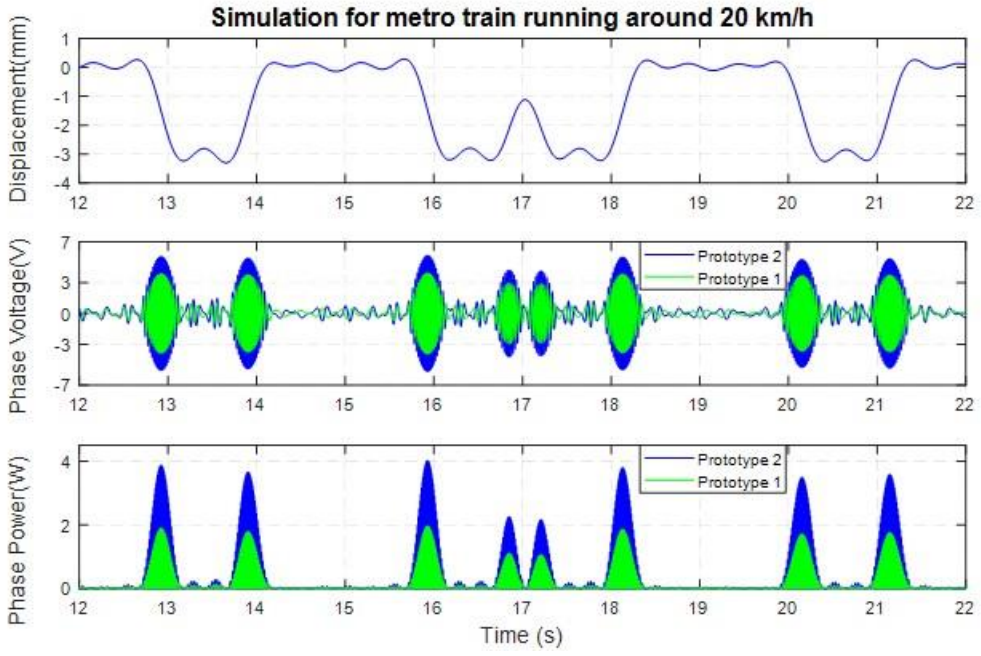

(a)

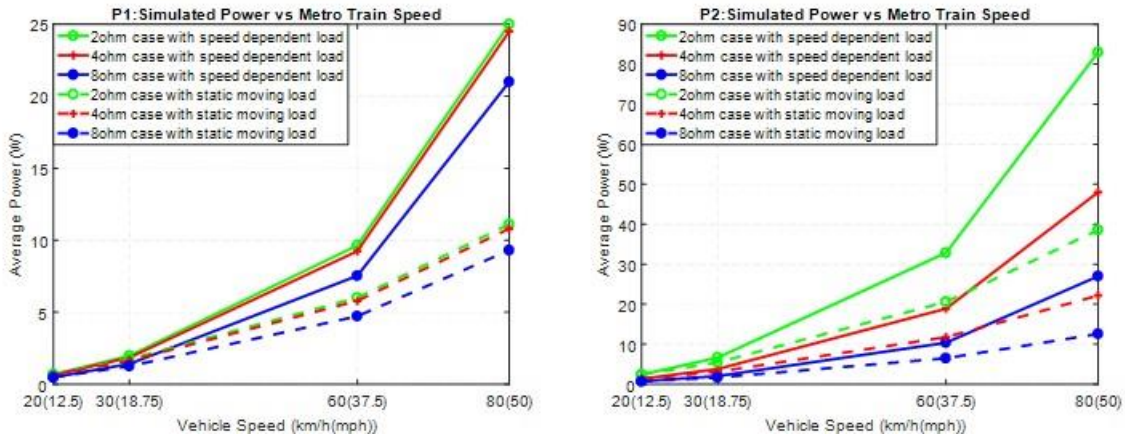

(b) (c)

Figure 3-6. (a) Simulation results with an 8 Ohm Wye shape resistive load when rapid transit speed is 20 km/hr: prototype 1 and prototype 2. Simulated average power under different train speed with different resistive loads: the solid line is the simulation results with speed-dependent moving load and the dashed line is the simulation result with static moving load: (b) prototype 1; (c) prototype 2.

3.3.5 Dynamic influence on the railway track and vehicle

The dynamic influence of the energy harvester to the railway track and vehicle is very important to the train operation safety. Figure 3-7(a) shows the simulated vertical displacement comparison of railway track with and without energy harvesters: the black solid line, representing the track displacement without any harvester beneath, matches very well with the red dash line, representing the track displacement with Harvester 1 beneath, and green dot line, representing the track displacement with Harvester 2, when the rapid transit train runs 20 km/hr and harvester connected to a 2 Ohm Wye shape external resistive load. Figure 3-7(b) shows the simulated displacement RMS differences between the track with the harvester 1 and 2 beneath (connected to 2 Ohm Wye shape external resistive load) and the track without energy harvester beneath, at different vehicle speeds. Compared with harvester 1, harvester 2 has a larger RMS difference; this is because harvester 2 provides more damping to the train-track system and recovers more power from the system. This difference increases when the rapid transit train runs faster; however, the overall RMS difference is still very small even at the maximum operation speed of 80 km/hr for the rapid transit train. In other words, the influence of integrating the harvester to the railway track is so small that it will not affect the track and train dynamics, which will not bring any safety issue to the train operation.

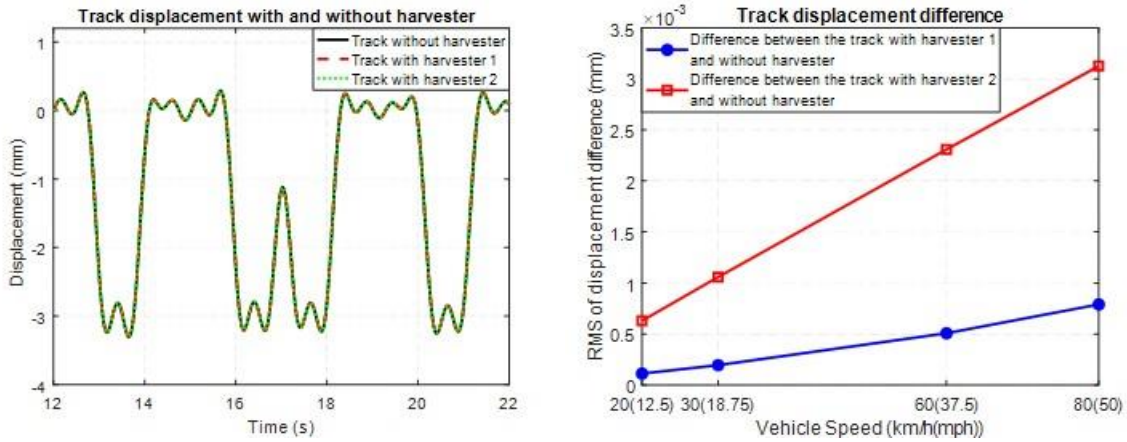

Figure 3-7. Dynamic influence of the energy harvester to the track: (a) railway track vertical displacement due to the wheel-rail vertical force when the train runs at around 20 km/hr: the black solid line represents the track displacement without any harvester beneath, the red dash line represents the track displacement with harvester 1 beneath connected to a 2 Ohms external resistive load and the green dot line represents the track displacement with harvester 2 beneath connected to a 2 Ohms external resistive load; (b) the displacement RMS differences between the tracks with the harvester 1 and harvester 2 beneath (connected to 2 Ohms external resistive load) and the tracks without the harvester beneath, at different vehicle speeds.

3.4 Lab Bench Test and Analysis

3.4.1 Experiment setup

Figure 3-8 shows the in-lab bench test setup for the proposed ball-screw based energy harvester. The ground plate was connected to the upper grip of the Instron hydraulic test machine through a T-shape adapter, and the input plate of the harvester was connected to the lower grip using an L-shape adapter and a connecting board. The lower grip could be driven by the hydraulic actuator and controlled by the built-in software and a 100 KN load cell together with an LVDT displacement sensor was used to measure the force and displacement during the test. A Wye shape resistive load with a 19:1 voltage divider was prototyped into a printed circuit board (PCB) which was connected to the generator of the harvester during the in-lab test. The voltage across the external resistor was measured and recorded by both Instron software and external dynamic analyzer (Spider 80) during each test. The ball-screw harvester was tested with both sinusoidal excitation and measured track displacement excitation, and the corresponding energy harvesting performance will be evaluated in the following.

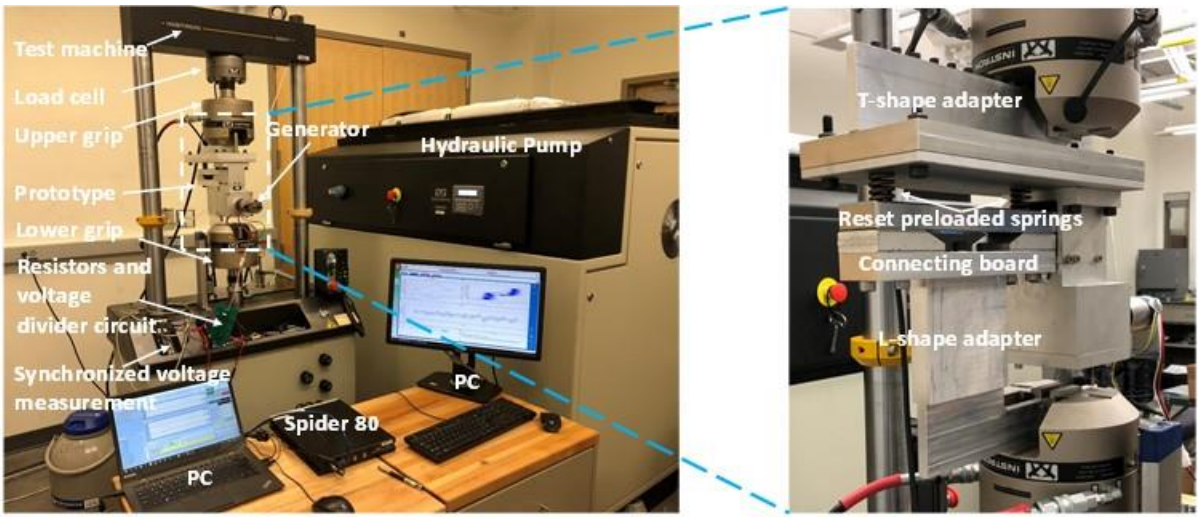

Figure 3-8. In-lab experiment setup

3.4.2 Harmonic excitation

A series of sinusoidal displacement excitations with different amplitudes and frequencies were input to the energy harvesters. During the test, the generator was observed to start to rotate at ±0.2 mm vibration amplitude, which indicates the overall prototype has a relatively small backlash and a high sensitivity towards the environmental vibration. The average power of the prototype 1 and prototype 2 under 1 Hz excitation frequency, 1-3mm amplitude with different resistive loads are summarized in Table 3-3, as well as the electrical damping coefficient for the two prototypes. As we can see, with the same external resistive load, the damping of prototype 2 is much larger than prototype 1, because the two prototypes use different generators and gearhead amplification ratios. The average power of the two prototypes in the harmonic test becomes larger when the vibration amplitude increases since the average input speed is increased. Meanwhile, the average power becomes larger when the external resistive load decreases, and this is because the electrical damping coefficient becomes larger, which means more mechanical energy could be converted to electrical energy within the same period. The energy harvesting output power of the prototype 2 is higher than that of the prototype 1 because the multiplication of speed constant of the generator 2 and its corresponding gearhead amplification ratio is larger.

Table 3-3. Test results under harmonic excitations with a 1 Hz frequency

Prototype 1	Damping	1 mm	2 mm	3mm	Prototype 2	Damping	1 mm	2 mm	3mm
2 *ohm*	67,762 Ns/m	0.8 W	3.2 W	7.1 W	2 *ohm*	168,640 Ns/m	0.9 W	6.5 W	17.7 W
4 *ohm*	46,182 Ns/m	0.5 W	2.0 W	4.6 W	4 *ohm*	89,908 Ns/m	0.8 W	4.9 W	12.3 W
8 *ohm*	28,212 Ns/m	0.3 W	1.40 W	3.0 W	8 *ohm*	46,495 Ns/m	0.5 W	3.0 W	7.3 W

Figure 3-9 shows the simulated and measured phase voltage and power of the ball-screw harvester 2 with a Wye shape external resistive load of 8 Ohms, under amplitude of ± 3 mm and frequency of 2Hz. The phase voltage subplot illustrates that the generator is still rotating when the

displacement reaches the peak or valley, showing the harvester disengages at that moment and generator rotates freely with viscous damping. An average power of 26.61W was achieved during this test and simulation results matched well with experimental results.

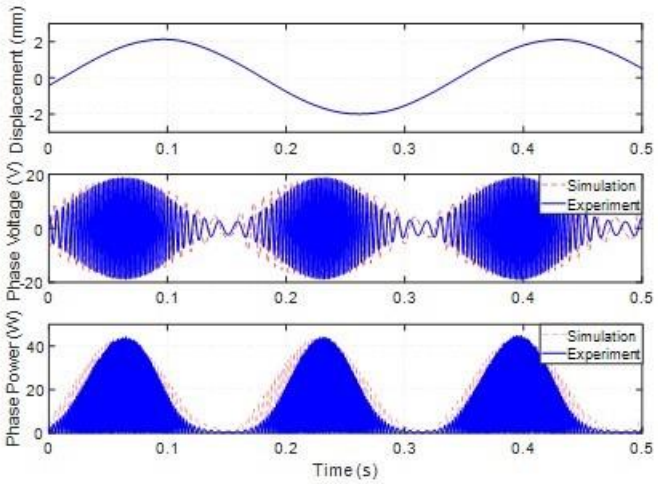

Figure 3-9. Measured and simulated phase voltage and power of harvester prototype 2 under sinusoidal excitation with amplitude ± 2 mm and frequency 3 Hz. The harvester is connected to an 8 Ohm resistive loads in a Wye shape and the average power of the total three phases is 26.61 W.

3.4.3 Measured freight train track vibration

A freight train track displacement previously measured in Transportation Technology Center, Inc. (TTCI) [29] was used as input to the harvester, to further investigate the performance of the proposed energy harvester. Figure 3-10 shows the phase voltage and power of ball-screw based energy harvester prototype 2 connected to 8 Ohm Wye shape resistive load under the measured displacement at the speed of 64km/hr (40mph), and a peak power of 114.98W at the single phase and an average power of 17.50W at three phases were achieved during the experiment. Simulation results by using harvester model with measured track displacement inputs are also illustrated in Figure 3-10. As we can see, the simulation results match well with the experiment results, which validates the effectiveness of the harvester model. Table 3-4 illustrates the damping coefficient and energy harvesting performance of the prototype 1 and prototype 2. It should be noted that, for both prototypes, when the external resistive load is reduced, the damping and average power will be increased. As we know, if the rotational speed of a generator is constant, the output power on the external resistor will be the maximum when the external resistive load approaches the internal resistive load. During the in-lab test, the displacement input can be regarded as constant, and prototype 1 has a 2.28 Ohms terminal resistance phase to phase, while prototype 2 has a 0.284 Ohm terminal resistance phase to phase. Therefore, for prototype 1, when the external resistive load is 2 Ohm, the output power should be around the maximum point, however, for prototype 2, if the external resistive load is reduced continuously, ideally the output power will be even larger. From table 3-4, when the external resistive load of prototype 2 decreases from 4 Ohm to 2 Ohm, the power should increase significantly, however, the output power remains almost the same. One possible reason for this abnormal phenomenon is that the resisting torque from the generator becomes larger when the external resistive load is reduced. Therefore, the clutches embedded in the large bevel gears reach their torque limit and slip which reduces the rotational transmission

from the shaft to the bevel gears, resulting in less output power than what it is expected when decreasing the external resistive load.

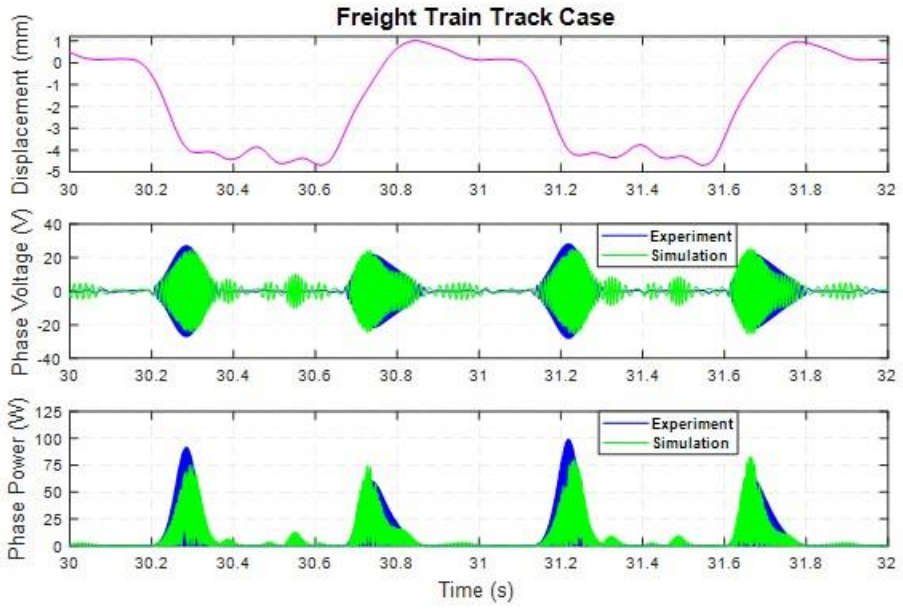

Figure 3-10. Energy harvesting performance of the ball-screw based harvester under measured freight train (running at 64 km/hr) track displacement with 8 Ohm resistive loads in a Wye shape. The peak power in a single phase is 114.98W and the average power in all three phases are 17.50 W.

Table 3-4. Energy harvesting performance under freight train track deflection for ball-screw based track energy harvesters.

Prototype 1	Damping	Avg. Power	Prototype 2	Damping	Avg. Power
2 *ohm*	67,762 Ns/m	20.10 W	2 *ohm*	168,640 Ns/m	**23.54 W**
4 *ohm*	46,182 Ns/m	17.60 W	4 *ohm*	89,908 Ns/m	23.17 W
8 *ohm*	28,212 Ns/m	11.40 W	8 *ohm*	46,495 Ns/m	17.50 W

3.4.4 Rapid transit track vibration

Rapid transit track deflections were measured with the vehicle running at different speeds on a rapid transit test line located at Tongji University campus, and harvesters were tested in lab with these measured track displacements. During the test, the preload of the reset springs was set to be around 2500 N. As shown in Figure 3-11(a), a single-phase peak power of 13.36W and a three-phase average power of 1.58W were obtained from prototype 2 under rapid transit track displacement (measured when rapid transit runs at 30 km/hr) with 8 Ohm resistive loads in the Wye shape. The force measured in the test and obtained in the simulation is the force from the upper grip to the harvester base plate, and negative force means that the upper grip is continuously supporting or pushing the base plate. As we can see, the simulation results match well with the experiment results, which validates the effectiveness of the harvester model. Figure 3-11(b) shows

single-phase peak power and three-phase average power of both prototype 1 and prototype 2 using the measured displacement with different resistive loads. 20 km/hr and 30 km/hr cases used real measured displacement as excitation input, and 60 km/hr and 80 km/hr cases used measured displacement with a compressed time, which means that the peak displacement will be kept as the same as low-speed case, while the time has been compressed to simulate higher train speed. As shown in Figure 3-11(b), the dash lines are the output power results for prototype 1 and the solid lines are for the prototype 2. The peak power and average power increase when the simulated train speed increases, and the average power at simulated 60km/hr and 80 km/hr cases could achieve around 5 and 9W for prototype 1 and 8 and 11W for prototype 2, which will be adequate for many trackside electronic applications and devices. The in-lab rapid transit track displacement track test results for prototype 1have the same trend with the simulation results in Figure 3-6 (c), and they match well with each other; however, for prototype 2, the test results and simulation results don't match well, especially when the external resistive load is small, such as the 2 Ohm case and 1 Ohm case. The reason for the mismatches at lower external resistor cases can be the resisting torque on the one-way clutch is larger than its limits, so that the clutch slipped during the experiment and cannot transmit the motion to the bevel gears, therefore the output rotational speed of the generator could not be fast enough as it is expected, and the output power will not be as high as we expected or even lower at a smaller resistor case compared with a higher resistive load.

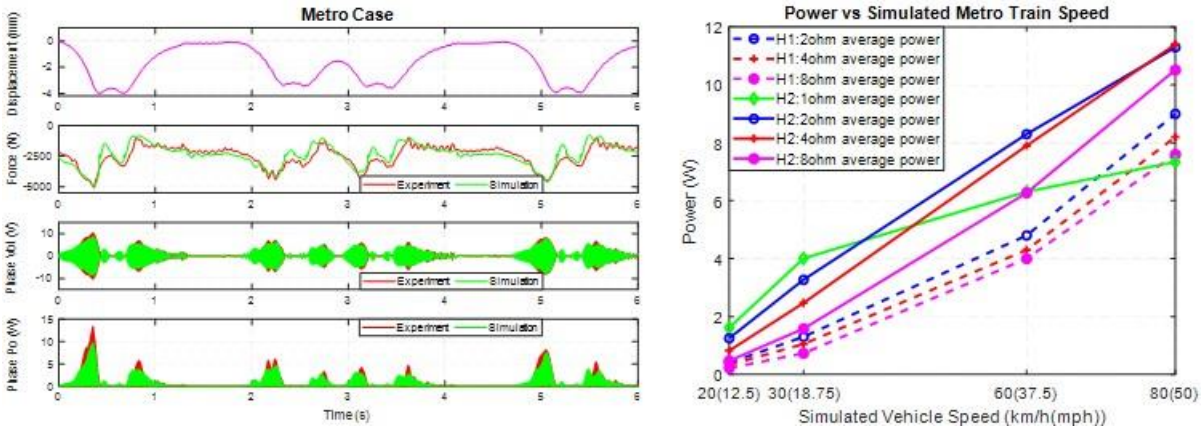

(a) (b)

Figure 3-11. (a) in-lab test and simulation results of prototype 2 under rapid transit train (running at around 30 km/hr) track displacement with an 8 Ohm resistive loads in Wye shape: single phase peak power in lab test is 13.36W and three-phase average power in lab test is 1.58 W; (b) three-phase average power of both ball-screw harvester prototype 1 and prototype 2 under simulated track displacement input using the measured displacement with different external resistive loads: the dash lines are for prototype 1 and the solid lines are for the prototype 2.

3.5 Field Test and Discussion

3.5.1 Test setup

Field test was carried out on a rapid transit test track located at Tongji University campus in Shanghai to validate the energy harvesting performance. Prototype 1 and 2 have been tested respectively. Fig. 12 shows the experimental setup. The harvester was placed between two wooden

sleepers on a ballast bed. The long input plate of the harvester was mounted rigidly under the test railway track. The ballast below the harvester prototype was cleared for fitting 4 jacks which supported the base plate of the harvester and provided a preload for the harvester input plate by compressing the reset springs. During the test, a two-unit rapid transit ran at around 20 km/hr and 30 km/hr on the ballast test line repeatedly. Two laser displacement sensors were used to measure the rail motion and harvester motion. Different Wye shape resistive loads were connected to the harvester during tests. A data acquisition system was employed to collect the displacement and voltage data and record the condition of harvester and rail when the rapid transit trains passed by.

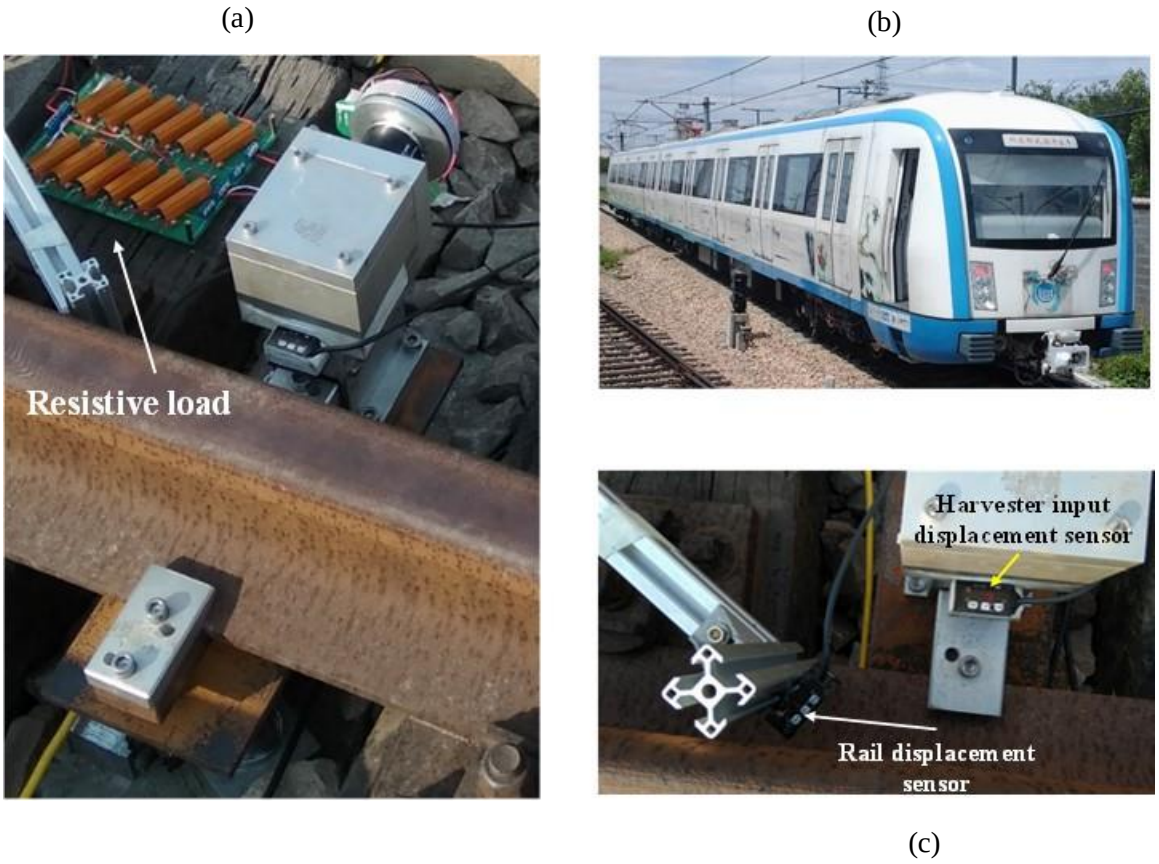

Figure 3-12. In field test setup: (a) Harvester prototype 1 was clamped on the railway track and positioned between two adjacent sleepers. (b) A two-unit Type A rapid transit ran with a speed of 20-30 km/hr; (c) Two laser displacement sensors measured the railway track displacement and harvester input displacement, respectively.

3.5.2 Results and discussion

Figure 3-13(a) shows the measured and simulated rail displacements, harvester input displacements and measured single-phase voltage over an 8 Ohm Wye shape external resistor at the train speed of 20 km/hr. The input displacement of the harvester followed closely with the rail displacement. A peak power of 1.64W and an average power of 0.27W were achieved.

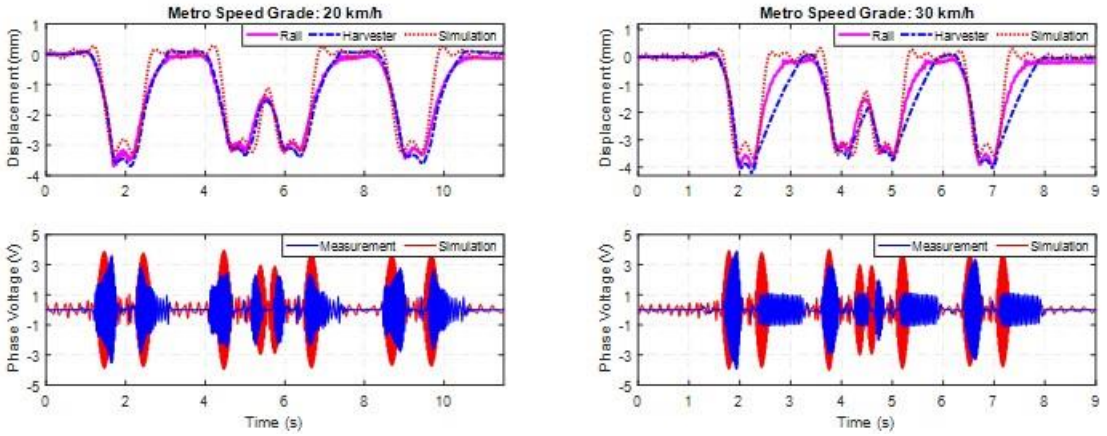

(a) (b)

Figure 3-13. Measured and simulated rail and harvester displacements and measured voltages at different vehicle speeds: (a) rapid transit train speed is 20km/hr and the external resistive load is 8 Ohm. The average power obtained in the test is 0.27W; (b) rapid transit speed is 30km/hr and the external resistive load is 2 Ohm. An average 1.12W was achieved in the test.

Figure 3-13(b) shows the measured and simulated rail displacements, harvester input displacement and measured single-phase voltage of generator of prototype 1 with a 2 Ohm Wye shape external resistor when the train passed with 30 km/hr speed. A peak power of 7.8W and an average power of 1.12W were achieved during this 8-second test. It is noted that during the test, the harvester displacement followed well when railway track moved downward, but not well when the track moved back. As a result, the voltage during the rail deflected was large, while relatively small when the track restores to its undeflected position. Possible reasons for this problem are as follows: (1) the spring force is not large enough, especially at a small resistive load or a large speed. When the vehicle speed increased, the track deflection speed and acceleration became large, so the damping force and the inertia force became larger, which means that the harvester needed larger spring force to push the base plate to keep still on the ground; (2) during the reciprocating test, ballast below the harvester became loose so that the preload provided by the reset spring was smaller than that of the first several tests. Inadequate spring force resulted in the base plate being separated with the rail foundation, so the restored speed of harvester was smaller, therefore, the voltage of the generator became smaller when the track restored back.

Table 3-5. Field test results summary for Prototype 2

Resistor / Speed	8 Ω	4 Ω	2 Ω
20 km/hr (12.4 mph)	1.16 W	1.24 W	1.36 W
30 km/hr (18.6 mph)	**2.24 W**	2.04 W	1.48 W

Table 3-4 summarizes the field test results of the prototype 2. A maximum average power of 2.24W was achieved with 8 Ohm Wye shape resistive loads at a rapid transit speed of 30 km/hr. This energy could be stored in a battery through self-designed or commercial battery charging circuits

and used to power different trackside electrical devices, such as signal lights, track switches, hot box detectors, rail health monitoring systems, and wireless communication modules, which could potentially increase the safety of train operation. The power outputs are expected to be larger with smaller resistive loads than that of 8 Ohm but ended up with a lower power due to possible inadequate spring forces and clutch slippage, which has been discussed above in this subsection and subsection *4.4*. More power could be expected by choosing a higher limit one-way clutch, increasing the reset spring stiffness and refining the installation condition.

3.6 Chapter Summary

In this chapter, a novel ball-screw based railway track energy harvester with mechanical motion rectifier mechanism was designed, modeled and tested. Due to the nonlinear characteristics induced by the one-way clutches in the mechanical motion rectifier (MMR) mechanism, the proposed energy harvester could convert the bi-directional track vibration into unidirectional rotation of the generator, which significantly improves the motion transmission by reducing the impact forces. A comprehensive model considering the coupled dynamic behaviors of the train, railway track and harvester was developed and validated. It is shown that the proposed ball-screw based energy harvester acts as a fixed inerter in parallel with pre-compressed springs and an adjustable damper tuned by external resistive load of the generator, when the one-way clutch is in engagement. When both one-way clutches disengage from the bevel gears, the energy harvester behaves as pre-compressed springs only, and the inertia of the generator drives the generator itself continuously to produce electricity. This piece-wise mass-spring-damper of the single freedom harvester is integrated into the train-track model and the performance of the harvester at different train speeds can be predicted by the model.

The in-lab and field tests were conducted to further validate the dynamic characteristics and evaluate the performance of the proposed energy harvester. The harvester could effectively work under a very small input with the amplitude of ±0.2 mm, which shows that the proposed harvester has an improved sensitivity to the environment vibrations. Field test results showed that an average power of 1.12 and 2.24W were achieved for prototype 1 and 2 respectively at 30 km/hr rapid transit speed. More power could be obtained by choosing a higher limit one-way clutch, increasing the reset spring stiffness and refining the installation condition.

Chapter 4 Design, Modeling and Test of a Smart Energy Harvesting Railroad Tie

This chapter presents the design, modeling and bench testing of a smart railroad tie for energy harvesting from the motion of railway track. The system is intended for applications that require trackside power in remote locations, such as wayside electrical devices and safety equipment, signal lights, crossing gates, wireless communication, as well as rail health monitoring systems. The smart tie, which is designed to have similar dimensions to a conventional railroad tie, is installed in the same manner as a standard tie on the track. In particular, the mechanical energy harvesting module, and its corresponding power management unit can be both embedded inside a composite, concrete or wooden tie, to shield the components from the harsh environment and protect the system against any potential theft or vandalism. Different from other railway track harvesters that typically harvest energy from bidirectional track deflections, the proposed smart tie only harvests the kinetic energy of the track when the wheels push it downwards, which resolves the preload and installation challenges of bidirectional harvesting and increases the overall system reliability. A nonlinear analytical model is developed to analyze the dynamic characteristic of the system, and the simulation is conducted to predict the performance. Bench tests are subsequently carried out under both harmonic and recorded tie displacement inputs to validate the model and assess the harvesting performance. During the bench tests, the generator shaft was observed to start rotation at 0.1 mm vibration amplitude, indicating that the overall prototype has a relatively small backlash. In-lab test results indicate that an average power of 26.1-42.2W on 4 Ohms and 2 Ohms external loads were achieved under simulated tie movement recorded from a service track.

4.1 Chapter Introduction

In the past decade, many emerging technologies have been applied to improve transportation conditions all over the world. Among them, the energy harvesting technique has been widely investigated in automobiles [51, 52], railcars [34, 57, 58], bridges [59, 60], roadways [8, 60], and railways [14, 29, 61], for potentially increasing the fuel economy, effectively powering onboard or wayside electronics, and smartly monitoring the health conditions, etc.

Rail transport is more economical compared with air transport and experiences much less traffic compared with highway transport, which make it a great choice for transferring passengers and goods. However, large portions of tracks are in tunnels, mountains and remote areas, where grid power is in short supply. Without the electricity, most of the auxiliary devices and smart technologies for improving the operational safety of railroad, such as the signal lights, track switches, health monitoring and wireless communication systems, are not able to function.

Facing this problem of lacking electricity along the railroad, researchers have proposed different alternative power sources to improve the predicament. Wischke *et al.* [12] designed a piezoelectric vibration energy harvester mounted on railroad tie for powering wireless sensor nodes in tunnels and achieved an average energy of 395 uJ per train in-field test. Yuan *et al.*

[15] developed a piezoelectric drum harvester that can be mounted below the railroad tie and tested it in a 1:10 test rig with a single wheel. In-lab test showed an average power of 0.1 mW when the wheel traveled at 0.5 km/hr. Pan *et al.* [62] proposed wind energy harvester for powering sensors in railroad tunnels and a maximum power of 107 mW was obtained in bench test with the wind speed of 11 m/s. Wang *et al*. [63] reported an acoustic energy harvesting noise barrier that can harvest sound energy when a high-speed train passes and in-lab test showed that an instantaneous power of 1.24 uW was obtained for a single honeycomb-structure unit of the barrier at 110 dB sound pressure level. Gao *et al.* [64] designed a thermoelectric generator (TEG) to harvest the thermal energy by utilizing the temperature difference between the track and substratum 200 mm below the track foundation. Field tests showed the TEG prototype could produce average 5.8 mW across a 7 Ohms resistive load at a temperature difference of 8 °C. Overall, these various energy harvesters are all promising solutions for low-power sensors, however, they are not suitable for most powering wayside electrical devices that usually require power at watt-level or higher.

To harvest more energy for the electrical devices along the railroad, motion-based electromagnetic energy harvesters have been investigated and developed. Pourghodrat *et al.* [14] developed a rack-pinion based track energy harvester and achieved an average power of 0.22W when the train passed by at 18.5 km/hr (11.5 mph). Lin *et al.* [29] proposed a rack-pinion based anchorless track energy harvester with a single shaft design, which can convert the bi-directional track vibration into unidirectional rotation of the electromagnetic generator. Field test results indicated that an average power of 6.9W was achieved when the loaded freight railcar traveled at 64 km/hr (40 mph). Later, Pan *et al.* [61] developed a compact ball-screw based track energy harvester, which is directly mounted between the track and railroad foundation and has a relatively small backlash. By harvesting the track energy bi-directionally, this compact prototype was able to generate an average power of 2.24W when the rapid transit train run at 30 km/hr (18.6 mph). However, a defect was observed on the bidirectional railway harvesters in [61], which is that the damping force and inertia force will lift up the harvester due to inadequate spring preload when the track moves upwards, resulting in less power output obtained. And simply increasing the preload of the spring will make the installation laborious and challenging in the limited space.

Overall, compared with other energy harvesting methods, motion-based electromagnetic track harvesters can convert the vibration energy of the railroad track into the electrical energy with a much better performance and a greater potential for improving the safety of railroad transportation. However, three inadequacies still remain: (i) the installation of the previous track harvesters might interfere the normal maintenance of the track, such as the railroad tamping; (ii) previous track harvesters are directly exposed to the harsh environment of railroad and lack of protection; (iii) the bi-directional harvesters require large preload to prevent the harvester being lifted when the track rebounds, which introduces difficulties in initial installation and later maintenance.

In this paper, a smart energy harvesting tie, which is designed to have similar dimensions to a conventional railroad tie, is proposed and presented. The smart tie can be installed in the same manner as a standard tie on the track. The two main parts of the smart tie, the mechanical energy harvesting module and power management unit, are both placed inside the railroad tie, to shield the components from the harsh environment and protect the system against any

potential theft or vandalism. Different from the previous railway track harvesters that typically harvest energy from bidirectional track deflections, the proposed smart tie only harvests the kinetic energy of the track when the wheels push it downward, which resolves the preload and installation challenges of bidirectional harvesting and increases the overall system reliability. A nonlinear model is developed to analyze the dynamic characteristic of the system, and the simulation is conducted to better understand the system and predict the performance. Bench tests are subsequently carried out under both harmonic and recorded tie displacement inputs to experimentally validate the model and assess the harvesting performance of the system.

The rest of the Chapter is organized as follows. Chapter 4.2 presents the detailed design of the proposed smart energy harvesting tie and the working principles, Chapter 4.3 introduces the dynamic model and simulation study of the energy harvesting module inside the smart tie, Chapter 4.4 shows the lab bench test of the prototype and Chapter 4.5 summarizes the conclusion.

4.2 Design and Working Principle

A railroad track deflects and the ties (sleepers) more down vertically due to the forces applied by the rolling wheels. Despite the fact that the track and ties displace with a small amplitude, the mechanical energy that is potentially available is quite large due to the high tonnage of the trainload [27].

The proposed smart energy harvesting tie, which is designed to have similar dimensions to a conventional railroad tie, can be installed in the same manner as a standard tie on the track and convert the vibrational energy into electricity to power wayside electrical devices. Figure 1 shows the overall design of a scaled smart tie prototype, which can be installed on a single track. This smart tie prototype mainly consists of an energy harvesting module, a tie housing, a tie box, and two coil springs. The top of the energy harvesting module is rigidly connected to the tie housing, while the bottom of the energy harvesting module is fixed on the base plate of the tie box. When the wheel of a railcar approaches, the tie housing is pushed downward; while when the wheel leaves, the tie housing rebounds due to the resilience of the track and coil springs.

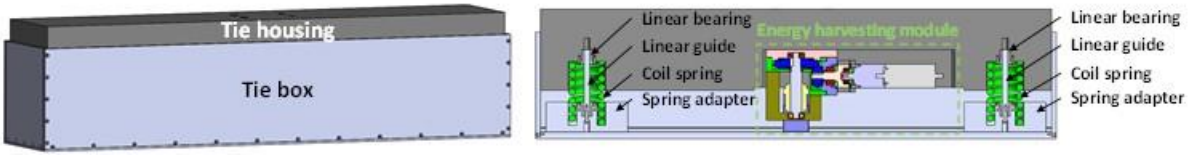

Figure 4-1. Overall design of the proposed smart energy harvesting tie. Half railroad tie is shown here. Similar design can be used for a full tie.

4.2.1 Design of the energy harvesting module

The energy harvesting module, playing an essential role as an energy transducer, is mainly comprised of a ball-screw with a nut, an enclosed gearbox with a single bevel gear-pair, an output shaft with an embedded one-way clutch, and an electromagnetic generator with a gearhead, as shown in Figure 2. The enclosed gearbox consists of casing 1, casing 2 and casing

3. The casing 1 and the nut adapter are rigidly connected to the tie housing and base plate of the tie box, separately. The ball-screw nut is embedded in and connected to the nut adapter by screws. Therefore, the gearbox of the energy harvesting module vibrates vertically together with the tie housing when the railcar passes by, while the tie box, where the nut adapter sits on, can be regarded as being stationary on the ballast. In this way, low speed reciprocal linear motion can be converted into the high-speed bidirectional rotation of the ball-screw shaft.

The enclosed gearbox includes a large bevel gear, a small bevel gear, three casings, and two angular contact bearings. The bearing casing holds another angular contact bearing for supporting the ball-screw shaft. The rotation can be transmitted from the larger bevel gear to the small bevel gear, and subsequently, the output shaft can also rotate in two directions. The one-way clutch bearing is pressed fitted into the output shaft, and the input shaft of the gearhead with a key on the shaft can be inserted into keyway on the inner ring of the clutch. This one-way clutch can only transmit the torque in one direction, and hence, only one directional rotation can be transmitted to the gearhead, and consequently, the generator can only rotate unidirectionally. The O-ring grooves and shaft seals enclose the lubricant oil or grease inside the gearbox, which increases the transmission reliability and reduces the undesired friction losses.

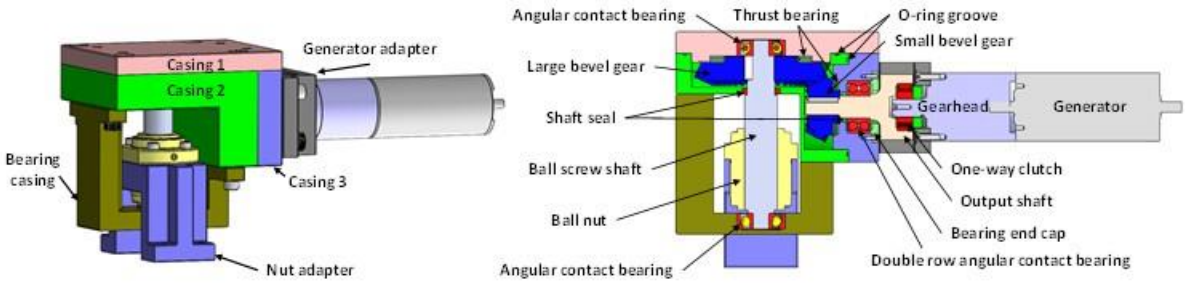

Figure 4-2. Detailed design of the energy harvesting module in the proposed smart tie

4.2.2 Working principle

Figure 3 illustrates the working principle of the energy harvesting module in the proposed smart tie. The solid line represents the motion transmission when the tie housing moves downwards and the one-way clutch engages with the gearhead shaft, while the dashed line represents the motion transmission when the tie housing rebounds back. Specifically, when the railcar wheel approaches, the enclosed gearbox with the generator moves downwards together with the tie housing. This linear downward motion of casings can be translated into the rotation of the ball-screw shaft and the large bevel gear, and subsequently, the small bevel gear and the output shaft both rotate. The embedded one-way clutch can be engaged with the generator shaft, depending on the rotational speed of the output shaft and the gearhead shaft, and the generator is driven to rotate as well to generate electricity. When the railcar wheel leaves, the enclosed gearbox with the generator moves upwards together with the tie. This linear upward motion will drive the ball nut and then drive the ball-screw shaft and two bevel gears to rotate

in opposite direction. The embedded one-way clutch is then disengaged with the generator shaft, and the generator can continue to spin freely under its rotation inertia with electrical damping until become stationary.

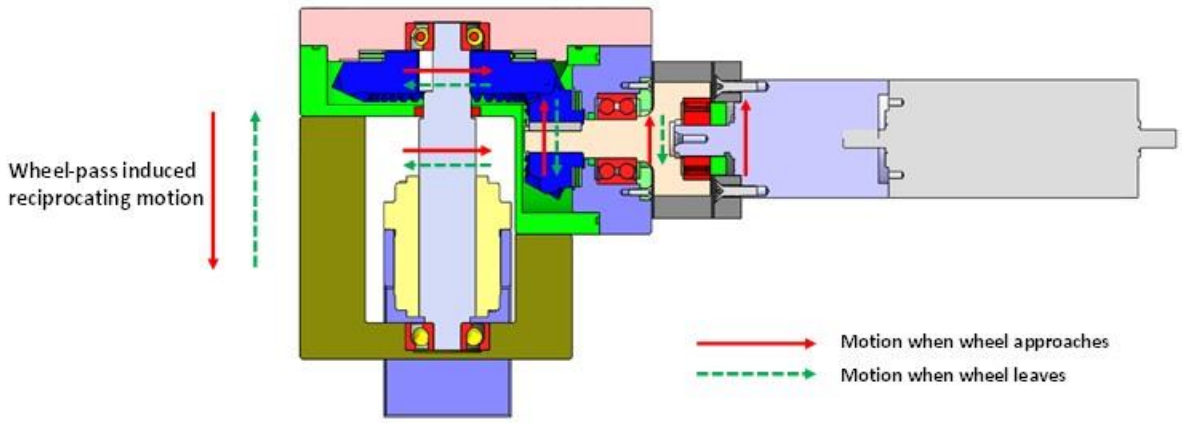

Figure 4-3. Wheel-pass induced reciprocating motion will drive the generator to spin using the proposed mechanism: the solid lines represent the motion transmission when the wheel approaches and the represent the motion transmission when the wheel leaves.

Previous energy harvesters [29, 61], that typically harvest energy from bidirectional track deflections, usually require relatively stiff springs to counteract the total force from the energy harvester during the track rebounds. The proposed design only harvests the kinetic energy of the tie when the wheels push it downwards, while the generator will be separated from the gearbox when the tie rebounds back. Therefore, there is no force transmitted back from the harvester during the disengagement period and the tie can rebound back quickly. The design resolves the preload and installation challenges [61] of bidirectional harvesting and increases the overall system reliability.

A scaled smart tie prototype for installing on a single-side track is fabricated, and the main parameters of this prototype are listed in Table 4-1.

Table 4-1. Parameters of the smart energy harvesting tie

Parameters	Value	Description
l	25 mm	Screw lead of ball-screw
J_m	0.264 kgcm^2	Generator inertia
J_{lg}	9.463 kgcm^2	Large gear inertia
J_{sg}	0.570 kgcm^2	Small gear inertia
J_{bs}	0.039 kgcm^2	Screw inertia
R_i	0.24 Ohm	Phase resistance of the generator
r_b	2	Bevel gear transmission ratio
r_g	19	Generator gearhead ratio
k_e	0.072 V/rads	Generator voltage constant
k_t	0.072 Nm/A	Generator torque constant
L	0.424 mH	Generator phase to phase inductance
$Stroke$	25.4 mm	Stroke

4.3 Modeling and Simulation

4.3.1 Modeling of the energy harvesting module

A three-phase AC motor is used as a generator in the proposed smart tie. Wye-shape external resistive loads are connected to the generator and the circuit model has been discussed in [29, 61] and shown in Figure 4. V_1, V_2, and V_3 are the induced voltages of the generator in each phase, respectively; and i_1, i_2, i_3 are induced current of the generator in each phase, respectively. L, which is relatively small, is the inductance per phase. R_i and R_e are internal and external resistive loads, respectively. From [61], the resistive torque T_{ge} induced by the electrical damping the AC generator is

$$T_{ge} = \frac{3k_t k_e}{2(R_i + R_e)}\omega_{ge} \tag{4.1}$$

where k_t and k_e are the speed and torque constants, and ω_{ge} is the angular velocity of the generator input shaft.
The induced voltages in each phase of the AC generator could be expressed as

$$\begin{cases} V_1 = k_e\omega_{ge}\sin(\omega_e t) \\ V_2 = k_e\omega_{ge}\sin\left(\omega_e t - \frac{2}{3}\pi\right) \\ V_3 = k_e\omega_{ge}\sin\left(\omega_e t + \frac{2}{3}\pi\right) \end{cases} \tag{4.2}$$

where ω_e is the angular frequency of the induced voltage of the generator, which will be ω_{ge} multiplied by the total number of generator pole pairs.

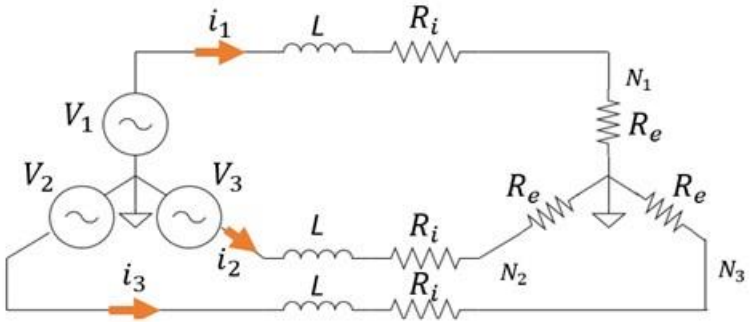

Figure 4-4. Model of a Wye-shape three-phase generator with Wye-shape external resistive loads [10].

Figure 4-5 shows the dynamic model of the energy harvesting module in the proposed smart tie. The overall operation of the energy harvesting module can be divided into two cases: engagement case and disengagement case. Assume the vertical tie displacement is x, and its corresponding velocity is $\dot{x}$. ω_{ge}, ω_{sb} are the rotational speed of the generator and small bevel gear. As shown in Table 4-1, l is the ball-screw lead, r_g is the gear ratio of the gearbox, and r_b is the gear ratio of the enclosed gearbox.

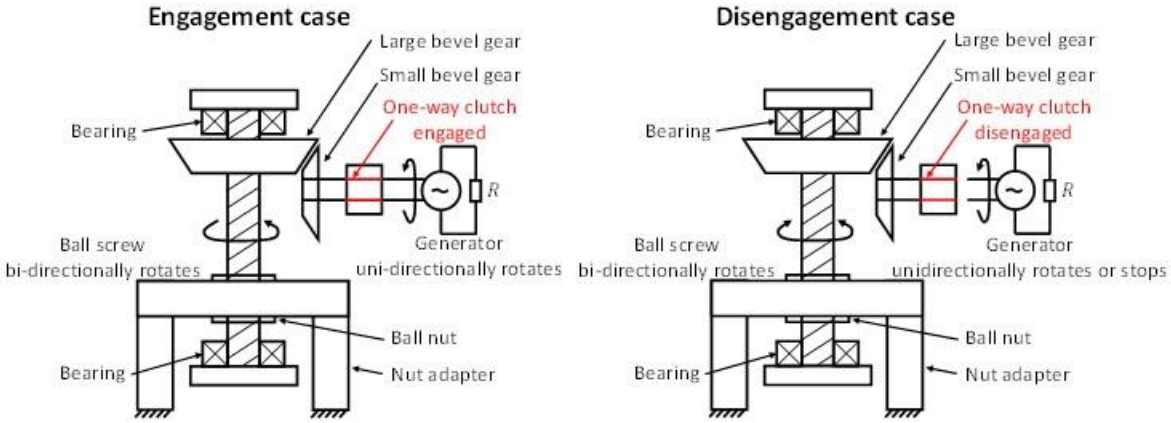

Figure 4-5. Dynamic model of the energy harvesting model: left side is the engagement case and the right side is the disengagement case.

When the tie moves downwards, $\dot{x} < 0$ and the system can be:

- In engagement, if $\omega_{ge} = r_g \omega_{sb} = \frac{2\pi r_b r_g}{l} \dot{x}$
- In disengagement, if $|\omega_{ge}| > r_g |\omega_{sb}| = \left| \frac{2\pi r_b r_g}{l} \dot{x} \right|$

More specifically, when the tie moves downward, the ball-screw shaft spins clockwise (from the bottom view) and drives the large bevel gear, small bevel gear, and output shaft successively. If the rotation speed of the generator gearhead equals that of the output shaft, the one-way clutch inner ring engages with the outer ring through a series of sprags in between, so that there is a torque transmission from the small bevel gear to the generator gearhead. In this case, by calculating the overall electrical resistance from the generator and using the energy method [61], we can get the expression for the equivalent electrical damping coefficient and equivalent mass of the system, written as below

$$c_e = \frac{6\pi^2 {r_b}^2 {r_g}^2 k_t k_e}{l^2(R_i + R_e)} \tag{4.3}$$

$$m_e \approx \frac{4\pi^2}{l^2} {r_b}^2 {r_g}^2 J_{ge} \tag{4.4}$$

The corresponding total force and output phase voltage during the engagement can be expressed as

$$F_{engage}^{down} = m_e\ddot{x} + c_e\dot{x} = \frac{4\pi^2}{l^2} {r_b}^2 {r_g}^2 J_{ge}\ddot{x} + \frac{6\pi^2 {r_b}^2 {r_g}^2 k_t k_e}{l^2(R_i + R_e)}\dot{x} \tag{4.5}$$

$$V_{k_{engage}}^{down} = 2\pi k_e r_b r_g sin\left(\int_0^t \omega_e dt + \frac{2k}{3}\pi\right)\frac{\dot{x}}{l} \tag{4.6}$$

If the rotation speed of the generator gearhead is larger than that of the output shaft, the inner ring of the clutch separates from the outer ring, so there is no motion transmission from the small bevel gear to the generator gearhead, as shown in Figure 5 (b). Then, the generator will freely spin with the electrical damping coming from the generator until stop.

The corresponding total force and output phase voltage during the disengagement can be expressed as

$$F_{disengage}^{down} = 0 \tag{4.7}$$

$$V_{k\_disengage}^{down} = e^{-\frac{c_e}{m_e}(t-t_0)}\dot{\theta_{s0}} \sin\left(\int_0^t \omega_e dt + \frac{k}{3}\pi\right) \tag{4.8}$$

where t_0 and $\dot{\theta}_{s0}$ are the time and angular velocity when disengagement occurs
When the tie moves upwards, $\dot{x} > 0$ and the system is always in disengagement mode. The expression of the force and the output phase voltage when the tie moves up can be written as follows

$$F^{up} = 0 \tag{4.9}$$

$$V_k^{up} = e^{-\frac{c_e}{m_e}(t-t_0)}\dot{\theta_{s0}} \sin\left(\int_0^t \omega_e dt + \frac{2k}{3}\pi\right) \tag{4.10}$$

4.3.2 Numerical simulations

Dynamic simulations have been conducted for the energy harvester module based on the developed model, considering engagement and disengagement, to better understand the system and predict the energy harvesting performance. Simulation results have been discussed in this section and presented in the following section together with the test results.

Figure 4-6 shows the simulated force and phase voltage with the input of 2 Hz, 3 mm harmonic excitation with different resistive loads. Results with 20-Ohm resistive loads are shown in Figure 4-6 (a), indicating that engagement happens only when the tie displacement moves downwards, while the generator can continue rotating after the engagement ends when the tie moves downward and when the tie moves upward, if the electrical damping is small. Figure 4-6 (b) demonstrates the simulated force and phase voltage with 2-Ohm resistive load. It shows that with the smaller resistive load (larger electrical damping from the generator), the disengagement period will be reduced, and the generator only rotates when the tie moves down. When the tie moves up, the system will always be in the disengagement period and the generator stays stationary.

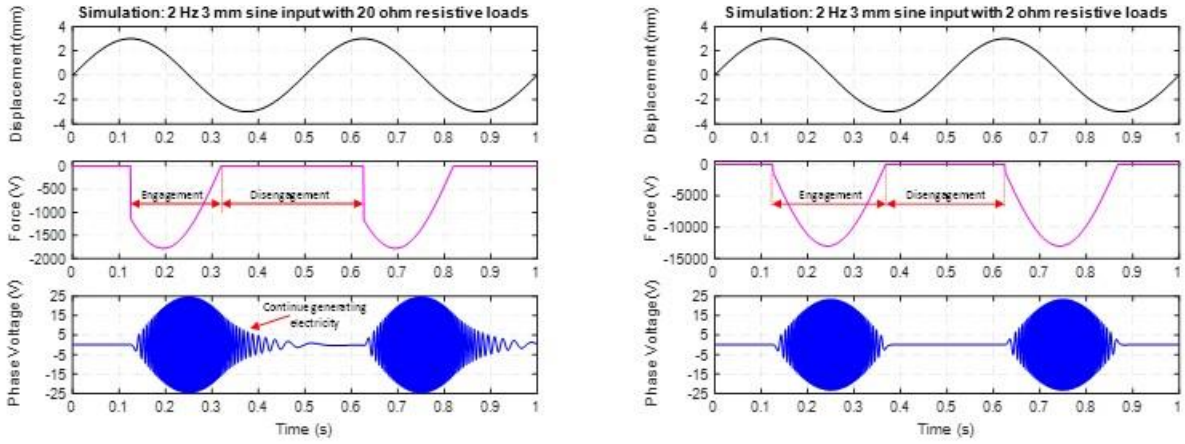

(a) (b)

Figure 4-6. Simulated force and phase voltage with the input of 2 Hz, 3 mm harmonic excitation with different resistive loads. (a) 20 Ohms, (b) 2 Ohms.

4.4 Bench Test and Analysis

4.4.1 Experimental setup

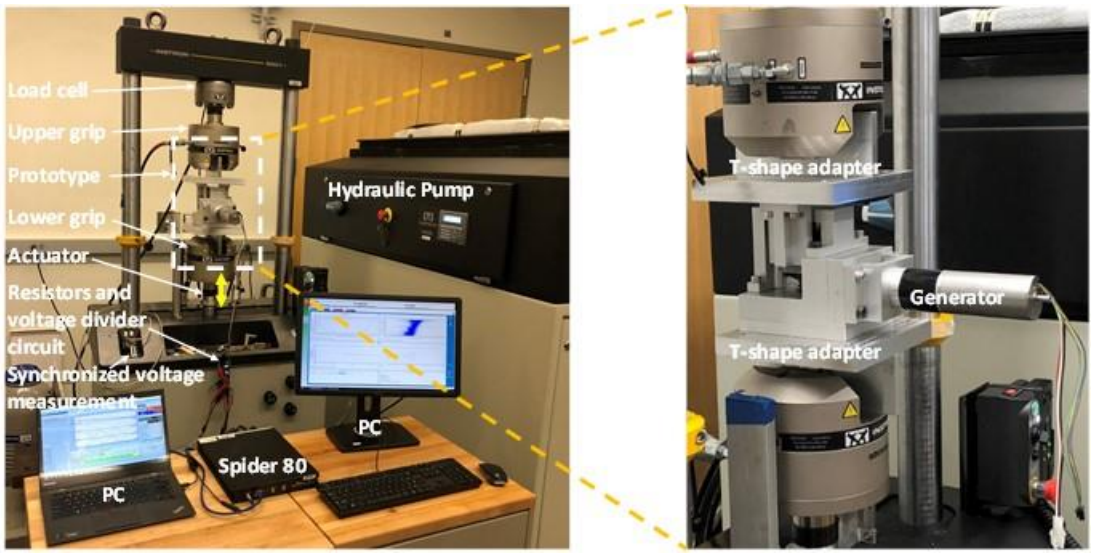

Figure 4-7. Bench test setup

Figure 4-7 shows the experimental setup for the energy harvesting module of the proposed smart tie. The nut adapter and the casing 1 of the energy harvester were connected to two T-shape adapters which are clamped by the upper and lower grips of the Instron machine, respectively. The hydraulic actuator with an LVDT displacement sensor, locating under the lower grip, can be controlled by the built-in software, and the 100 kN load cell, locating above the upper grip, can measure the dynamic force applied on the nut adapter. The external resistive load was connected to the generator in "wye" configuration, together with a 19:1 voltage divider. The energy harvesting module of the proposed smart tie was tested with both harmonic excitation and recorded tie displacement during the experiment and the results will be analyzed in the following subsection.

4.4.2 Results with harmonic excitation

A series of harmonic excitation tests with different input frequencies, amplitudes and external resistive loads were conducted. During the experiment, the generator was observed to rotate and generate electricity at 0.1 mm vibration amplitude input, indicating that the smart tie that we proposed has a relatively small backlash and can sense and harvest energy from minor vibrations. The calculated average power and the measured peak force under the 1 Hz frequency with amplitudes varying from 1-5 mm and different resistive loads were shown in Figure 4-8. As we can see, with the increasing of the input vibration amplitude, both the average power and peak force increase due to a higher rotational speed. Meanwhile, with the same amplitude, both the average power and peak force increase when the external resistive load decrease. This is because the electrical damping increases, which means more mechanical energy could be converted into electrical energy when the loads are reduced. Figure 4-9 shows the measured and simulated force, phase voltage and phase power of the energy harvesting module under the harmonic excitation with 2 Hz frequency and 3 mm amplitude. The solid lines represent the measured or calculated data while the dash lines represent the simulated

ones. An average power of 88W was achieved with 2-Ohm resistive load and from plot, we can see that the experiment results match well with the simulation result.

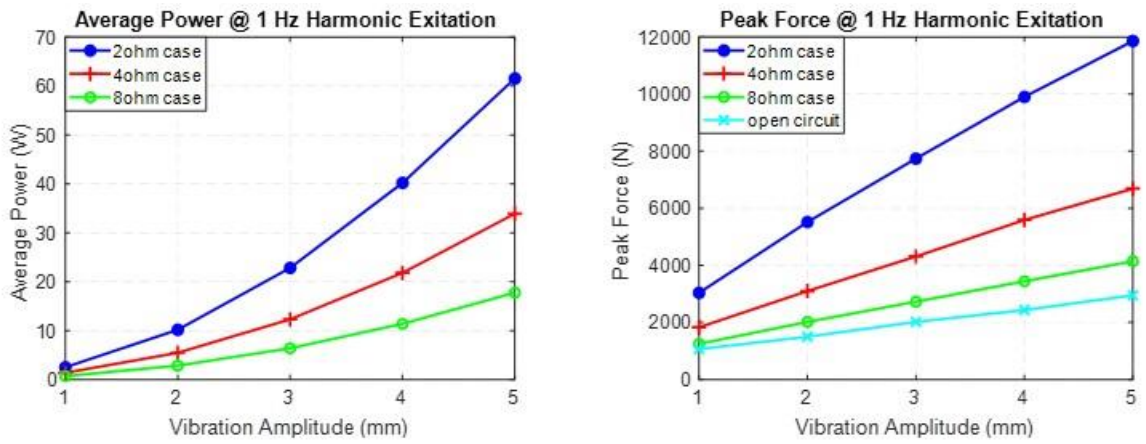

(a) (b)

Figure 4-8. Bench test results under 1 Hz frequency harmonic excitation with different amplitudes and resistive loads: (a) average power; (b) peak force.

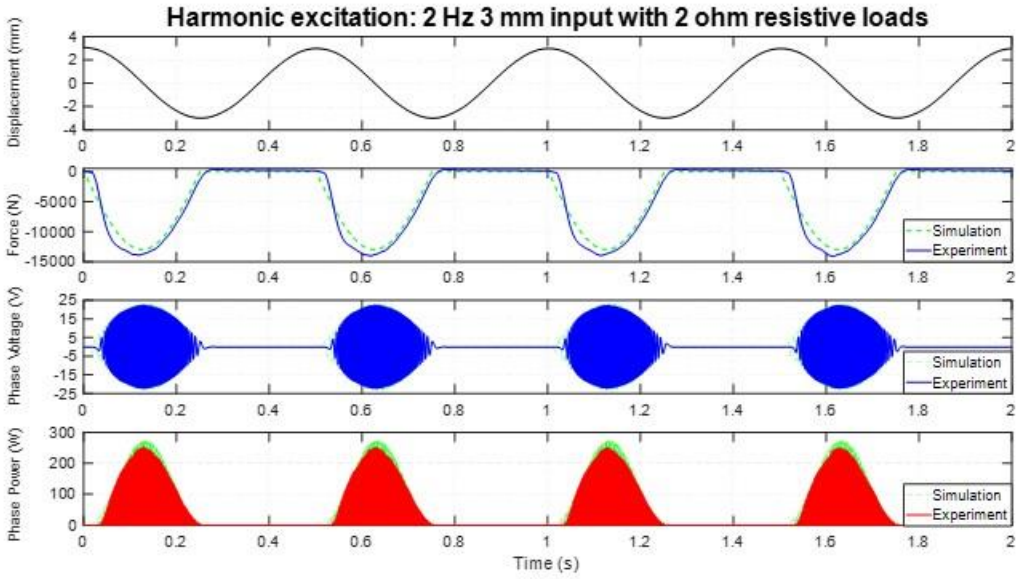

Figure 4-9. Measured and simulated force, phase voltage and phase power of the energy harvesting module under the harmonic excitation 2 Hz of frequency and 3 mm of amplitude. The external resistive loads are 2 Ohms, and the average power is 88 W.

4.4.3 Results with recorded railroad tie vibration

In order to further evaluate the energy harvesting performance of the proposed smart tie, a railroad tie movement recorded in *Transportation Technology Center, Inc.* (TTCI) when the freight railcars passed by at around 64 km/hr (40 mph) [28] was used as an excitation input for

in-lab bench testing. Figure 4-10 illustrates the measured and simulated force, phase voltage and phase power of the energy harvesting module under the recorded railroad tie movement when several consecutive railcars traveling at 64 km/hr (40 mph). The external resistive loads were 2 Ohms and the average power of 42.2W was obtained during the experiment. Experimental results match well with the simulated ones, which validates the accuracy and effectiveness of the energy harvester model. As indicated in Figure 4-10, the energy harvesting module only generates electricity when the tie moves downward, while when the tie moves upward, output power is zero and the force is positive but with a relatively small amplitude. Therefore, different from the need of strong reset springs for previous railroad bi-directional energy harvesters [29, 61], the proposed smart energy harvesting tie doesn't require a large spring resilience force for keeping the tie box being stationary, resolving the preload and installation challenges of bidirectional harvesting and increasing the overall system reliability.

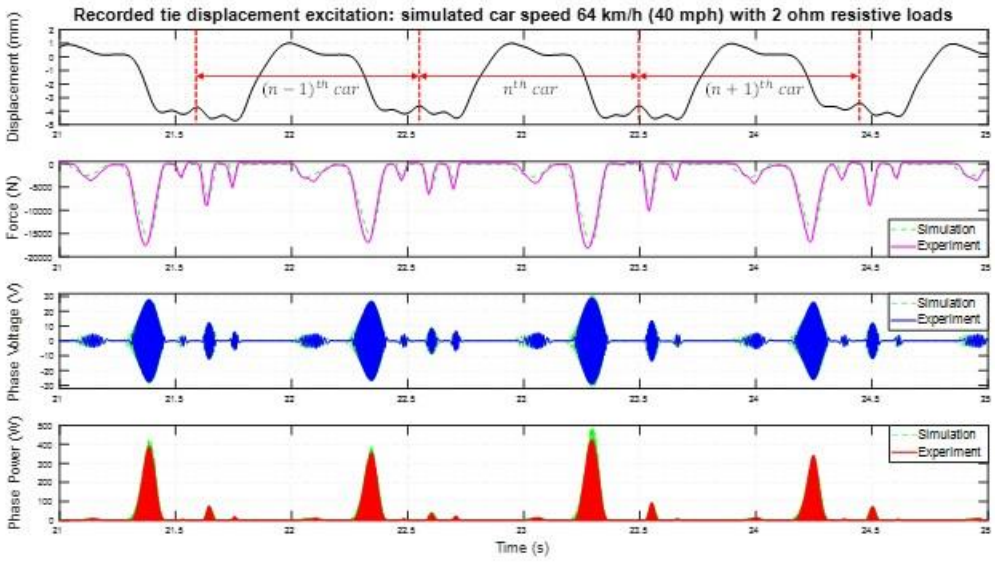

Figure 4-10. Measured and simulated force, phase voltage and phase power of the energy harvesting module under the recorded railroad tie movement when railcars traveling at 64 km/hr (40 mph). The external resistive loads are 2 Ohms and the average power of 42.2W was obtained.

Table 4-2 summarizes the test results about the peak force and average power obtained during this recorded tie displacement input test. As expected, the peak force and average power increase when the external resistive load gets reduced.

Table 4-2. Bench test results under recorded tie movement with various resistive loads

Resistive load	Peak force	Average Power
2 ohm	19535 N	**42.2 W**
4 ohm	12129 N	26.1 W
8 ohm	9759 N	15.3 W

open circuit	8012 N	NA

4.5 Chapter Summary

In this chapter, a smart energy harvesting railroad tie to power the trackside electrical device has been proposed, designed, modeled and tested for potentially improving the train operational efficiency and safety. The smart tie, which is designed to have similar dimensions to a conventional railroad tie, can be installed in the same manner as a standard tie on the track. Through a ball-screw, a pair of bevel gear and an output shaft with a single one-way clutch, the generator can be driven to generate electricity. Different from bidirectional energy harvesters, the proposed smart tie only harvests the kinetic energy of the railroad tie when the tie moves downwards due to the approaching wheel, which resolves the preload and installation challenges and increases the overall system reliability. An analytical model is developed, and the dynamic simulation is conducted to better understand the system nonlinearity and predict the performance. During the bench tests, the smart tie demonstrates great sensitivity to the environment vibration due to its small backlash (less than 0.1 mm). In-lab test results show that an average power of 26.1 and 42.2W on 4 Ohms and 2 Ohms external loads are obtained under simulated tie movement, indicating that the proposed smart tie is capable to power most wayside electrical devices, which has a great potential to improve the train operational safety.

Chapter 5 Design, Modeling and Onboard Test of an Electromagnetic Energy Harvester for Railway Cars

To enable the smart technologies on the freight railcars, such as the global positioning system (GPS), real-time train condition monitoring and positive train control, a cost-effective power source is required. This paper presents the design, modeling, in-lab and onboard field-tests of an electromagnetic energy harvester for freight railcars. The proposed harvester with a mechanical motion rectification (MMR) mechanism can scavenge the vibration energy that is usually dissipated or wasted. An analytical model considering the train-harvester interaction is established to analyze the dynamic characteristic and predict the performance of the harvesters on different tracks at various train speeds. An in-lab bench test is carried out to experimentally validate the harvester model and evaluate the characteristics of the proposed energy harvester. The experimental results show that an average power of 14.5 and 9.2W are achieved respectively for the harvester using 66:1 and 43:1 gearheads under typical suspension vibrations recorded on an operational railcar at 90 km/hr. An onboard field test is also performed using the harvester with 43:1 gearhead on a test track, which yields a peak phase power of 73.2W and an average power of 1.3W at 30 km/hr. Both the in-lab and onboard test results indicate that the proposed energy harvester could continuously generate an amount of power useful for the implementation of smart technologies to improve the operational safety on the freight cars.

5.1 Chapter Introduction

As discussed in Chapter 2.2, compared with other technologies (solar, axle generator, and thermoelectric), vibrational energy harvesters, especially the mechanical-based electromagnetic ones, have a great potential to scavenge the dissipated energy from the railcar vibrations without adding energy loss to the train operation. However, three main challenges remain in the existing onboard energy harvesting technologies for freight cars: (i) increasing the power output of the harvesters under realistic train vibrations since many onboard applications of electrical devices require more power (watts to tens of watts level); (ii) improving the conversion efficiency through simple and reliable designs; and (iii) developing a train-harvester coupled model to predict the energy harvesting performance at different train speeds and on different tracks.

In this chapter, a rack-pinion based suspension energy harvester with a simplified structure is designed, modeled, and tested both in lab and onboard, for smart freight railcars. Facing the severe vibration and huge load conditions during the operation of the freight cars, an enclosed lubricated gearbox and a unique two guide-rail mechanism are specifically designed for the harvester to reduce the friction loss and increase transmission reliability and durability. A nonlinear systematic model considering the train-harvester interaction is developed to predict the energy harvesting performance at different train speeds and on different tracks. In-lab tests are then carried out at various conditions to experimentally characterize the proposed energy harvester. An average power of 14.5 and 9.2W are achieved respectively for the harvester with the 66:1 and 43:1 gearhead under typical suspension vibrations recorded at 90 km/hr on an operational track. On-board tests are also conducted on a low-speed freight car on a test track

in CRRC Yangtze Co., Ltd. An average power of 1.3W was obtained when the train traveled at around 30 km/hr, which is close to the model prediction. The paper shows that the proposed harvester could generate a useable amount of power for certain on-board auxiliary electronic devices, which has the potential to improve the operational safety of the freight railcars.

This chapter is organized as follows. Chapter 5.2 introduces the detailed design and working principle of proposed rack-pinion based train suspension energy harvester. Chapter 5.3 introduces the systematic modeling for the proposed suspension energy harvester. Chapter 5.4 summarizes the in-lab testing of the proposed energy harvesters and Chapter 5.5 introduces the harvester onboard testing. Chapter 5.6 provides the concluding remarks.

5.2 Design and Working Principle

5.2.1 Design and installation of the freight railcar suspension energy harvester

Figure 5-1(a) shows the detailed design of the proposed rack-pinion based train suspension energy harvester. The harvester consists of a rack, a pinion gear integrated with a shaft, an enclosed gearbox with lubricant inside, and an electromagnetic generator with a planetary gearhead. One guide rail is mounted on the back of the rack and the rack is connected to the upper square case, while the corresponding carriage is installed in the lower square case. Another pair of guide rail and carriage are connected to the upper square case and lower square case, respectively. By using these two face-to-face pairs of guide rail and carriage, the upper and lower case could slide smoothly vertically. The pinion gear shaft is driven by the rack to rotate bi-directionally. Lubricant grease is placed in the chamber between the rack teeth and pinion teeth to increase the transmission durability. The enclosed gearbox is composed of two large bevel gears, one small bevel gear, two one-way sprag clutches, bearings, O-rings and shaft seals. The two one-way clutches are positioned between the large bevel gears and the pinion gear shaft. A small bevel gear is connected to the shaft of the geared generator. The shaft seals and O-ring enclose the gearbox so that lubricant could be sealed inside. A flywheel could be added at the end of the generator shaft at the bottom side to adjust the total inertia property of the suspension energy harvester.

Figure 5-1(b) illustrates the installation of the energy harvester on a freight K5 bogie (an improved version of the traditional three-piece bogie). The overall dimensions of the energy harvester are chosen so that they can be retrofitted into the majority of the commercial freight railcars, such as those by CRRC Yangtze Co. LTD. The harvester dimensions are 283 mm (fully compressed) and 378 mm (fully extended), for an overall stroke of 95 mm. The K5 bogie is mainly comprised of two wheelsets, side frames, bolster, spring plank, center plate, roller bearing adapters, and coil springs. The primary stiffness comes from the roller bearing adapters, which is very stiff. The secondary suspension consists of coil springs and wedge friction dampers between the bogie and car body. The harvester is designed to be installed at the secondary suspension (between the spring plank and the bolster) in parallel with the coil springs.

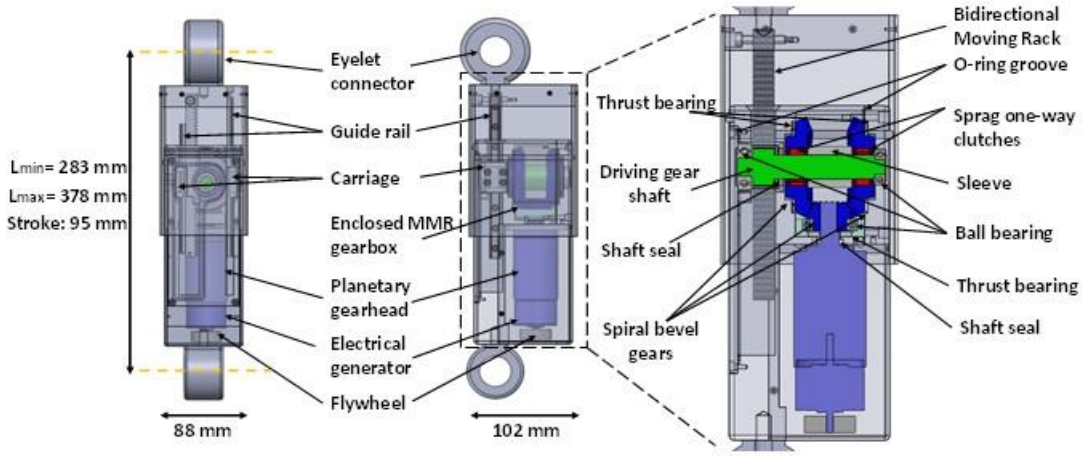

(a)

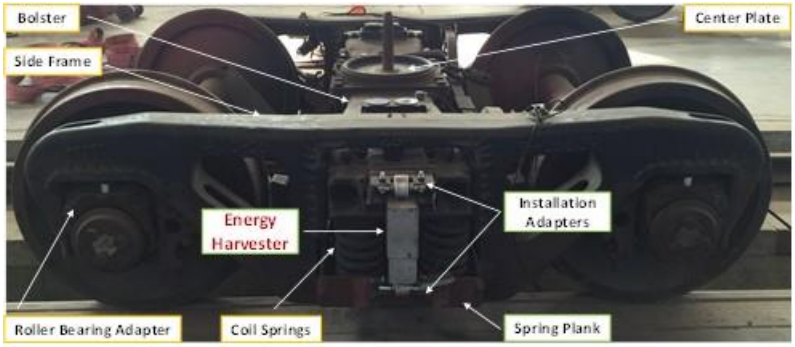

(b)

Figure 5-1. Design and installation of a rack-pinion based train suspension energy harvester: (a) design details (b) installation of the prototype.

5.2.2 Working principle

A special mechanism, named mechanical motion rectification (MMR) [23], which could convert the bidirectional linear motion of the rack into the unidirectional rotation of the generator, is adopted in the design. Figure 5-2 illustrates the working principle of the harvester. In Case 1, when the rack moves downward, it drives the pinion gear shaft to rotate counterclockwise (from the left side view). At this moment, the left one-way clutch between the pinion shaft and the left large bevel gear is engaged, while the right clutch between the pinion shaft and the right large bevel gear is disengaged. The left bevel gear becomes the driving gear, and the right large bevel gear becomes an idler. Therefore, the small bevel gear and the electromagnetic generator will be driven to rotate clockwise (from the bottom side). If the rack moves upward, as shown in Case 2 of Figure 5-2, it drives the pinion gear shaft to rotate clockwise (from the left side view). Currently, the right one-way clutch is engaged while the left clutch is disengaged. The right bevel gear behaves as the driving gear and drives the small bevel gear and electromagnetic generator to rotate clockwise (from the bottom side), while the left large bevel gear becomes an idler. With this unique MMR mechanism, no matter

the rack moves upward or downward, the generator will always rotate in one direction, resulting in a high energy harvesting performance and low impact force during transmission [24]. The main parameters of the proposed suspension energy harvester are listed in Table 5-1.

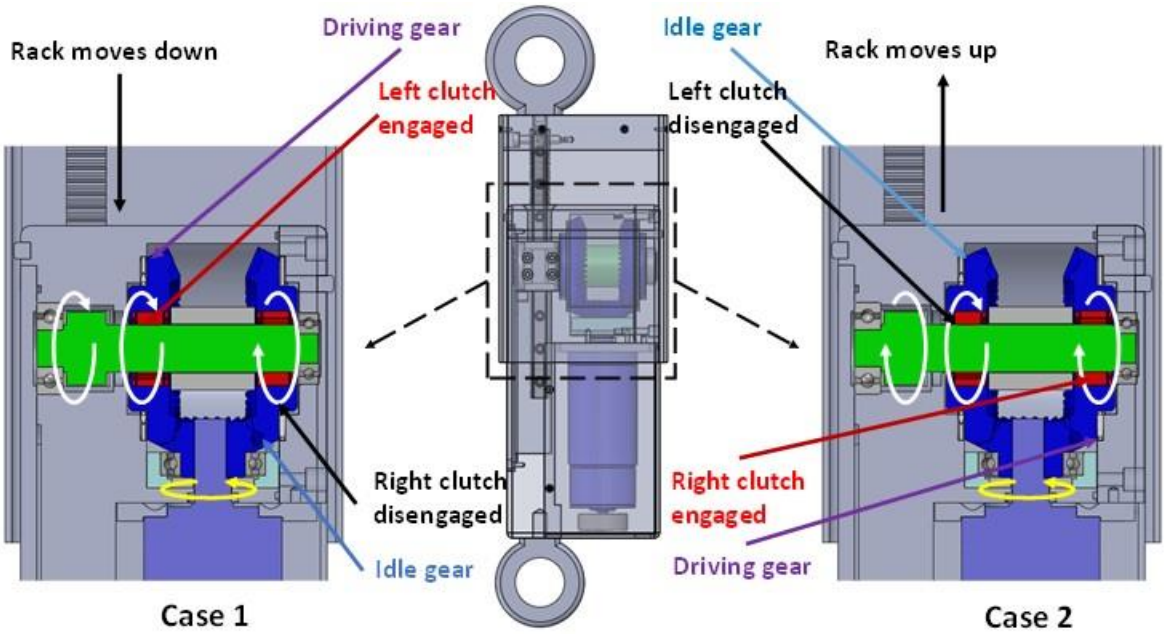

Figure 5-2. Irregular reciprocating suspension vibration will drive the generator to rotate in one direction using the MMR mechanism: Case 1 represents rack moving downward and Case 2 represents the rack moving upward

Table 5-1. Parameters of the proposed suspension energy harvester

Parameters	Value	Description	Parameters	Value	Description
m	1.25	Pinion gear/rack modulus	l_{min}	283 mm	Harvester compression length
α	20°	Pinion gear/rack pressure angle	$Stroke$	95 mm	Harvester stroke
n_L	40	Large bevel gear teeth number	$Weight$	5.5 kg	Harvester weight
n_S	20	Small bevel gear teeth number	$Backlash$	0.5 mm	Rack and pinion gear backlash
n_P	16	Pinion gear teeth number	$Compliance$	0-1 mm	Mechanical compliance
r_p	10 mm	Pinion gear pitch radius	R_i	1.44 Ω	Terminal resistance phase to phase
J_{lg}	2.16 kgcm^2	Large bevel gear inertia	L	1.15 mH	Terminal inductance phase to phase
J_{sg}	0.13 kgcm^2	Small bevel gear inertia	I_n	1.61 A	Norminal (max. continuous) current
J_m	0.0128 kgcm^2	Generator inertia	I_{max}	25 A	Maximum peak current
n_b	2	Bevel gear transmission ratio	V_{nv}	36 V	Nominal voltage
n_{g1}	4.3	Gearhead 1 transmission ratio	V_{ns}	6080 rpm	Nominal speed
n_{g2}	12	Gearhead 2 transmission ratio	k_e	0.0461 V/rad	Generator voltage constant

l_{max}	378 mm	Harvester extension length	k_t	0.0461 Nm/A	Generator torque constant

5.3 Modeling and Dynamics

5.3.1 Dynamics of the three-phase AC generator and energy harvesting circuit

In the proposed train suspension energy harvester, a three-phase AC electromagnetic generator is adopted. Figure 3 shows the dynamic model of the three-phase AC generator with Wye shape resistive loads. V_1, V_2, V_3 are the back electromotive forces (EMF) or induced voltages of the generator, and i_1, i_2, i_3 are induced current per phase, respectively. L is the inductance of coils per phase, which has a very small value and could be ignored. R_i and R_e represent the internal phase resistance and the external electrical load of the generator, respectively.

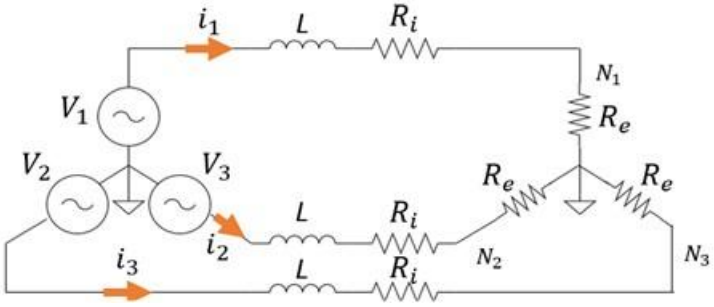

Figure 5-3. Modeling of Wye shape three-phase generator with Wye shape resistive loads [25].

The dynamics of the generator and its damping characteristics have been studied in [29, 51]. Since the inductance of the coils is ignorable, the resistive torque T_{ge} induced by the electrical currents of the three-phase electromagnetic generator could be obtained as $T_{ge} = C_{ge}\omega_{ge}$, where $C_{ge} = \frac{3k_t k_e}{2(R_i+R_e)}$ is the rotary damping coefficient of the generator with shunt resistance. The k_t and k_e are the speed and torque constants of the AC generator, respectively, and ω_{ge} is the angular velocity of the generator.

From Newton's second law, the equation of motion for the generator could be written as

$$T_m - T_{ge} = J_{ge}\dot{\omega}_{ge} \tag{5.1}$$

where T_m and J_{ge} are the external driving torque and rotary inertia of the generator, respectively. Therefore, the driving torque T_m can be expressed as

$$T_m = J_{ge}\dot{\omega}_{ge} + \frac{3k_t k_e}{2(R_i + R_e)}\omega_{ge} \tag{5.2}$$

5.3.2 Dynamic model of the suspension energy harvester

The simplified model of the energy harvester is illustrated in Figure 5-4. Different from the linear and rotary harvesters, MMR energy harvester can convert the bi-directional vibration into unidirectional rotation of the generator by utilizing the one-way clutches embedded inside the large bevel gears. Specifically, the one-way clutch embedded in that bevel gear is engaged

to the shaft when the pinion gear shaft angular velocity ω_{gs} equals that of the large bevel gears ω_{lb}, enabling the torque to be transmitted from the pinion gear shaft to the generator. Conversely, when the instant angular velocity ω_{gs} of pinion gear shaft is smaller than that of the large bevel gears ω_{lb}, both one-way clutches are disengaged from the shaft, resulting in no motion transmission from the pinion shaft to the bevel gears, so that the generator will rotate freely due to the inertia.

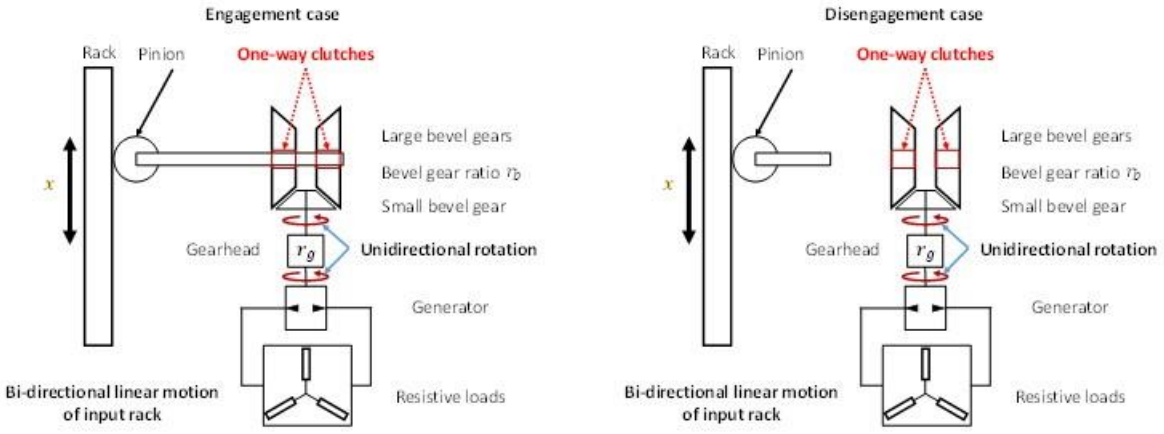

(a) (b)

Figure 5-4. Dynamic model of the proposed train suspension energy harvester: (a) engagement case; (b) disengagement case

Let x, $\dot{x}$ and $\ddot{x}$ be the suspension vibration displacement, velocity, and acceleration, respectively. The pinion gear radius is r_p, the transmission ratio from large bevel gears to the small bevel gear is n_b, and the planetary gearhead transmission ratio is n_g. Therefore, at the engagement period, the rotational speed of the generator is $\omega_{ge} = n_b n_g \frac{\dot{x}}{r_p}$.

Therefore, the motion for the small bevel gear, larger bevel gear, and pinion gear shaft could be obtained. Let J_{sb}, J_{lb} and J_{gs} represent the rotational inertia of the small bevel gear, large bevel gear and gear shaft, respectively, and m_r represents the mass of the rack and the upper casing. The driving force F_{engage} on the rack (the harvester) during the engagement could be derived as

$$F_{engage} = \left(\frac{{n_b}^2 {n_g}^2}{{r_p}^2} J_m + \frac{{n_b}^2 J_{sb} + 2J_{lb} + J_{gs}}{{r_p}^2} + m_r \right) \ddot{x} + \frac{{n_b}^2 {n_g}^2 k_t k_e}{{r_p}^2 (R_i + R_e)} \dot{x} \qquad (5.3)$$

From Equation (3), the suspension energy harvester during engagement could be considered as a linear inertia mass in parallel with a viscous damper. The damping coefficient of such a damper could be tuned by adjusting the external resistive loads. The equivalent linear inertia mass and equivalent linear viscous damping could be expressed as

$$\begin{cases} m_e = \dfrac{{n_b}^2 {n_g}^2}{{r_p}^2} J_m + \dfrac{{n_b}^2 J_{sb} + 2J_{lb} + J_{gs}}{{r_p}^2} + m_r \approx \dfrac{{n_b}^2 {n_g}^2}{{r_p}^2} J_m \\ C_e = \dfrac{{n_b}^2 {n_g}^2 k_t k_e}{{r_p}^2 (R_i + R_e)} \end{cases} \tag{5.4}$$

In Equation (4), when the transmission gear ratio n_g of the planetary gearhead is large (the ratios are 43 and 66 for the two prototyped harvesters), the total equivalent linear mass of the bevel gears, gear shaft and rack $\frac{{n_b}^2 J_{sb} + 2J_{lb} + J_{gs}}{{r_p}^2} + m_r$ is much smaller than that of the electromagnetic generator $\frac{{n_b}^2 {n_g}^2}{{r_p}^2} J_m$. Therefore, the dominant contribution of the inertance of the suspension energy harvester comes from the electromagnetic generator (and the flywheel on the generator shaft). Therefore, the driving force at the end of the rack (the harvester) during the engagement could be approximated as $F_{engage} = \frac{{n_b}^2 {n_g}^2}{{r_p}^2} J_m \ddot{x} + \frac{{n_b}^2 {n_g}^2 k_t k_e}{{r_p}^2 (R_i + R_e)} \dot{x}$, and the induced phase voltages can be expressed as

$$V_{ge} = k_e n_b n_g \frac{\dot{x}}{r_p} \sin\left(\int_0^t \omega_e dt + \frac{2k}{3}\pi \right) \tag{5.5}$$

where $k = 0, 1, 2$, represent the 1st, 2nd and 3rd phase of the generator. ω_e is the angular frequency of the induced voltage of the generator, which will be ω_{ge} multiplied by the total number of generator pole pairs.

When both one-way clutches are disengaged, as shown in Fig. 4(b), the generator separates with the gearbox and there is no torque transmission from the pinion shaft to the bevel gears. The generator rotates freely due to the inertia and damping, which means that the rotor continues to spin with the stored momentum and exponentially decelerates due to its damping. Therefore, the driving force at the end of the rack (the harvester) will be $F_{disengage} = \left(m_r + \frac{J_{gs}}{r_p^2} \right) \ddot{x} \approx 0$, and the single-phase voltage during the disengagement could be expressed as

$$V_{ge} = \dot{\theta}_s(t) = e^{-\frac{c_e}{m_e}(t - t_0)} \dot{\theta_{s0}} \sin\left(\int_0^t \omega_e dt + \frac{2k}{3}\pi \right) \tag{5.6}$$

where t_0 and $\dot{\theta}_{s0}$ are the instant time and angular velocity when disengagement occurs.

In summary, the dynamics driving force equation, and the induced single-phase voltage of the proposed train suspension energy harvester could be obtained and derived as

$$\begin{cases} F_{engage} \approx \dfrac{{n_b}^2{n_g}^2}{{r_p}^2} J_m \ddot{x} + \dfrac{{n_b}^2{n_g}^2 k_t k_e}{{r_p}^2 (R_i + R_e)} \dot{x} & Engagement: \left|\omega_{gs}\right| = \left|\omega_{lb}\right| \\ F_{disengage} \approx 0 & Disengagement: \left|\omega_{gs}\right| < \left|\omega_{lb}\right| \end{cases} \tag{5.7}$$

$$\begin{cases} V_{ge} = k_e n_b n_g \dfrac{\dot{x}}{r_p} \sin\left(\displaystyle\int_0^t \omega_e dt + \frac{2k}{3}\pi\right) & Engagement: \left|\omega_{gs}\right| = \left|\omega_{lb}\right| \\ V_{ge} = \dot{\theta}_s(t) = e^{-\frac{c_e}{m_e}(t-t_0)} \dot{\theta_{s0}} \sin\left(\displaystyle\int_0^t \omega_e dt + \frac{2k}{3}\pi\right) & Disengagement: \left|\omega_{gs}\right| < \left|\omega_{lb}\right| \end{cases} \tag{5.8}$$

5.3.3 System dynamics

To investigate the power output of the harvester at different train speeds and on different tracks, a systematic vertical model of the freight railcar coupled with suspension harvesters at the secondary suspension is developed in the following. In this coupled railcar-harvester model, the suspension harvester can be modeled as a tunable damper in parallel with an inerter between the car body and each side frame, as discussed in Subsection 3.2. While for the freight railcar, the bounce motions of the car body, side frames, and wheelsets, as well as the pitch motions of the car body and side frames, are taken into consideration. The wheel-rail contact is a complex but very essential part for the train dynamics and has been continuously researched and studied in the past several decades [53, 65, 66]. For simplicity, the wheel-rail contact can be modelled as a stiff spring in parallel with damper between the track and every wheelset, as discussed in [67].

In this dynamic study, the simplified wheel-rail contact model is adopted, and the vertical vehicle-harvester coupled model is shown in Figure 5-5, which consists of 10 degrees of freedom: the bounce and pitch motions of the car body and both side frames, as well as the bounce motions of the four wheelsets. Being consistent with the K5 bogie where the suspension harvester is installed in the onboard experiment, the secondary suspension consists of coil springs with stiffness K_{sz} and friction boards and wedges (behaving as the friction damper) with damping coefficient C_f in the model. For the primary suspension, the roller bearing adapters provide stiffness K_{pz}, while there is no oil damper or friction damper. K_{wr} and C_{wr} are the wheel/rail contact stiffness and damping [67], respectively. The railcar is assumed to travel longitudinally on a tangent track with a constant speed V_0.

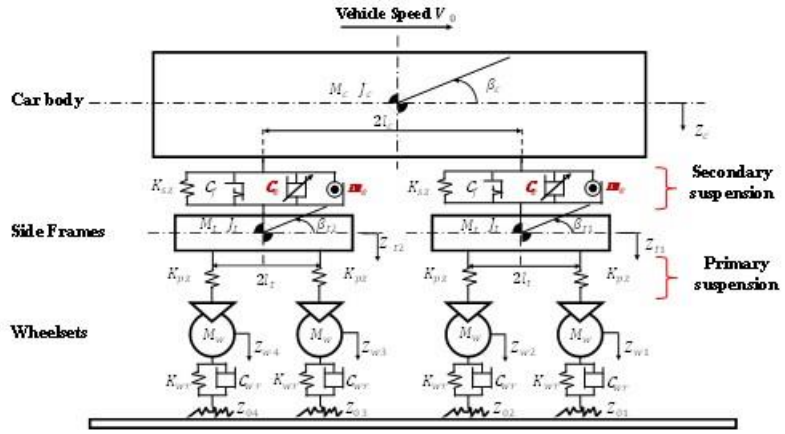

Figure 5-5. The dynamic model of a half freight car with energy harvesters installed at the secondary suspension

M_c, M_t and M_w are the mass of the car body, the side frame and the wheelset, respectively; J_c and J_t are moment inertia of the car body and side frames, respectively; Z_c, Z_{t1} and Z_{t2} are the vertical displacements, relative to the static balanced position, of the car body, front side frame and rear side frame, respectively; β_c, β_{t1} and β_{t2} are the pitch angle of the car body, front side frame and rear side frame, respectively. Z_{w1}, Z_{w2}, Z_{w3} and Z_{w4} are the vertical displacements of the four wheelsets, and Z_{01}, Z_{02}, Z_{03} and Z_{04} are the track irregularity at the wheel-rail contact point. l_c is the semi-longitudinal distance between bogies, and l_t is the semi-longitudinal distance between wheelsets in the bogie.

The friction forces mainly come from the relative motion between the wedges and friction boards on the side frames in the secondary suspension [68] and they could be simplified to be the total spring force in secondary suspension multiplied by a relative friction coefficient φ. The spring forces could be expressed as

$$\begin{cases} F_{s1} = K_{sz}(f_{st} + Z_c - l_c\beta_c - Z_{t1}) \\ F_{s2} = K_{sz}(f_{st} + Z_c + l_c\beta_c - Z_{t2}) \end{cases} \tag{5.9}$$

where F_{s1} represents the spring force between the front bogie and car body, and F_{s2} represents the spring force between the rear bogie and the car body. $(Z_c \mp l_c\beta_c - Z_{t1})$ represents the dynamic relative displacement between the front/rear bogie and car body. f_{st} is the static deflection of the springs at the secondary suspension.

Therefore, the friction forces could be expressed in the Coulomb friction model as

$$\begin{cases} F_{f1} = \alpha_1\varphi F_{s1} = sgn(\dot{Z}_c - l_c\dot{\beta}_c - \dot{Z}_{t1})\varphi K_{sz}(f_{st} + Z_c - l_c\beta_c - Z_{t1}) \\ F_{f2} = \alpha_2\varphi F_{s2} = sgn(\dot{Z}_c + l_c\dot{\beta}_c - \dot{Z}_{t2})\varphi K_{sz}(f_{st} + Z_c + l_c\beta_c - Z_{t2}) \end{cases} \tag{5.10}$$

where φ is the relative fiction coefficient, $\alpha_1 = sgn\left(\dot{Z}_c - l_c\dot{\beta}_c - \dot{Z}_{t1}\right) = \begin{cases} \dot{Z}_c - l_c\dot{\beta}_c - \dot{Z}_{t1} > 0 & 1 \\ \dot{Z}_c - l_c\dot{\beta}_c - \dot{Z}_{t1} = 0 & 0 \\ \dot{Z}_c - l_c\dot{\beta}_c - \dot{Z}_{t1} < 0 & -1 \end{cases}$ and $\alpha_2 = sgn\left(\dot{Z}_c + l_c\dot{\beta}_c - \dot{Z}_{t2}\right) = \begin{cases} \dot{Z}_c + l_c\dot{\beta}_c - \dot{Z}_{t2} > 0 & 1 \\ \dot{Z}_c + l_c\dot{\beta}_c - \dot{Z}_{t2} = 0 & 0 \\ \dot{Z}_c + l_c\dot{\beta}_c - \dot{Z}_{t2} < 0 & -1 \end{cases}$.

$\left(\dot{Z}_c - l_c\dot{\beta}_c - \dot{Z}_{t1}\right)$ and $\left(\dot{Z}_c + l_c\dot{\beta}_c - \dot{Z}_{t2}\right)$ represent the relative velocities in the secondary suspension for the front bogie and rear bogie, respectively.

The suspension harvester could be in the engaged mode or disengaged mode while the train is moving. When the rotational speed of the bevel gears inside the harvester equals the input rotational speed of the pinion gear shaft, the harvester will be in the engaged mode. However, if the rotational speed of the bevel gears is larger than that of the input rotational speed of the pinion gear shaft, then the harvester will be in the disengaged mode. The forces of the harvesters in the secondary suspension could be expressed as

$$\begin{cases} F_{EH1} = \beta_1\left[m_e\left(\ddot{Z}_c - l_c\ddot{\beta}_c - \ddot{Z}_{t1}\right) + C_e\left(\dot{Z}_c - l_c\dot{\beta}_c - \dot{Z}_{t1}\right)\right] \\ F_{EH2} = \beta_2\left[m_e\left(\ddot{Z}_c + l_c\ddot{\beta}_c - \ddot{Z}_{t2}\right) + C_e\left(\dot{Z}_c + l_c\dot{\beta}_c - \dot{Z}_{t2}\right)\right] \end{cases} \tag{5.11}$$

where m_e and C_e represent the equivalent mass and damping of the harvester, respectively; $\left(\ddot{Z}_c - l_c\ddot{\beta}_c - \ddot{Z}_{t1}\right)$ and $\left(\ddot{Z}_c + l_c\ddot{\beta}_c - \ddot{Z}_{t2}\right)$ are the relative accelerations in the secondary suspension for the front and rear bogie, respectively. $\beta_1 = \begin{cases} 1 & engage \\ 0 & disengage \end{cases}$ and $\beta_2 = \begin{cases} 1 & engage \\ 0 & disengage \end{cases}$.

Therefore, the dynamic equations of the motion for railcar coupled with suspension energy harvesters at secondary suspension could be derived as follows

Car body bounce motion:

$$M_c\ddot{Z}_c + 2K_{sz}Z_c - K_{sz}Z_{t1} - K_{sz}Z_{t2} + \alpha_1\varphi F_{s1} + \alpha_2\varphi F_{s2} + F_{EH1} + F_{EH2} = 0 \tag{5.12}$$

Car body pitch motion:

$$\begin{aligned} J_c\ddot{\beta}_c + 2K_{sz}l_c^2\beta_c + K_{sz}l_cZ_{t1} - K_{sz}l_cZ_{t2} - \alpha_1\varphi F_{s1}l_c + \alpha_2\varphi F_{s2}l_c \\ -F_{EH1}l_c + F_{EH2}l_c = 0 \end{aligned} \tag{5.13}$$

Front bogie bounce motion:

$$\begin{aligned} M_t\ddot{Z}_{t1} + \left(2K_{pz} + K_{sz}\right)Z_{t1} - K_{sz}Z_c - K_{pz}Z_{w1} - K_{pz}Z_{w2} + K_{sz}l_c\beta_c \\ -\alpha_1\varphi F_{s1} - F_{EH1} = 0 \end{aligned} \tag{5.14}$$

Front bogie pitch motion:

$$J_t\ddot{\beta}_{t1} + 2K_{pz}l_t^2\beta_{t1} + K_{pz}l_tZ_{w1} - K_{pz}l_tZ_{w2} = 0 \tag{5.15}$$

Rear bogie bounce motion:

$$M_t\ddot{Z}_{t2} + \left(2K_{pz} + K_{sz}\right)Z_{t2} - K_{sz}Z_c - K_{pz}Z_{w3} - K_{pz}Z_{w4} - K_{sz}l_c\beta_c - \alpha_2\varphi F_{s2} - F_{EH2} = 0 \quad (5.16)$$

Rear bogie pitch motion:

$$J_t\ddot{\beta}_{t2} + 2K_{pz}l_t^2\beta_{t2} + K_{pz}l_tZ_{w3} - K_{pz}l_tZ_{w4} = 0 \quad (5.17)$$

First wheelset bounce motion:

$$M_w\ddot{Z}_{w1} + C_{wr}\dot{Z}_{w1} - C_{wr}\dot{Z}_{01} - K_{pz}Z_{t1} + K_{pz}l_t\beta_{t1} + \left(K_{pz} + K_{wr}\right)Z_{w1} - K_{wr}Z_{01} = 0 \quad (5.18)$$

Second wheelset bounce motion:

$$M_w\ddot{Z}_{w2} + C_{wr}\dot{Z}_{w2} - C_{wr}\dot{Z}_{02} - K_{pz}Z_{t1} - K_{pz}l_t\beta_{t1} + \left(K_{pz} + K_{wr}\right)Z_{w2} - K_{wr}Z_{02} = 0 \quad (5.19)$$

Third wheelset bounce motion:

$$M_w\ddot{Z}_{w2} + C_{wr}\dot{Z}_{w2} - C_{wr}\dot{Z}_{02} - K_{pz}Z_{t1} - K_{pz}l_t\beta_{t1} + \left(K_{pz} + K_{wr}\right)Z_{w2} - K_{wr}Z_{02} = 0 \quad (5.20)$$

Fourth wheelset bounce motion:

$$M_w\ddot{Z}_{w2} + C_{wr}\dot{Z}_{w2} - C_{wr}\dot{Z}_{02} - K_{pz}Z_{t1} - K_{pz}l_t\beta_{t1} + \left(K_{pz} + K_{wr}\right)Z_{w2} - K_{wr}Z_{02} = 0 \quad (5.21)$$

5.3.4 Numerical simulation for energy harvesting performance

The excitation input comes from the irregularities on the surface of the railroad track, which are due to the track formation technology limit, track wear, clearances, ground subsidence, contemporary mechanical maintenance, settlement and other factors [69]. Based on a large quantitative field measurements data in the United States, the Association of American Railroad (AAR) proposed that the track irregularity in the vertical profile could be characterized by a one-sided power spectral density function (PSD) [70, 71], which is

$$S_v = \frac{KA_v\Omega_c^2}{\Omega^2(\Omega^2 + \Omega_c^2)} \quad (5.22)$$

where K (usually chosen as 0.25) and A_v (value listed in Table. 2) are the vertical track irregularity parameters, Ω is spatial frequency, and $\Omega_c = 0.8245$ is the critical number. Table 5-2 also lists the operating speed limits and the percentage of the mileages for each class track.

Table 5-2. Parameters for track vertical profile PSD

Parameter \ Class	Class 6	Class 5	Class 4	Class 3	Class 2	Class 1
$A_v(\text{cm}^2 \cdot \text{rad/m})$	0.0339	0.2095	0.5376	0.6816	1.0181	1.2107
Speed limit (freight)	177 km/hr	129 km/hr	96 km/hr	64 km/hr	40 km/hr	16 km/hr
Percentage of mileages	0.6%	6.0%	10%	21.9%	25.8%	35.7%

*Total track mileage measured in the United States is 513380 km (319,000 miles) [33].

For Chinese railways (not including high-speed rails), the spectrum of the rail vertical profile irregularities is usually located between those of the AAR Class 5 and Class 6 track [35]. In this simulation study, the AAR Classes 5 and 6 track irregularities are both chosen as the excitation inputs, respectively. By transforming the spatial spectrum in the frequency domain into the general geometry variations in the time domain, AAR Classes 5 and 6 railway track irregularities under the different vehicle speeds could be generated. Figure 5-6 shows the time domain Class 6 and 5 track irregularity (deflection) under 30 km/hr vehicle speed.

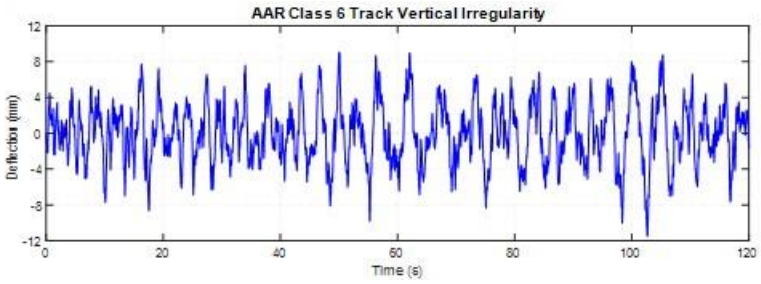

(a)

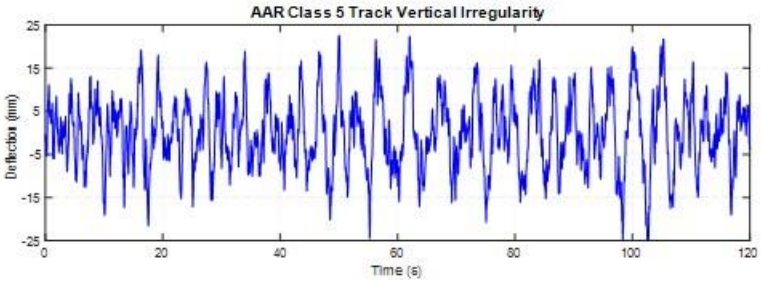

(b)

Fig. 5-6. Simulated track vertical irregularity in the time domain with 30 km/hr train speed: (a) AAR Class 6 track; (b) AAR Class 5 track

Table 5-3. Parameters (half vehicle) for the simulation

Parameter	Value	Description	Parameter	Value	Description
M_c	11472.5 kg	Car body mass	K_{sz}	1.841 MN/m	Secondary suspension stiffness
M_t	377 kg	Bogie frame mass	K_{wr}	6×10^8 N/m	Wheel/rail contact stiffness
M_w	570.5 kg	Wheelset mass	C_{wr}	10 kNs/m	Wheel/rail contact damping
J_c	205000 kgm^2	Moment of inertia of car body	φ	0.121	Relative friction coefficient
J_t	155.38 kgm^2	Moment of inertia of side frame	l_c	4.605 m	Semi-longitudinal distance between bogies
K_{pz}	35 MN/m	Primary suspension stiffness	l_t	0.9 m	Semi-longitudinal distance between wheelsets

The half-vehicle parameters are listed in Table 5-3 for the simulation. The wheel/rail contact stiffness and damping coefficient are adopted from [67], while other parameters are provided by CRRC Yangtze Co. Ltd. A railcar with an 8t weight in the car body (empty full car body is 14945 kg) was simulated in the simulation, and the results of the train suspension energy harvester with 66:1 transmission ratio are shown in Figure 5-7. Backlash and compliance phenomenon are taken into consideration, which will also be discussed in the lab test sections. Figure 5-7(a) illustrates the simulated secondary suspension relative displacement, single-phase voltage and single-phase power with a 4 Ohm Wye-shape resistive load at for 66:1 harvester at 30 km/hr train speed on an AAR Class 5 track. The secondary suspension displacement is in the range of $\pm$3mm, and the root mean square (RMS) relative velocity is 0.017 m/s. The total power gained in this simulation is 3.2W and the total energy obtained in this 3-min period is 1140 J.

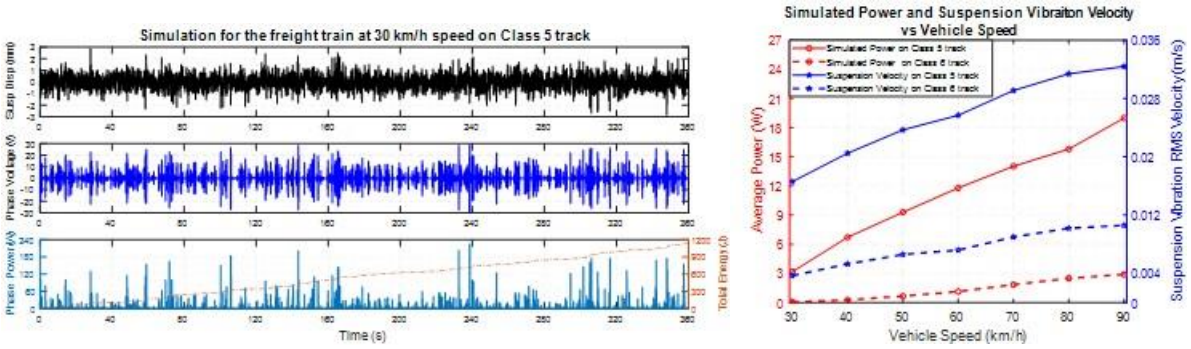

Figure 5-7. Simulation results for the harvester (66:1 gear ratio) with a 4 Ohm Wye-shape resistive load: (a) simulated suspension displacement, single-phase voltage and single-phase power with train speed of 30 km/hr for 66:1 harvester; (b) simulated average power and suspension vibration RMS speed under different train speeds on both 3 km-length AAR Class 5 and 6 track.

Figure 5-7(b) shows the simulated average power of the 66:1 harvester with 4 Ohms external resistive loads versus different train speeds on both Class 5 and 6 tracks. Since most freight railcars in China are running less than 90 km/hr, the simulation study is performed with the train speed range of 0-90 km/hr. The red line (solid for Class 5 and dashed for Class 6) with circle markers represents the results of the simulated average power for the harvester at different train speeds. The blue line (solid for Class 5 and dash for Class 6) with star makers represents the RMS velocity of the secondary suspension. The average power and RMS velocity are calculated at different freight railcar speed conditions, but all with 3 km-length

track irregularities. It should be noted that the generated power and suspension RMS velocities on both track classes increase with the train speeds. As indicated by Figure 5-7(b), for Class 5 track, the RMS velocity increases from 0.017 m/s to 0.033 m/s when the train speed increases from 30 km/hr to 90 km/hr; the corresponding average power gained shows the similar trend towards suspension vibration speed, which also increases with the rising speeds achieved around 19W at 90 km/hr. As mentioned in Subsection 3.3, the railcar is assumed to travel longitudinally on a tangent track with a constant speed V_0 and only the bounce and pitch motion are taken into consideration, while roll motion and yaw motion are ignored. In the real case, the suspension vibration could be larger due to the difference of irregularities between left and right track, etc. Therefore, the energy harvester performance could be larger during real train operation than that in the simulated condition.

In addition, as discussed in Subsection 5.3.2, the proposed energy harvester can be modeled as a viscous damper (due to harvesting) in parallel with an inerter (due to rotational inertia), with dynamic engagement and disengagement. A Preliminary study in [72] indicates that such a suspension harvester can further improve the vehicle dynamics and ride comfort if the damping coefficient and rotational inertia are selected properly.

5.4 Lab Bench Test and Analysis

5.4.1 Experimental setup

The prototype of the energy harvester and in-lab experiment setup are shown in Figure 5-8. Eyelets on both ends of the harvester were removed and replaced by two screw bolts to connect the harvester with the upper and lower grip of the Instron® hydraulic test machine. The lower grip is rigidly connected to the hydraulic actuator, which is controlled by built-in software. An LVDT displacement sensor inside the actuator was used to measure the input displacement and a 100 KN load cell connected to the upper grip is used for force measurement. The three-phase wye resistive loads with a 20:1 voltage divider was connected to the generator, and both the Instron® built-in software and Spider 80 dynamic analyzer recorded the voltage across the external resistor during each test. The train suspension harvester was tested under both harmonic excitation and recorded suspension displacement excitation, and the corresponding energy harvesting performance will be analyzed in the subsections that follow.

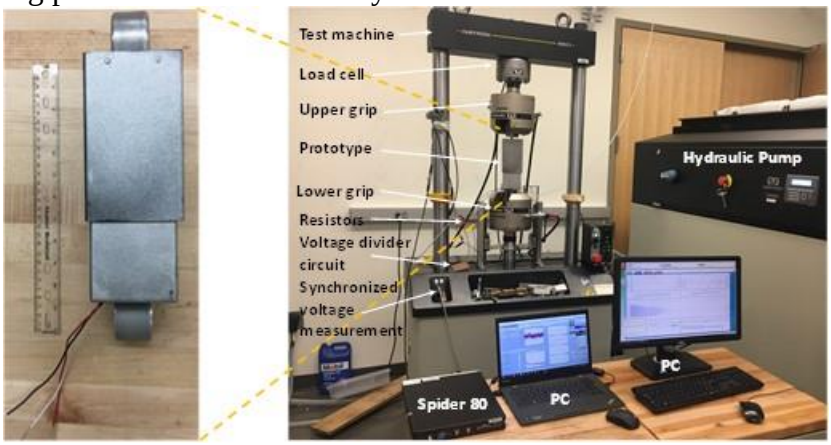

Figure 5-8. In-lab bench test setup

5.4.2 Harmonic excitation

A series of harmonic-excitation tests with different amplitudes and frequencies were carried out. During the tests, a combination of backlash and compliance of the prototype in the range of $\pm$0.5mm was observed, mainly from the rack teeth and pinion gear teeth. The average power of the harvester with transmission ratio 43:1 under 2-4 Hz excitation frequency, 2-4 mm amplitude with a Wye-shape 10 Ohm resistive load are summarized in Table 5-4, along with the engaged electrical damping calculated from Equation (7). It should be noted that the average power of the energy harvester could reach tens of watts in the sinusoidal-wave test, and this average power becomes larger when the vibration amplitude and excitation frequency increase.

Table 5-4. Test result under harmonic excitation with 10 Ohms resistive loads.

Load Resistance: 10 Ohms		2 mm	3 mm	4mm
Transmission ratio 43:1	2 Hz	2.16 W	10.92 W	16.47 W
Engaged damping: 14,076 Ns/m	3 Hz	9.93 W	22.73 W	38.56 W
	4 Hz	18.06 W	40.57 W	62.62 W

Furthermore, the mechanical efficiency of the energy harvester can be obtained by calculating the ratio of total electrical energy obtained and mechanical input work. The mechanical work input is $W_{mech} = \int_0^t F(t) \cdot D(t)dt$, where $F(t)$ is the input force of the harvester and $D(t)$ is the harvester input displacement. The total electrical energy obtained in all three phases could be expressed as $E_{elec} = 3 \times \int_0^t \frac{(R_i+R_e)Ve^2}{Re^2} dt$, where V_e is the instant phase voltage across the external resistor, R_i is the internal resistance of the generator and R_e is the external resistive load. Therefore, the mechanical efficiency η of the train suspension energy harvester could be expressed as

$$\eta = \frac{E_{elec}}{W_{mech}} = \frac{3 \times \int_0^t \frac{(R_i + R_e)Ve^2}{Re^2} dt}{\int_0^t F(t) \cdot D(t)dt} \tag{5.23}$$

In the harmonic excitation experiment, after calculating η for every single case, we found that the maximum efficiency was achieved at 4Hz, 3mm excitation with a 2 Ohm resistive load. The mechanical work input obtained in one period at this condition is 71 J, and the total electrical energy in this period is 48J, therefore, the maximum mechanical efficiency obtained in the harmonic excitation tests is around 68%. The loss of the mechanical efficiency includes the frictions and damping in the rack and pinion, bevel gears sets, bearings and clutches, and the gearhead. By selecting low-friction bearings, using proper lubricants for the motion transmission system, and increasing the machining precision (such as avoiding undesired machining misalignment) will increase the mechanical efficiency.

Figure 5-9 shows the simulated and measured phase voltage and power (transmission ratio 43:1) with a Wye shape external resistive load of 10 Ohms, under amplitude of ± 3 mm and frequency of 2 Hz. An average power of 10.92W was achieved during this test, and a total energy obtained in this one-second period is 10.92 J. The red dashed lines in the phase voltage subplot and phase power subplot are the simulation results (backlash and compliance were set to be zero in this simulation), and it should be noted that there is a difference between the simulation and test results. This is due to the backlash between rack teeth and pinion teeth and the compliance of the mechanical system, resulting in no voltage or power since there is no rotation of the generator when the opposite direction displacement input happens at the beginning.

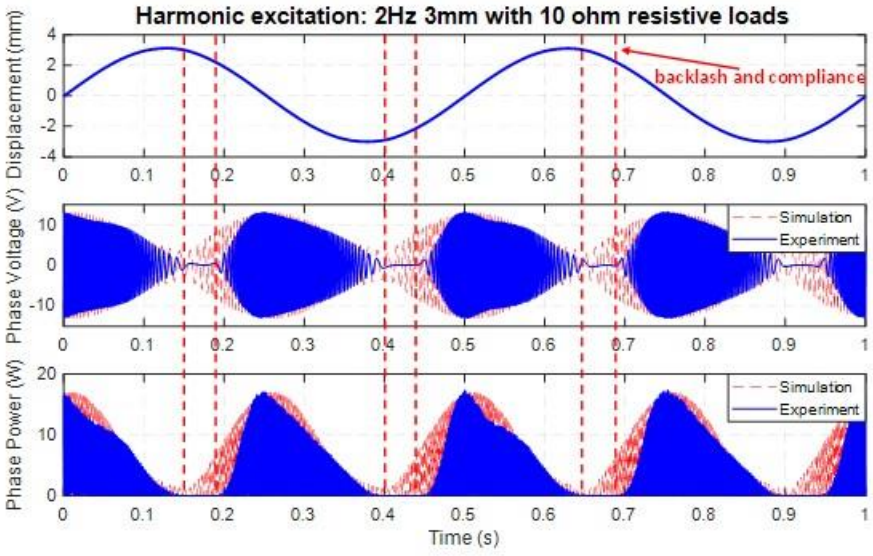

Figure 5-9. Measured and simulated phase voltage and power of harvester with transmission ratio 43:1 under sinusoidal excitation with an amplitude of ± 3 mm and a frequency of 2 Hz. The generator is connected to an external 10 Ohm resistive load in a "Wye" shape and the average power of the total three phases is 10.92 W, and the energy obtained is 10.92 J in this one-second experiment.

5.4.3 Bench tests with recorded freight railcar vibrations

5.4.3.1 Recorded freight railcar suspension displacement on the test train in CRRC

A freight railcar suspension displacement which was recorded on a train tested in CRRC Yangtze, Co., Ltd, Wuhan, China, was used as the input to investigate the performance of the proposed harvester in the lab bench test. Figure 10 shows the phase voltage and power of the harvester with the transmission ratio 66:1 connected to a 4 Ohm Wye shape resistive load under the recorded train secondary suspension displacement at the train speed of 30km/hr. A peak phase power of 88.8W and a total average power of 3.3W were achieved. Figure 5-10 shows that the vibration amplitude (mostly less than 2mm) and frequency (dominant frequency is 0.5-0.6 Hz) are small when the test train moves at the low speed of 30 km/hr. The calculated RMS velocity of this 20-second recorded suspension displacement is 0.017 m/s.

The zoomed-in plot on the right shows the simulation results together with the bench test results. The simulation results agree well with the experiment results. However, a difference can be observed when the force is large. One possible explanation is that the corresponding torque on the one-way clutch is larger than its torque capacity due to the large damping coefficient of the harvester during the engagement. This over-limit torque might make the slip happen between the clutch and bevel gears or the shaft (which means that the clutches cannot transmit the entire torque from the shaft to the bevel gear), resulting in less generated voltage and power in the experiment than the expectation in the simulation. One way to increase the torque capacity of the clutch and avoid the slippage is to select appropriate materials for the shaft and gears, which can withstand more torque transmission and can be heat treated to obtain proper surface hardness.

Table 5-5 lists the engaged damping coefficients and energy harvesting performance of the harvester with different gear transmission ratios and resistive loads under the recorded suspension displacement on the CRRC test track. A maximum average power of 3.3W was achieved with 4 Ohm resistors for the large gear ratio harvester, and the total energy obtained in this 20-second period is 66 J. For the small gear ratio case, the power output and the damping coefficients are higher when the resistive load decreases. However, for the large gear ratio case, the power outputs with a 2 Ohm resistive load are a little bit lower than those of the 4 Ohms case. The explanation for this abnormality is that the clutches slip due to the higher damping and large required torque, resulting in lower power output in the experiment.

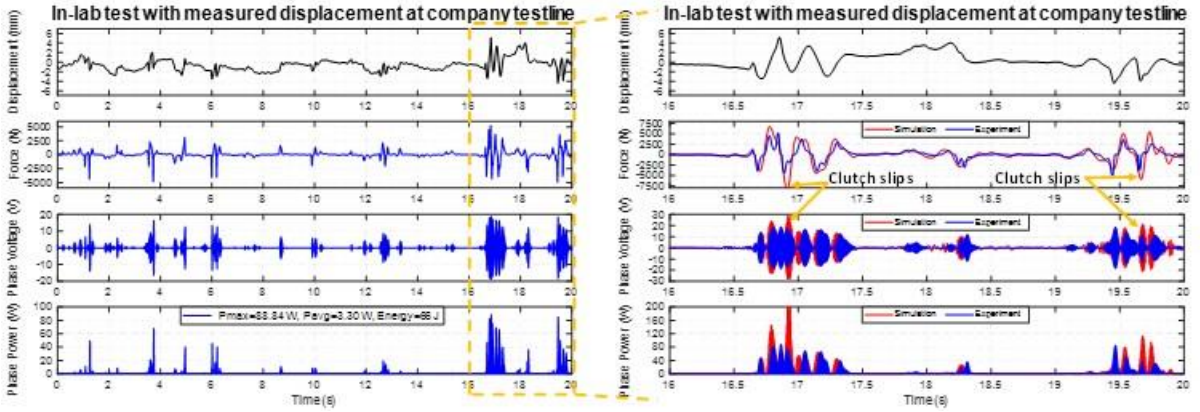

Figure 5-10. Measured phase voltage and power of rack-pinion based energy harvester (transmission ratio 66:1) connected to a 4 Ohm Wye shape resistive load under the recorded train secondary suspension displacement at the train speed of 30km/hr: the left figure is the 20-second in-lab test result, and the right figure is zoomed in test results with simulations.

Table 5-5. Performance of the harvesters under the recorded suspension displacement at 30 km/hr train speed in CRRC.

Ratio 43:1	Engaged Damping	Avg. Power	Ratio 66:1	Engaged Damping	Avg. Power
2 *ohm*	55,475 Ns/m	2.4 W	2 *ohm*	130,690 Ns/m	3.0 W
4 *ohm*	31,969 Ns/m	2.0 W	4 *ohm*	75,315 Ns/m	**3.3 W**
8 *ohm*	17,304 Ns/m	1.8 W	8 *ohm*	40,767 Ns/m	2.9 W

5.4.3.2 Recorded freight railcar suspension displacement of a normal operational train on operational tracks

To further investigate the performance of the proposed harvester on the train running at higher speeds, bench tests were performed with recorded suspension displacements of a freight railcar (parameters the same as Table 3) on different operational track sections in China. Figure 5-11(a) shows the phase voltage and power of the harvester with a transmission ratio of 66:1 connected to a 4 Ohm Wye shape resistive loads at the train speed of 90km/hr. In this test condition, the corresponding calculated peak current, RMS current, peak voltage, and generator rotational speed are 5.25 A, 1.1 A, 21 V, and 3908 rpm, respectively, which is reasonable compared with the suggested values of listed in Table 1. The total energy obtained in this around 20-second period is 278.4 J, and a peak phase power of 117.18W and a total average power of 14.5W were achieved during the bench test. In order to store the energy into a battery, a two-stage energy harvesting circuit (AC-DC and buck-boost converter) [73] with a battery charger circuit could be applied. The buck-boost could be placed between the AC/DC rectifier and the battery charger circuit, which can set an ideal effective resistance [73, 74] for the harvester. Commercial battery charging circuits [75] are able to handle the irregular and multi-gap voltage/current effectively.

Compared with the recorded CRRC test train suspension displacement with the RMS velocity of 0.017 m/s, the amplitude and frequency of the displacement at 90 km/hr are much higher with the RMS velocity of 0.030 m/s, resulting in larger power output. Figure 5-11(b) shows the average power versus different train speeds at 4 Ohms external resistive loads for the harvester with both transmission ratio 66:1 and 43:1. The 20-second suspension displacements recorded at different track sections and different speeds, which are used as inputs for the harvester during the tests, are provided by CRRC. The red lines (circle markers for 66:1 and squares makers are for 43:1) represent the average power obtained at different train speeds. The blue dashed line with star makers represents the corresponding RMS velocity of the secondary suspension at different train speeds. As shown in Figure 11(b), the RMS velocity increases from 30 km/hr to 90 km/hr and the corresponding average powers show a similar trend towards speed.

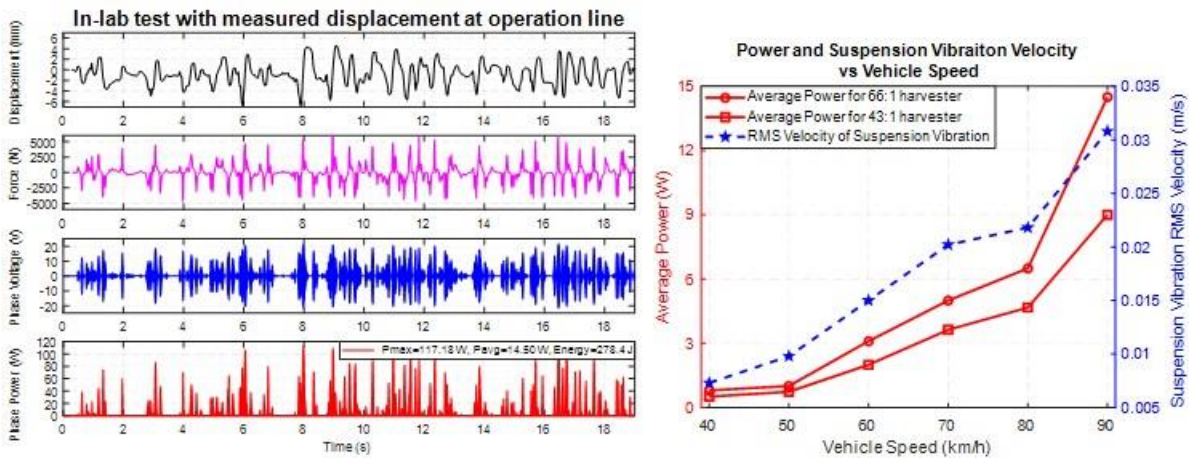

(a) (b)

Figure 5-11. Lab test results of the suspension harvester with 4 Ohms Wye shape resistive loads under recorded secondary suspension displacements of a freight railcar running on an operational track: (a) suspension displacement, force, phase voltage and phase power at 90 km/hr train speed; an average power of 14.5W and a total energy 278.4 J were obtained for 66:1 harvester; (b) average power and suspension vibration RMS velocity for both 66:1 and 43:1 harvester at different train speeds.

Compared with the simulations conducted in Subsection 5.3.4, the power outputs and suspension velocities in this experiment have a similar value and the trend agrees well with the simulation, which could validate the effectiveness of the model. Note that the tested suspension RMS velocities are between the simulated suspension RMS velocities on Class 5 and Class 6 tracks, corresponding to the average power outputs in the tests and simulations. This also agrees with the statement mentioned before that Chinese rail roughness is usually located between those of the AAR Class 5 and Class 6 tracks [76].

For the sake of comparison, Table 5-6 lists the calculated damping coefficients and average power outputs of the harvesters with different gear transmission ratios and resistive loads. Maximum average power of 14.5 and 9.2W were obtained at the 90 km/hr train speed with 66:1 and 43:1 gear ratios, respectively. Average power outputs are expected to be higher with the 2 Ohm load for the 66:1 gearhead ratio case; however, these are lower compared to the 4 Ohms case. This is consistent with subsection 4.3.1, with the same explanation for this abnormality: the clutches slip due to the higher damping coefficient and large required torque with 66:1 ratio at 2 Ohms load condition, resulting in lower power output in the experiment.

Table 5-6. Energy harvesting performance of train suspension harvester under the recorded suspension displacement on an operational track: (a) 43:1 transmission ratio harvester; (b) 66:1 transmission ratio harvester

Table 5-6(a): prototype with 43:1 gear ratio

External Resistance	Engaged Damping	Avg. Power @40 km/hr	Avg. Power @60 km/hr	Avg. Power @90 km/hr
2 *ohm*	55,475 Ns/m	0.6 W	2.2 W	**9.2 W**

4 *ohm*	31,969 Ns/m	0.5 W	2.0 W	9.0 W
8 *ohm*	17,304 Ns/m	0.4 W	1.5 W	7.2 W

Table 5-6(b): prototype with 66:1 gear ratio

External Resistance	Engaged Damping	Avg. Power @40 km/hr	Avg. Power @60 km/hr	Avg. Power @90 km/hr
2 *ohm*	130,690 Ns/m	0.7 W	3.0 W	12.5 W
4 *ohm*	75,315 Ns/m	0.8 W	3.1 W	**14.5 W**
8 *ohm*	40,767 Ns/m	0.6 W	2.8 W	13.4 W

5.5 Onboard Field Test and Discussion

5.5.1 Test setup

The onboard experiment was carried out on a test track located inside CRRC Yangtze, Co., Ltd in Wuhan, China, to validate the proposed suspension energy harvester. The harvester with the 43:1 gearhead transmission ratio was tested. Figure 5-12 shows that the harvester was installed at the secondary suspension of a C70H general-purpose Gondola car by using two welded adapters. The adapters are welded on the bolster and spring plank, respectively; and two elastic rubber attachments are placed between the adapters and eyelets of the harvester for reducing the impact force to the harvester during train operation. The loaded car has a total weight of around 23 tons. The onboard test maintained a constant locomotive speed of 30 km/hr for around 20 seconds and then started to brake on a ballast track. Due to the overall length limit of the testing track in the company, the train speed could not be higher than 30 km/hr; otherwise, there is not enough time for the train to stop. A pull rod linear position displacement sensor was used to measure the relative displacement of the secondary suspension. Wye shape 4 Ohms resistive loads were connected to the harvester during the onboard tests. A data acquisition (DAQ) system was employed to collect the displacement and phase voltage data.

Figure 5-12. Onboard experiment setup

5.5.2 Results and discussions

Figure 5-13 shows the recorded relative displacement (harvester displacement input) in the secondary suspension, single-phase voltage across a 4 Ohms external resistive load, and the calculated single-phase power. A peak phase power of 73.2W and an average power of 1.3W in total three phases were achieved. The total energy obtained in this 20-second period is 26 J. Higher power output could be obtained at higher train speeds. The harvested energy is enough to power some onboard devices, such as sensors for real-time structure health monitoring, GPS and wireless communication systems, which could potentially increase the safety of the train operation. Some onboard electronic devices, like electronic anti-skid, may demand much larger power (like 100W) for a short period time. These can be enabled in intermittent operation mode with onboard battery energy storage.

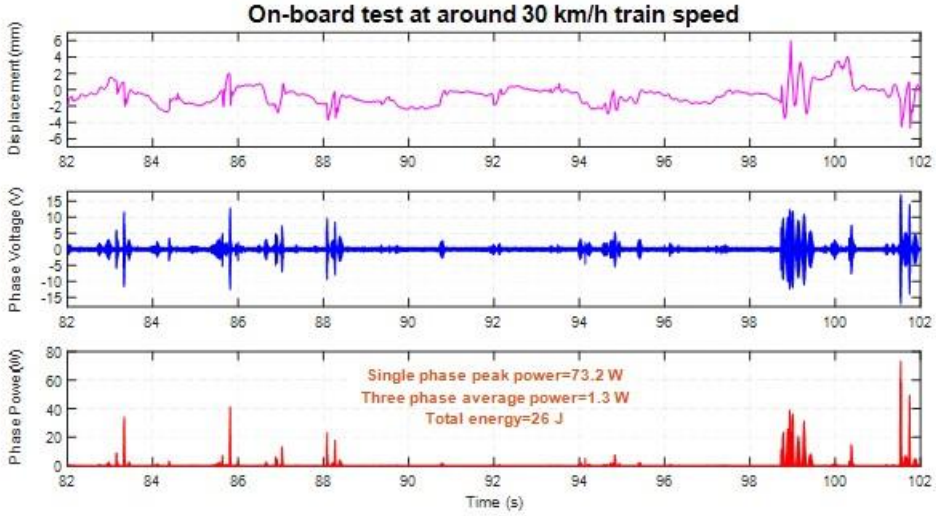

Figure 5-13. Recorded harvester displacement, phase voltage, and the corresponding phase power for the suspension energy harvester with 43:1 transmission ratio and 4 Ohms resistive loads at 30 km/hr train speed: suspension vibration RMS velocity is **0.017 m/s** and an average of 1.3W was achieved during the onboard test. The total energy obtained in this 20-second period is 26 J.

During the onboard experiment, the freight railcar ran at a low speed (30 km/hr) on the ballast track located in the company, resulting in a small amplitude (mostly less than 2 mm) and low frequency (0.5-0.6 Hz) vibration of the secondary suspension. Compared with the in- lab test of subsection 4.3.1, the power output in the onboard test with 1.3W is smaller than that in the lab test with 1.96W for the harvester with 43:1 gearhead transmission ratio. The difference is that for the onboard tests rubber bushings were used at each end to connect the harvester to the railcar, which absorbs some of the fact forces. For the lab tests, the harvester was attached to the Instron® test machine by steel grippers.

5.6 Chapter Summary

In this chapter, a rack-pinion based freight railcar energy harvester with a mechanical motion rectifier (MMR) mechanism was designed, modeled, and tested both in the lab and in the field. The proposed energy harvester could translate the bidirectional freight railcar suspension vertical vibration into unidirectional rotation of the electromagnetic generator by utilizing two one-way clutches embedded in transmission bevel gears. An enclosed MMR gearbox with lubricant inside was designed to increase the transmission durability and decrease the friction loss.

A coupled model for the freight railcar integrated with the proposed energy harvesters at the secondary suspensions was developed. A simulation study was performed with the Association of American Railroad (AAR) Class 5 and 6 track irregularities as the system input, showing that the generated power from the harvester and the suspension vibration RMS velocity increase with the train speeds. Energy harvesting performances at different train speeds for the proposed harvester were also predicted through modeling and numerical simulations.
The in-lab and onboard field tests were carried out to evaluate the performance of the proposed train suspension energy harvester. In-lab test results showed that an average power of 14.5 and 9.2W were achieved with the typical recorded suspension displacement (vibration RMS velocity is 0.030 m/s) at 90 km/hr on an operational track for the prototype harvesters with 66:1 and 43:1transmission ratios, respectively. The model was validated through bench tests using both the sinusoidal inputs and the recorded displacement inputs. An onboard test was also carried out on a test track in CRRC Yangtze, Co., Ltd., and test results showed a peak of 73.2W phase power and an average of 1.3W were achieved at a train speed of 30 km/hr (vibration RMS velocity is 0.017 m/s) for the harvester with 43:1 transmission ratio. Both the in-lab and onboard test results indicate that the proposed train suspension energy harvester could continuously generate an amount of power (watts to tens of watts level) useful for powering onboard auxiliary electrical devices, which can potentially improve the freight railcar operational safety.

Chapter 6 Power Management System of Energy Harvester for Railcar Suspension and Performance Evaluation of Energy Harvesting Shock Absorber on Railway Vehicle Dynamics

6.1 Chapter Introduction

Without dependable electrical supplies, modern smart devices and technologies, such as GPS, electromagnetic braking, train condition real-time monitoring system and positive train control, cannot be applied to the freight vehicles to improve the operational safety and efficiency. A suspension energy harvester, which has been discussed in the previous section, could potentially improve the awkward situation for freight trains lack of electricity. To store the energy that harvested from the suspension vibration and manage the power, a power management system for the electromagnetic harvester is needed.

In this chapter, a power management system with an energy storage circuit is designed, prototyped and tested. AC-DC and buck-boost (DC-DC) converters are employed in the energy storage circuit to convert the AC voltage to DC voltage and set an effective resistance (equivalent damping) to the transducers. The oscillator circuit in the self-designed buck-boost converter controls the switching frequency and duty cycle of the power MOSFET. A modified commercial battery charging circuit is located at the output side of the buck-boost converter to maximally store the electrical energy into the lead-acid battery. Power management system is also integrated with the self-designed energy storage circuit, battery indicator circuits and two boost converters. Tests were conducted in CPES, and results showed the overall power management system could perform well in the bench test conditions.

The ongoing studies of the influence of the MMR-EHSA on railway vehicle dynamics are also included in this chapter. A nonlinear railway vehicle model integrating EHSAs at the secondary suspension with six degrees of freedom is built and simulations with analysis about the train ride comfort are presented.

6.2 Power Management System for Train Suspension Energy Harvester

6.2.1 Power management system overview

The suspension energy harvester, which can be also called the transducer, can convert the mechanical energy into the electrical energy. In other to further store or utilize the energy that harvested through the transducer, a power management system with an energy storage circuit is needed. Figure 6-1 shows the diagram of the power management system with an energy storage circuit for the train suspension energy harvester. The energy storage circuit consists of four parts: the AC-DC converter, DC-DC converter, oscillator circuit and battery charger circuit. The voltage generated from the electromagnetic (EMG) is a three-phase AC voltage with a 120° phase difference between each phase. Therefore, for the energy storage circuit connected to the EMG, the first step is converting the AC oscillating voltage to DC voltage

through an AC-DC converter. Afterwards, a DC-DC converter is employed to set a resistance to the EMG. The oscillator circuit controls the switching frequency and duty cycle of the MOSFET inside the DC-DC converter. A commercial battery charger circuit is connected to the output of the DC-DC converter to storage the electricity into the lead acid battery.

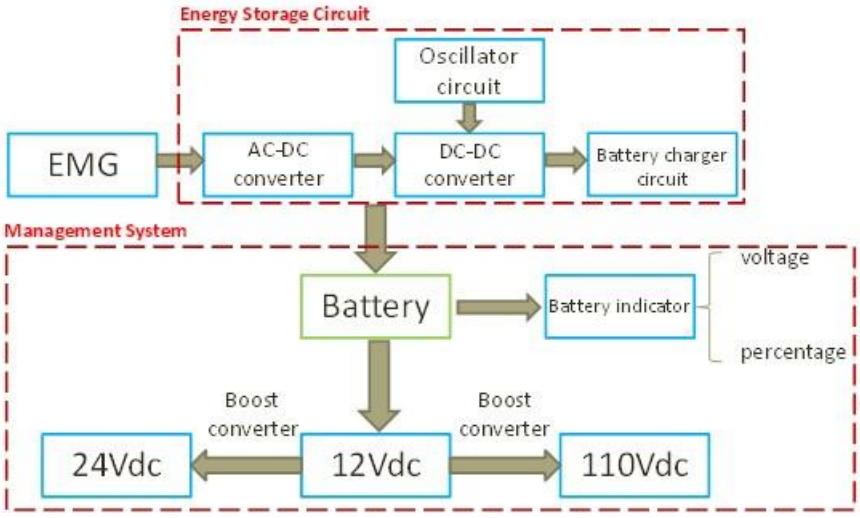

Fig. 6-1. Diagram of the power management system for the suspension energy harvester

The management system consists of a 12V lead acid battery, a battery indicator and 2 boost converters. The battery indicator could show real-time voltage and capacity percentage of the battery. Two boost converter could boost the 12V DC voltage to 24V and, respectively. In this way, during the train operation, the vibration energy in the train suspension could be converted into the electrical energy, which could be stored in the battery and boosted to higher voltages for different electronic devices to use.

6.2.2 Energy storage circuit

Figure 6-2 shows the energy harvesting storage circuit diagram, which includes a self-designed converter with oscillator circuit and a commercial battery charger. The self-designed converter sets an equivalent resistance for the harvester to control a reasonable damping of the mechanical part, while the battery charger circuit functions as storing the electricity into the lead acid battery. Figure 6-3 shows the layout of the printed circuit board (PCB) for the train suspension energy harvester.

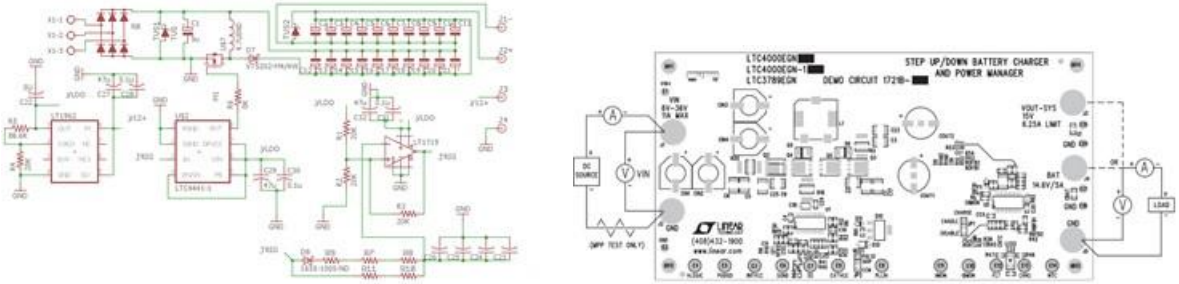

(a) (b)

Figure 6-2. Energy storage circuit schematic: (a) the self-designed converter with oscillator circuit; (b) the commercial battery charger circuit

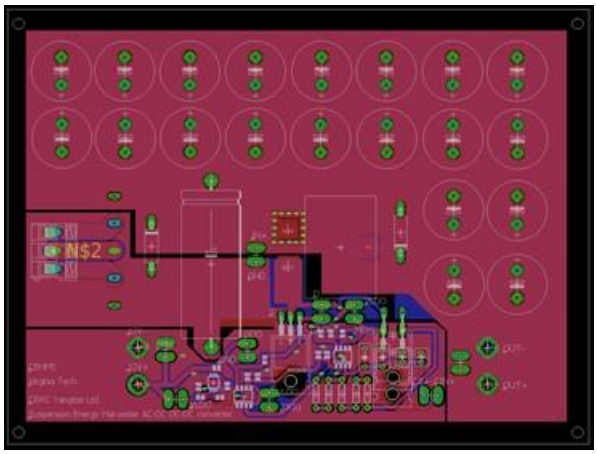

Figure 6-3. Print Circuit Board (PCB) layout of AC-DC and DC-DC converter for suspension energy harvester

6.2.2.1 AC-DC converter

The electromagnetic generator used in the suspension energy harvester is a three-phase AC generator. The reciprocating vibration input results in an oscillating AC output voltage, which is the input of the conditioning circuit. As shown in Figure 6-4, a three-phase AC-DC rectifier is employed in the circuit to convert the AC voltage to a DC voltage. A TVS diode is connected right after the AC-DC rectifier for clamping the voltage back to its breakdown. With the help to the front TVS diode, the following converter circuit could be protected from high voltage spike due to sudden impacts on the suspension harvester. An electrolytic capacitor is placed after the TVS diode and before the DC-DC converter to smooth the output voltage of the AC-DC rectifier.

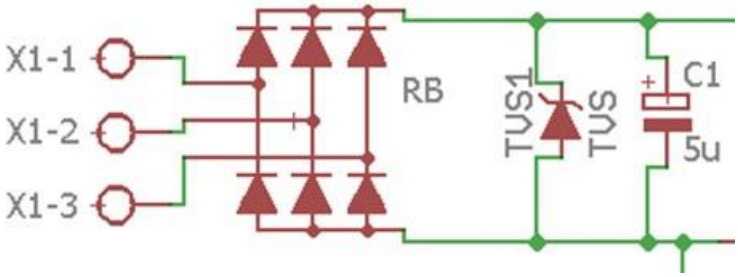

Figure 6-4. AC-DC rectifier circuit

6.2.2.2 Buck-boost converter

Traditional buck-boost converter includes buck, boost, buck-boost, flyback and Sepic converters. Among these converters, buck-boost converter is widely used in energy harvesting

area for the following reasons: (a) it can step up or step down the input voltage; (b) compared with flyback and Sepic converters, the buck-boost converter requires a smaller number of components; (c) when buck-boost converter works in discontinuous conduction mode (DCM), it behaves as a resistor and the equivalent resistive load is independent of the output load of the circuit. The effective input load of a DCM buck-boost converter could be expressed as [77].

$$R_{in} = \frac{2L}{D^2 T_s} \tag{6.1}$$

where R_{in} represents the effective resistance of the buck boost converter, L represents the inductance of the inductor in the buck-boost converter, D represents the duty cycle of the switch and T_s represents the period when the switch is on.

Figure 6-5 shows the schematic of the self-designed buck-boost converter. In this design, to maintain a reasonable damping, we set a 7 Ohm effective resistive load to the designed buck-boost converter. From large number of trials in the simulations and in-lab tests, the inductance is finally selected as 4.7 uH, switching frequency is 40 KHz and the duty cycle is 23.3%. And calculated from the Equation (6.1), the corresponding effective resistance is 6.925 Ohm theoretically. 20 electrolytic capacitors are located at the output side of the buck-boost converter to smooth the output voltage and to distribute the output current.

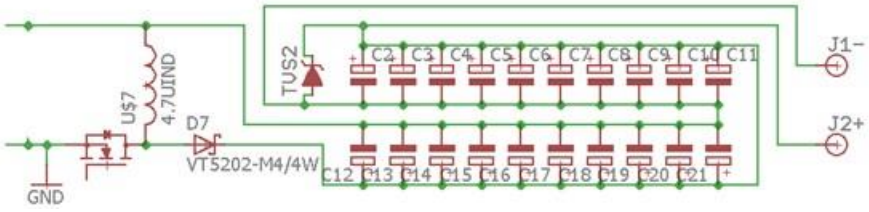

Figure 6-5. Buck-boost converter schematic

6.2.2.3 Oscillator circuit

Oscillator circuit is very important in the buck-boost converter, and it decides the switching frequency and duty cycle of the MOSFET in the buck-boost main circuit. Figure 6-6 shows the schematic of the oscillator circuit for the energy storage circuit, which consists of a linear drop off regulator (LDO), comparator circuit and a gate driver.

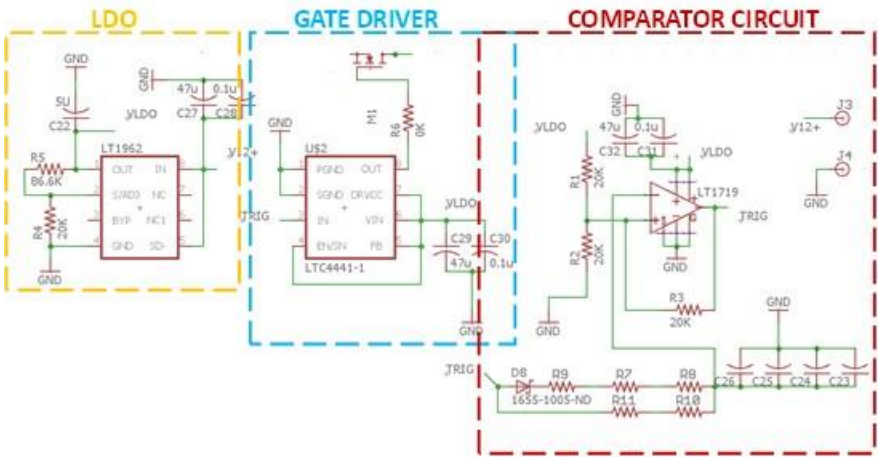

Figure 6-6. Oscillator circuit schematic

An LDO (LT1962) is located at the first stage of the oscillator circuit, regulating the 12Vdc voltage from the battery to lower DC voltage for powering the comparator. By tuning the resistor R_4 and R_5, the LDO output voltage could be adjusted to be in the range of 1.22Vdc-20Vdc. In this design, the LDO output is tuned to be 6.5 V for powering the comparator.

A comparator circuit is located at the second stage of the oscillator circuit. LT1719 is used in this circuit to output the switching signal to turn on or off the MOSFET. By tuning the $(R_7 + R_8 + R_9)$, $(R_{10} + R_{11})$ and $(C_{23} + C_{24} + C_{25} + C_{26})$, the charging and discharging period could be adjusted and therefore, the duty cycle and switching frequency could be tuned [78, 79]. From the simulation and experiment together, the duty cycle is chosen as 23.3% and the switching frequency is chosen as 40 KHz.

A gate driver is a power amplifier that accepts a low-power input from a controller IC and produces a high-current drive input for the gate of a high-power transistor such as an IGBT or power MOSFET. A gate driver (LTC4441-1) is located at the last stage of the self-designed oscillator circuit to amplify the current to the MOSFET. The resistor R_6 is the tuning resistor to make sure there is no false turn on for the MOSFET by removing or suppressing the ringing signals. Figure 6-7 shows the final prototyped PCB of the AC-DC and buck-boost converter.

Figure 6-7. PCB of AC-DC and DC-DC (buck-boost) converter

6.2.2.4 Battery charger circuit

A demonstration circuit (DC-1721B), as shown in Figure 6-8 is located at the output side of the buck-boost converter. This commercial demo board is a 14.6V, 5A battery charger with an input range of 6-36V, which is suitable for a wide variety of portable applications including instruments, industrial equipment, power tools and computers. The chip LTC4000-1 on the board has an input voltage regulation loop for Maximum Power Point (MPP) control, which can extract near maximum power from the former circuit. Overall, by connecting the battery charging circuit between the buck-boost converter and the lead acid battery, the electricity could be stored in the battery.

Figure 6-8. Commercial battery charging circuit demo board

6.2.3 In-lab test of the buck-boost converter

To test the self-designed buck-boost converter with high power (watts to tens of watts level) input and output, we seek the help from Center of Power Electronic System (CPES) to use their equipment. The buck-boost converter was tested in both DC condition and AC condition

with a large input range. Extreme conditions were also considered, and the harvester successfully passed the tests, showing the circuit could work in the severe train suspension vibration conditions.

6.2.3.1 DC test of buck-boost converter

Figure 6-9 shows the DC test diagram of the buck boost converter. The DC power supply has an output voltage range of 0-100V and an output current range of 0-30A, which is good enough to test our circuits. The buck-boost converter is connected to the DC power supply and a 20 Ohm power resistor is connected at the output side of the buck-boost converter. Voltages and currents of the input and output of the buck-boost converter were measured. Table 6-1 shows the test result of the DC condition test. It shows that with the input range of 1.9-24.9 V input voltage, the circuit can function well with a maximum 77.28% efficiency. The effective resistance of the buck-boost converter is also calculated for each case, and it shows that the effective resistance stays in the range of 7-7.5 Ohm, which is very close to the designed value (6.925 Ohm).

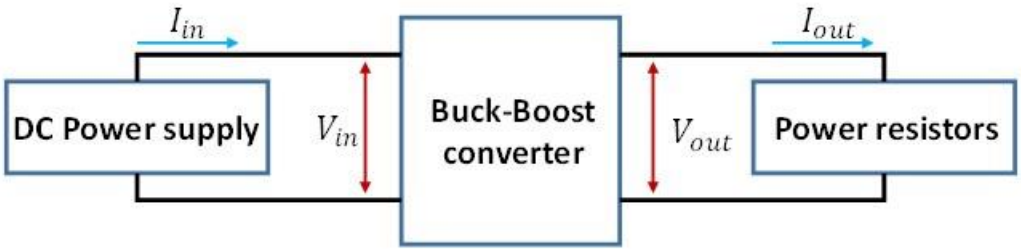

Figure 6-9. DC test of the buck-boost converter

Table 6-1 Test results with DC inputs

V_{in} (V)	I_{in} (A)	V_{out} (V)	I_{out} (A)	Efficiency	R_{in_test} (Ω)
1.9	0.27	2.39	0.11	51.24%	7.03
4.96	0.69	6.58	0.32	61.52%	7.19
10.22	1.40	13.48	0.69	65.00%	7.3
14.65	1.96	20.40	0.99	70.33%	7.47
19.2	2.63	27.29	1.43	**77.28%**	7.30
24.9	3.35	32.43	1.89	73.48%	7.43

6.2.3.2 AC test of the AC-DC and buck-boost converters

Figure 6-10 shows the AC test diagram of the buck boost converter. The function generator generates some sine wave AC signal, and in this case, a 3000 Hz signal was generated as an extreme case for the testing. The goal of this high frequency input is that test the circuit in an extreme condition and if it can pass, then we can conclude that the circuit should be able to survive in the train suspension case. Through the power amplifier, the current could be amplified to power the following buck-boost converter with a constant power resistor. The buck-boost converter is connected to the power amplifier and a 20 Ohm power resistor is

connected at the output side of the buck-boost converter. Voltages and currents of the input and output of the buck-boost converter were measured. Table 6-2 shows the test result of the AC condition test. Due to the current limit of the power amplifier, the voltage cannot be increased over 15 Vrms. The measured results showed that the circuit can function well with a maximum 66.82% efficiency. The power loss could mainly come from the full bridge rectifier, MOSFET and Diodes. To work in a high range of voltage, a robust bridge rectifier was chosen and each diode in the 3-phase full bridge rectifier has a forward voltage drop 1.06V, which might cause a not small power loss in the circuit.

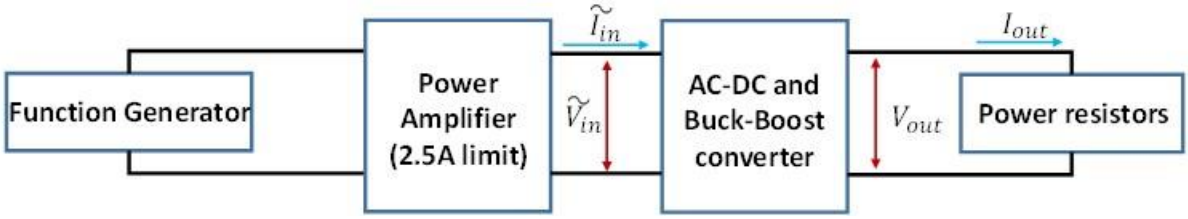

Figure 6-10. AC test of the buck-boost converter

Table 6-2 Test results with AC inputs

V_{in_pp} (V)	V_{in_RMS} (V)	I_{in_RMS} (A)	V_{o_RMS} (V)	I_{o_RMS} (A)	Efficiency
NA	7.83	1.74	9.09	0.46	30.70%
44.00	12.44	2.46	16.74	0.86	47.04%
48.6	14.86	2.51	22.32	1.15	**68.82%**

6.2.3.3 Test of the energy storage circuits

Figure 6-11 shows the testing diagram of the energy storage circuit. The converters, battery chargers and the battery are tested together. Table 6-3 shows the test results of the energy storage circuit, indicating that the whole circuit could function well for a large range of voltage and current input. The overall system maximum efficiency is around 43% during the test. Besides the power loss from the converters, the battery charger will also have some power loss due to the battery current capacity. The battery tested in lab is a nearly fully charged battery, therefore, the output power to the battery is not large and the overall efficiency is not high.

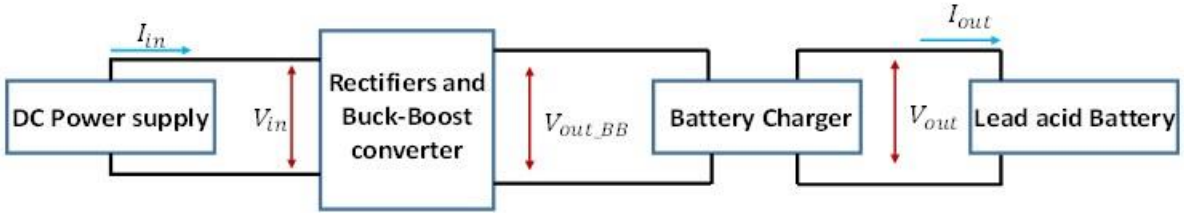

Figure 6-11. Test of the energy storage circuit

Table 6-3 Test results of the energy storage circuit

V_{in} (V)	I_{in} (A)	V_{out_BB} (V)	V_{out} (V)	I_{out} (A)	Efficiency
2.03	0.18	0->6	12.80	0.006	21.02%
5.01	0.57	~6	12.87	0.04	18.06%
10.25	1.34	~6	12.93	0.36	33.89%
15.25	2.10	~6	13.16	0.91	37.39%
20.21	2.90	6->36	14.2	1.77	**42.88%**

6.2.4 Test of the other subsystem of the management system

The other commercial components, including the battery indicator and boost converters are also tested and validated for their functionalities. Figure 6-12 shows the overall power management system for the train suspensions.

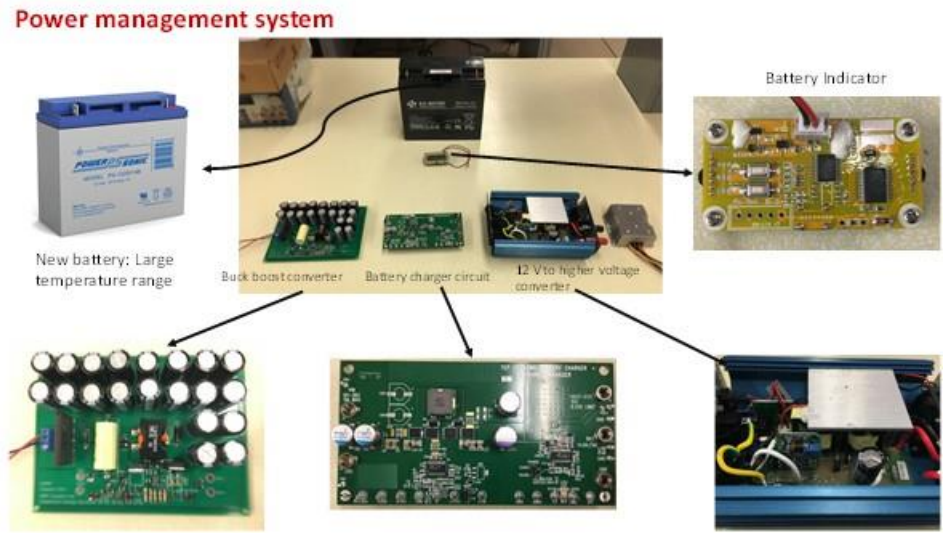

Figure 6-12 Power management system

6.3 Performance Evaluation of MMR Energy Harvesting Shock Absorber (EHSA) on Railway Vehicle Dynamics

The railcar suspension energy harvester has a similar appearance of a shock absorber; therefore, we can also call the energy harvester as the energy harvesting shock absorber (EHSA). Although the energy harvesting performance of the MMR suspension energy harvester has been validated from Chapter 5, the influences of this type of unique harvester/shock absorber on the railway vehicle dynamics have not been studied yet. The MMR-EHSA, as discussed before, could be regarded as a tunable nonlinear damper in parallel with a nonlinear inerter. The influence of the linear inerter on the railway vehicle has been studied by several researchers [80-85]. *Zhang et al.* [80] proved that a 12.84% improvement

of later acceleration of vehicle body could be obtained by parallel inerter after optimizing parameters in the primary and secondary suspension. *Wang et al.* [83-85] proved that adding the inerter into the railway vehicle could enhance vertical ride comfort and reduce the settling time. However, these previous investigations only focused on the influences of the linear inerter on the vehicle dynamics, while MMR-EHSA involves a nonlinear inerter in parallel with a nonlinear damping induced by the engagement and disengagement, which shall have different performances and has not been researched yet on railway vehicles. In this sub-chapter, the vehicle dynamics with the MMR-EHSA in the primary suspension is studied. A six degree-of-freedom vehicle model with the MMR-EHSA at primary suspension is built. Simulations towards system nonlinearity due to engagement and disengagement are conducted, to analyze the characteristics of vehicle dynamics with the random rail surface irregularities. Results show vertical ride comfort could be improved if the nonlinear equivalent inertance and damping could be properly designed.

6.3.1 Dynamics of the railway vehicle with EHSA at primary suspension

From the view of dynamics and energy, the difference between the traditional shock absorber and energy harvesting shock absorber are: (a) the EHSA could be regarded as a tunable nonlinear damper (by adjusting the external resistive load) in parallel with a nonlinear inerter, while the traditional shock absorber can only function as a damper with fixed damping coefficient; (b) the traditional shock absorber mitigates the suspension vibration by dissipating the suspension vibration energy into heat, while the EHSA can convert the vibration energy into electrical energy and harvest it.

In this sub-chapter, the traditional shock absorber in the primary suspension is replaced with our MMR-EHSA. Figure 6-13 illustrates the components of the vehicle model integrated with energy harvesting shock absorber. The car body is supported on the two double-axle bogies at both end. The EHSAs replace the original hydraulic shock absorber in the primary suspension, which linked the bogie frame and the wheelsets. The two bogies are also linked with the rail car body through the secondary suspensions, which consists of the two-stage springs. The displacement of the wheelsets is assumed to be the same as the track movement at the wheel-rail contact. The overall vertical vehicle system involves six degrees of freedom, as the car body and two bogies have bouncing and pitching motion, respectively. The railcar is assumed to run along with the track with a constant speed V_0.

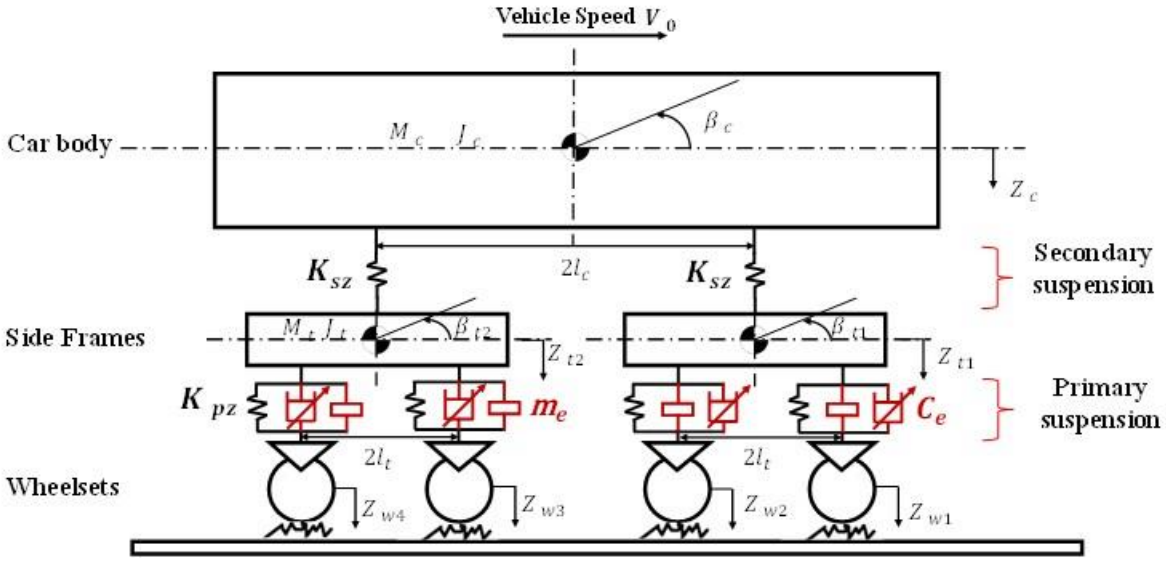

Figure 6-13 Railway vehicle model with MMR-EHSA at primary suspension

M_c and M_t are mass of car body and side frames, respectively; J_c and J_t are moment inertia of the car body and side frames, respectively; Z_c, Z_{t1} and Z_{t2} are the vertical displacements, relative to the static balanced position, of car body, front side frame and rear side frame, respectively; β_c, β_{t1} and β_{t2} are the pitch angle of the car body, front side frame and rear side frame, respectively. Z_{w1}, Z_{w2}, Z_{w3} and Z_{w4} are the vertical displacements of the four wheelsets due to the irregularity of the railway track. l_c is the semi-longitudinal distance between bogies, and l_t is the semi-longitudinal distance between wheelsets in bogie.

The suspension harvester could be in the engaged mode or disengaged mode during the railway car is running. When the rotational speed of one of the bevel gears inside the harvester equals the input rotational speed of the pinion gear shaft, the harvester will be in the engage mode. While if the rotational speed of the bevel gears inside the harvester is larger than that of the input rotational speed of the pinion gear shaft, then the harvester will be in the disengaged mode. The forces of the harvesters in the primary suspension could be expressed as

$$F_{EHSA1} = m_e\left(\ddot{Z}_{t1} - l_t\ddot{\beta}_{t1} - \ddot{Z}_{w1}\right) + C_e\left(\dot{Z}_{t1} - l_t\dot{\beta}_{t1} - \dot{Z}_{w1}\right) \quad (6.2)$$

$$F_{EHSA2} = m_e\left(\ddot{Z}_{t1} + l_t\ddot{\beta}_{t1} - \ddot{Z}_{w2}\right) + C_e\left(\dot{Z}_{t1} + l_t\dot{\beta}_{t1} - \dot{Z}_{w2}\right) \quad (6.3)$$

$$F_{EHSA3} = m_e\left(\ddot{Z}_{t2} - l_t\ddot{\beta}_{t2} - \ddot{Z}_{w3}\right) + C_e\left(\dot{Z}_{t2} - l_t\dot{\beta}_{t2} - \dot{Z}_{w3}\right) \quad (6.4)$$

$$F_{EHSA4} = m_e\left(\ddot{Z}_{t2} + l_t\ddot{\beta}_{t2} - \ddot{Z}_{w4}\right) + C_e\left(\dot{Z}_{t2} + l_t\dot{\beta}_{t2} - \dot{Z}_{w4}\right) \quad (6.5)$$

where m_e and C_e represent the equivalent mass and damping of the harvester, respectively; $\alpha_{1\sim4} = \begin{cases} 1 & engage \\ 0 & disengage \end{cases}$.

Therefore, the dynamic equation of the motion for car body and side frames could be derived as follows

Car body bounce motion:

$$M_c\ddot{Z}_c + 2C_{sz}\dot{Z}_c - C_{sz}\dot{Z}_{t1} - C_{sz}\dot{Z}_{t2} + 2K_{sz}Z_c - K_{sz}Z_{t1} - K_{sz}Z_{t2} = 0 \quad (6.6)$$

Car body pitch motion:

$$J_c\ddot{\beta}_c + 2C_{sz}l_c^2\dot{\beta}_c + C_{sz}l_c\dot{Z}_{t1} - C_{sz}l_c\dot{Z}_{t2} + 2K_{sz}l_c^2\beta_c + K_{sz}l_cZ_{t1} - K_{sz}l_cZ_{t2} = 0 \quad (6.7)$$

Former bogie bounce motion

$$\begin{aligned} &M_t\ddot{Z}_{t1} - K_{sz}(Z_c - l_c\beta_c - Z_{t1}) - C_{sz}\left(\dot{Z}_c - l_c\dot{\beta}_c - \dot{Z}_{t1}\right) \\ &+K_{pz}(Z_{t1} - l_t\beta_{t1} - Z_{w1}) + \alpha_1C_e\left(\dot{Z}_{t1} - l_t\dot{\beta}_{t1} - \dot{Z}_{w1}\right) \\ &+\alpha_1m_e\left(\ddot{Z}_{t1} - l_t\ddot{\beta}_{t1} - \ddot{Z}_{w1}\right) + K_{pz}(Z_{t1} + l_t\beta_{t1} - Z_{w2}) \\ &+\alpha_2C_e\left(\dot{Z}_{t1} + l_t\dot{\beta}_{t1} - \dot{Z}_{w2}\right) + \alpha_2m_e\left(\ddot{Z}_{t1} + l_t\ddot{\beta}_{t1} - \ddot{Z}_{w2}\right) = 0 \end{aligned} \quad (6.8)$$

Former bogie pitch motion:

$$\begin{aligned} &J_t\ddot{\beta}_{t1} - K_{pz}(Z_{t1} - l_t\beta_{t1} - Z_{w1})l_t - \alpha_1C_e\left(\dot{Z}_{t1} - l_t\dot{\beta}_{t1} - \dot{Z}_{w1}\right)l_t \\ &-\alpha_1m_e\left(\ddot{Z}_{t1} - l_t\ddot{\beta}_{t1} - \ddot{Z}_{w1}\right)l_t + K_{pz}(Z_{t1} + l_t\beta_{t1} - Z_{w2})l_t \\ &+\alpha_2C_e\left(\dot{Z}_{t1} + l_t\dot{\beta}_{t1} - \dot{Z}_{w2}\right)l_t + \alpha_2m_e\left(\ddot{Z}_{t1} + l_t\ddot{\beta}_{t1} - \ddot{Z}_{w2}\right)l_t = 0 \end{aligned} \quad (6.9)$$

Latter bogie bounce motion:

$$\begin{aligned} &M_t\ddot{Z}_{t2} - K_{sz}(Z_c + l_c\beta_c - Z_{t2}) - C_{sz}\left(\dot{Z}_c + l_c\dot{\beta}_c - \dot{Z}_{t2}\right) \\ &+K_{pz}(Z_{t2} - l_t\beta_{t2} - Z_{w3}) + \alpha_3C_e\left(\dot{Z}_{t2} - l_t\dot{\beta}_{t2} - \dot{Z}_{w3}\right) \\ &+\alpha_3m_e\left(\ddot{Z}_{t2} - l_t\ddot{\beta}_{t2} - \ddot{Z}_{w3}\right) + K_{pz}(Z_{t2} + l_t\beta_{t2} - Z_{w4}) \\ &+\alpha_4C_e\left(\dot{Z}_{t2} + l_t\dot{\beta}_{t2} - \dot{Z}_{w4}\right) + \alpha_4m_e\left(\ddot{Z}_{t2} + l_t\ddot{\beta}_{t2} - \ddot{Z}_{w4}\right) = 0 \end{aligned} \quad (6.10)$$

Latter bogie pitch motion:

$$\begin{aligned} &J_t\ddot{\beta}_{t2} - K_{pz}(Z_{t2} - l_t\beta_{t2} - Z_{w3})l_t - \alpha_3C_e\left(\dot{Z}_{t2} - l_t\dot{\beta}_{t2} - \dot{Z}_{w3}\right)l_t \\ &-\alpha_3m_e\left(\ddot{Z}_{t2} - l_t\ddot{\beta}_{t2} - \ddot{Z}_{w3}\right)l_t + K_{pz}(Z_{t2} + l_t\beta_{t2} - Z_{w4})l_t \\ &+\alpha_4C_e\left(\dot{Z}_{t2} + l_t\dot{\beta}_{t2} - \dot{Z}_{w4}\right)l_t + \alpha_4m_e\left(\ddot{Z}_{t2} + l_t\ddot{\beta}_{t2} - \ddot{Z}_{w4}\right)l_t = 0 \end{aligned} \quad (6.11)$$

6.3.2 Numerical Simulation and Analysis

The main function of the shock absorber is to mitigate vehicle car body vibration induced by the rail surface irregularities. The influence of MMR-EHSA on the ride performance is analyzing the car body vertical acceleration, which is a main and important index when evaluating the vertical ride comfort. Simulation study is conducted using the developed railway vehicle model with EHSA at the primary suspension. The system inputs come from the railway track irregularities, which has been discussed in Chapter 5. The parameters of a 160 km/hr freight railcar for the simulation are listed in Table 6-4. CRRC Yangtze Co., Ltd. provides this set of parameter.

Table 6-4 List of the main parameters of a fast 160 km/hr freight railcar

Parameter	Value	Discription	Parameter	Value	Description
M_{c_empty}	20300 kg	Car body mass (empty)	K_{pz_empty}	0.905 MN/m	Primary stiffness (empty)
M_{c_loaded}	59000 kg	Car body mass (fully loaded)	K_{pz_loaded}	1.896 MN/m	Primary stiffness (fully loaded)
M_t	2767 kg	Side frame mass	K_{sz}	15 MN/m	Secondary stiffness
J_{c_empty}	545800 kgm^2	Moment of inertia of car body (empty)	C_{pz}	40/60 kNs/m	Primary damping (empty/fully loaded)
J_{c_loaded}	1677900 kgm^2	Moment of inertia of car body(fully loaded)	l_c	4.605 m	Semi-longitudinal distance between bogies
J_t	833 kgm^2	Moment of inertia of side frame	l_t	0.9 m	Semi-longitudinal distance between wheelsets

Figure 6-14 shows the car body bouncing and pitching accelerations with MMR energy harvesting shock absorber when the railcar is empty. The green stars represent the accelerations with the traditional shock absorber. As we can see, with the optimal pair of equivalent inertial mass and damping, the car body vertical central acceleration and pitching acceleration can be reduced by 5~6%, which potentially improve the railcar dynamics while harvesting the energy.

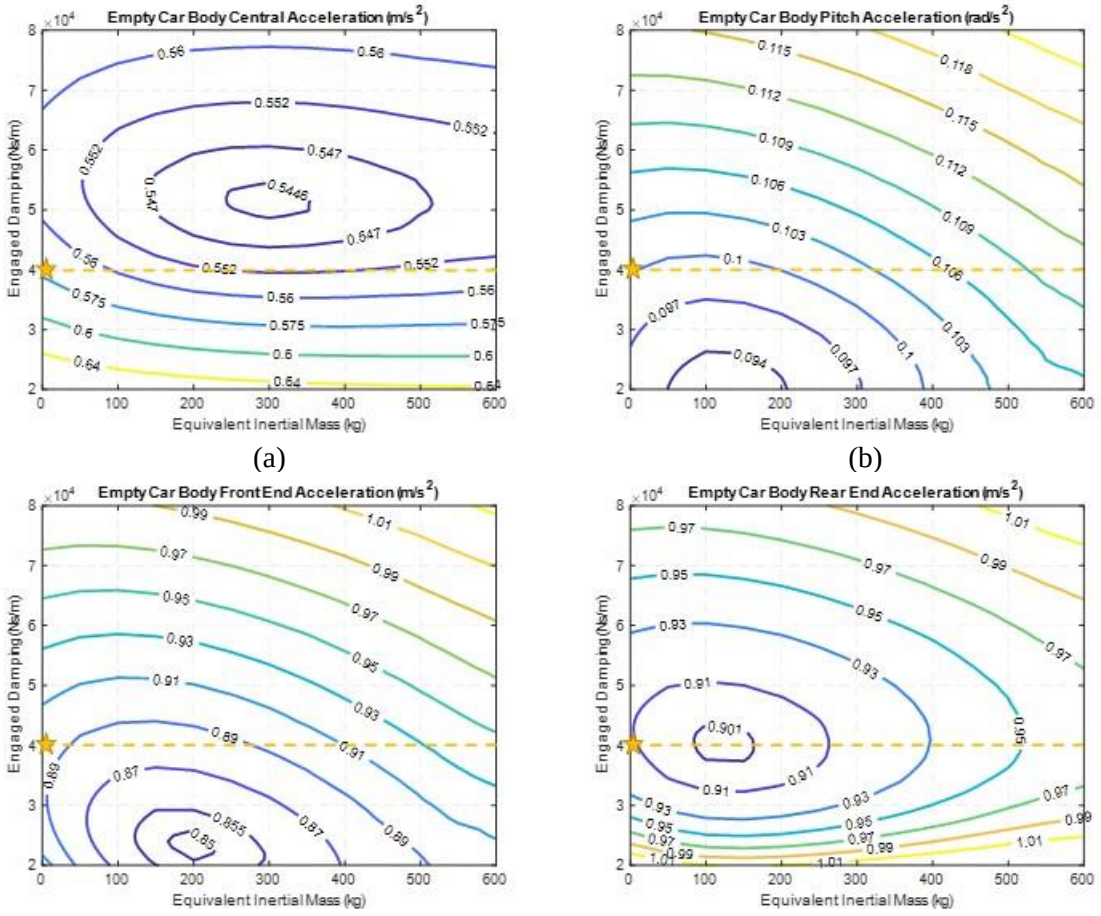

Figure 6-14. RMS accelerations for empty car condition: (a) car body central vertical acceleration; (b) car body pitching acceleration; (c) car body front-end vertical acceleration; (d) car body rear-end vertical acceleration.

Figure 6-15 shows the car body bouncing and pitching accelerations with MMR energy harvesting shock absorber when the railcar is fully loaded. The green stars represent the accelerations with the traditional shock absorber. As we can see, with the optimal pair of equivalent inertial mass and damping, the car body vertical central acceleration and pitching acceleration can be reduced by 5~12.3%, which potentially improve the railcar dynamics while harvesting the energy.

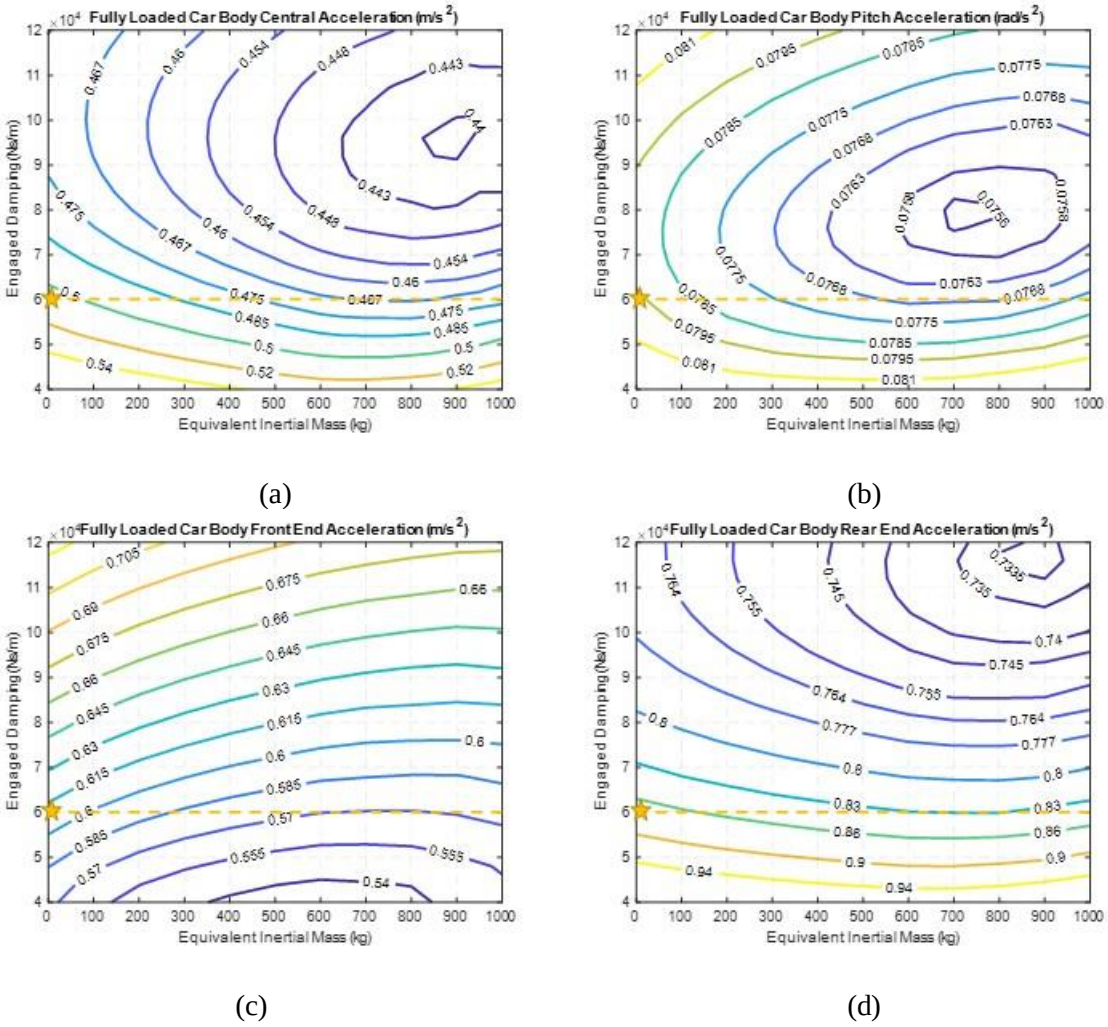

Figure 6-15. RMS accelerations for fully loaded car condition: (a) car body central vertical acceleration; (b) car body pitching acceleration; (c) car body front-end vertical acceleration; (d) car body rear-end vertical acceleration.

6.4 Chapter Summary

In this chapter, a power management system with an energy storage circuit is designed, prototyped and tested. AC-DC and buck-boost (DC-DC) converters are employed in the energy storage circuit to convert the AC voltage to DC voltage and set an effective resistance (equivalent damping) to the transducers. The oscillator circuit in the self-designed buck-boost

converter controls the switching frequency and duty cycle of the power MOSFET. A modified commercial battery charging circuit is located at the output side of the buck-boost converter to maximally store the electrical energy into the lead-acid battery. Power management system is also integrated with the self-designed energy storage circuit, battery indicator circuits and two boost converters. Tests were conducted in CPES, and results showed that an around 7 Ohm resistance and a maximum 77% efficiency could be achieved for the buck-boost converter. The overall power management system could perform well in the bench test conditions.

The influence of the MMR-EHSA on railway vehicle dynamics has been also investigated in this chapter. A nonlinear railway vehicle model integrating EHSAs at the primary suspension with six degrees of freedom is built and simulations with analysis are presented. Results shows that compared with vehicle with traditional shock absorbers, trains with MMR-EHSAs could reduce 5~12.3% accelerations when the equivalent inertia mass is properly designed according to the vehicle parameter, which will improve the ride comfort of the railway cars.

Chapter 7 Conclusion and Future Work

This chapter will provide a summary of the work completed, draw some conclusions, and suggest future direction on the energy harvesting research on railroad and railcar application.

7.1 Conclusion

Up to now, the following conclusions can be drawn from the work accomplished in this dissertation.

1. A novel ball-screw based railway track energy harvester with mechanical motion rectifier mechanism was designed, modeled and tested.

    - Due to the nonlinear characteristics induced by the one-way clutches in the mechanical motion rectifier (MMR) mechanism, the proposed energy harvester could convert the bi-directional track vibration into unidirectional rotation of the generator, which significantly improves the motion transmission by reducing the impact forces.
    - A comprehensive model considering the coupled dynamic behaviors of the train, railway track and harvester was developed and validated. It is shown that the proposed ball-screw based energy harvester acts as a fixed inerter in parallel with pre-compressed springs and an adjustable damper tuned by external resistive load of the generator, when the one-way clutch is in engagement. When both one-way clutches disengage from the bevel gears, the energy harvester behaves as pre-compressed springs only, and the inertia of the generator drives the generator itself continuously to produce electricity. This piece-wise mass-spring-damper of the single freedom harvester is integrated into the train-track model and the performance of the harvester at different train speeds can be predicted by the model.
    - The in-lab and field tests were conducted to further validate the dynamic characteristics and evaluate the performance of the proposed energy harvester. The harvester could effectively work under a very small input with the amplitude of ±0.2 mm, which shows that the proposed harvester has an improved sensitivity to the environment vibrations. Field test results showed that an average power of 1.12 and 2.24W were achieved for prototype 1 and 2 respectively at 30 km/hr rapid transit speed. More power could be obtained by choosing a higher limit one-way clutch, increasing the reset spring stiffness and refining the installation condition.

2. A smart energy harvesting railroad tie to power the trackside electrical device has been proposed, designed, modeled and tested for potentially improving the train operational efficiency and safety.

    - The smart tie, which is designed to have similar dimensions to a conventional railroad tie, can be installed in the same manner as a standard tie on the track.
    - Through a ball-screw, a pair of bevel gear and an output shaft with a single one-way clutch, the generator can be driven to generate electricity. Different from bidirectional energy harvesters, the proposed smart tie only harvests the kinetic energy of the railroad tie when the tie moves downwards due to the approaching wheel, which resolves the preload and installation challenges and increases the overall system reliability.
    - An analytical model is developed, and the dynamic simulation is conducted to better understand the system nonlinearity and predict the performance.

- During the bench tests, the smart tie demonstrates great sensitivity to the environment vibration due to its small backlash (less than 0.1 mm). In-lab test results show that an average power of 26.1 and 42.2W on 4 Ohms and 2 Ohms external loads are obtained under simulated tie movement, indicating that the proposed smart tie is capable to power most wayside electrical devices, which has a great potential to improve the train operational safety.

3. A rack-pinion based freight railcar energy harvester with a mechanical motion rectifier (MMR) mechanism was designed, modeled, and tested both in the lab and in the field.

    - The proposed energy harvester could translate the bidirectional freight railcar suspension vertical vibration into unidirectional rotation of the electromagnetic generator by utilizing two one-way clutches embedded in transmission bevel gears. An enclosed MMR gearbox with lubricant inside was designed to increase the transmission durability and decrease the friction loss.
    - A coupled model for the freight railcar integrated with the proposed energy harvesters at the secondary suspensions was developed. A simulation study was performed with the Association of American Railroad (AAR) Class 5 and 6 track irregularities as the system input, showing that the generated power from the harvester and the suspension vibration RMS velocity increase with the train speeds. Energy harvesting performances at different train speeds for the proposed harvester were also predicted through modeling and numerical simulations.
    - The in-lab and onboard field tests were carried out to evaluate the performance of the proposed train suspension energy harvester. In-lab test results showed that an average power of 14.5 and 9.2W were achieved with the typical recorded suspension displacement (vibration RMS velocity is 0.030 m/s) at 90 km/hr on an operational track for the prototype harvesters with 66:1 and 43:1transmission ratios, respectively. The model was validated through bench tests using both the sinusoidal inputs and the recorded displacement inputs.
    - An onboard test was also carried out on a test track in CRRC Yangtze, Co., Ltd., and test results showed a peak of 73.2W phase power and an average of 1.3W were achieved at a train speed of 30 km/hr (vibration RMS velocity is 0.017 m/s) for the harvester with 43:1 transmission ratio. Both the in-lab and onboard test results indicate that the proposed train suspension energy harvester could continuously generate an amount of power (watts to tens of watts level) useful for powering onboard auxiliary electrical devices, which can potentially improve the freight railcar operational safety.

4. A power management system with an energy storage circuit is designed, prototyped and tested.

    - AC-DC and buck-boost (DC-DC) converters are employed in the energy storage circuit to convert the AC voltage to DC voltage and set an effective resistance (equivalent damping) to the transducers. The oscillator circuit in the self-designed buck-boost converter controls the switching frequency and duty cycle of the power MOSFET.
    - A modified commercial battery charging circuit is located at the output side of the buck-boost converter to maximally store the electrical energy into the lead-acid battery. Power management system is also integrated with the self-designed energy storage circuit, battery indicator circuits and two boost converters.

- Tests were conducted and results showed that an around 7 Ohm resistance and a maximum 77% efficiency could be achieved for the buck-boost converter. The overall power management system could perform well in the bench test conditions.

5. The MMR energy harvester on railcar dynamics has been also investigated.
    - A nonlinear railway vehicle model integrating EHSAs at the primary suspension with six degrees of freedom is built and simulations with analysis are presented.
    - Results shows that compared with vehicle with traditional shock absorbers, railcars with MMR energy harvester as new-type shock absorber could perform better for ride comfort when the equivalent inertia mass and damping coefficient is properly designed.

7.2 Future Work

This sub-chapter discusses future work based on the knowledge accumulated thus far. Future work should primarily address the following:

1. Energy harvesting Tie project
    - Field test of the smart energy harvesting tie.
2. Performance evaluation of train suspension energy harvesting shock absorber on railway vehicle and its dynamic influence
    - Optimizing the primary suspension stiffness, inertia mass and engaged damping for further improving the railcar dynamics.
    - Use commercial software *Simpack* to validate the model. (Might collaborate with CRRC engineer.)

References

[1] Tai W-C, Liu M, Yuan Y, Zuo L. On Improvement of the Frequency Bandwidth of Nonlinear Vibration Energy Harvesters Using a Mechanical Motion Rectifier. Journal of Vibration and Acoustics. 2018;140:051008--11.

[2] Zhou S, Zuo L. Nonlinear dynamic analysis of asymmetric tristable energy harvesters for enhanced energy harvesting. Communications in Nonlinear Science and Numerical Simulation. 2018;61:271-84.

[3] Viet NV, Xie XD, Liew KM, Banthia N, Wang Q. Energy harvesting from ocean waves by a floating energy harvester. Energy. 2016;112:1219-26.

[4] Younesian D, Alam M-R. Multi-stable mechanisms for high-efficiency and broadband ocean wave energy harvesting. Applied Energy. 2017;197:292-302.

[5] Zhou S, Wang J. Dual serial vortex-induced energy harvesting system for enhanced energy harvesting. AIP Advances. 2018;8:075221.

[6] Zhang R, Wang X, Al Shami E, John S, Zuo L, Wang CH. A novel indirect-drive regenerative shock absorber for energy harvesting and comparison with a conventional direct-drive regenerative shock absorber. Applied Energy. 2018;229:111-27.

[7] Bowen L, Vinolas J, Olazagoitia J, Otero JE. An Innovative Energy Harvesting Shock Absorber System using Cable Transmission. IEEE/ASME Transactions on Mechatronics. 2019;99:1-.

[8] Xiong H, Wang L. Piezoelectric energy harvester for public roadway: On-site installation and evaluation. Applied Energy. 2016;174:101-7.

[9] Gao M, Wang Y, Wang Y, Wang P. Experimental investigation of non-linear multi-stable electromagnetic-induction energy harvesting mechanism by magnetic levitation oscillation. Applied Energy. 2018;220:856-75.

[10] Coelho B, Hölscher P, Priest J, Powrie W, Barends F. An Assessment of Transition Zone Performance. Proceedings of the Institution of Mechanical Engineers, Part F: Journal of Rail and Rapid Transit. 2011;225:129-39.

[11] Vorster J, Grabe H. Axle load and track deflection on a heavy haul line. Civil Engineering : Magazine of the South African Institution of Civil Engineering. 2010;18:44-9.

[12] Wischke M, Masur M, Kröner M, Woias P. Vibration harvesting in traffic tunnels to power wireless sensor nodes. Smart Materials and Structures. 2011;20:085014.

[13] Nelson CA, Platt SR, Albrecht D, Kamarajugadda V, Fateh M. Power harvesting for railroad track health monitoring using piezoelectric and inductive devices. Active and Passive Smart Structures and Integrated Systems: International Society for Optics and Photonics; 2008. p. 69280R.

[14] Pourghodrat A, Nelson CA, Hansen SE, Kamarajugadda V, Platt SR. Power harvesting systems design for railroad safety. Proceedings of the Institution of Mechanical Engineers, Part F: Journal of Rail Rapid Transit. 2014;228:504-21.

[15] Yuan T, Yang J, Song R, Liu X. Vibration energy harvesting system for railroad safety based on running vehicles. Smart Materials and Structures. 2014;23:125046.

[16] Wang J, Shi Z, Xiang H, Song G. Modeling on energy harvesting from a railway system using piezoelectric transducers. Smart Materials and Structures. 2015;24:105017.

[17] Nelson CA, Pourghodrat A, Fateh M. Energy harvesting from vertical deflection of railroad track using a hydraulic system for improving railroad track safety. ASME International Mechanical Engineering Congress and Exposition. p. 259-66.

[18] Gao M, Wang P, Cao Y, Chen R, Cai D. Design and verification of a rail-borne energy harvester for powering wireless sensor networks in the railway industry. IEEE Transactions on Intelligent Transportation Systems. 2017;18:1596-609.
[19] Gatti G, Brennan MJ, Tehrani MG, Thompson DJ. Harvesting energy from the vibration of a passing train using a single-degree-of-freedom oscillator. Mechanical Systems and Signal Processing. 2016;66:785-92.
[20] Brennan MJ, Gatti GA. Harvesting Energy From Time-Limited Harmonic Vibrations: Mechanical Considerations. Journal of Vibration and Acoustics. 2017;139:051019.
[21] Pourghodrat A, Nelson CA, Phillips KJ, Fateh M. Improving an energy harvesting device for railroad safety applications. Active and Passive Smart Structures and Integrated Systems: International Society for Optics and Photonics; 2011. p. 9.
[22] Pourghodrat A, Nelson CA. A system for generating electricity using the passage of train wheels for improving railroad track safety. ASME International Design Engineering Technical Conferences and Computers and Information in Engineering Conference. p. 1025-31.
[23] Wang JJ, Penamalli G, Zuo L. Electromagnetic energy harvesting from train induced railway track vibrations. Proceedings of IEEE/ASME International Conference on Mechatronic and Embedded Systems and Applications 2012. p. 29-34.
[24] Zhang X, Zhang Z, Pan H, Salman W, Yuan Y, Liu Y. A portable high-efficiency electromagnetic energy harvesting system using supercapacitors for renewable energy applications in railroads. Energy Conversion and Management. 2016;118:287-94.
[25] Zhang X, Pan H, Qi L, Zhang Z, Yuan Y, Liu Y. A renewable energy harvesting system using a mechanical vibration rectifier (MVR) for railroads. Applied Energy. 2017;204:1535-43.
[26] Wang J, Lin T, Zuo L. High efficiency electromagnetic energy harvester for railroad application. ASME 2013 International Design Engineering Technical Conferences and Computers and Information in Engineering Conference2013. p. V004T08A37-VT08A37.
[27] Lin T, Wang JJ, Zuo L. Efficient electromagnetic energy harvester for railroad transportation. Mechatronics. 2018;53:277-86.
[28] Lin T, Pan Y, Zuo L. Dynamics Modeling of Train-Track-Harvester System and In-Field Testing of Railroad Energy Harvester. ASME 2016 Dynamic Systems and Control Conference2016. p. V001T13A-VT13A.
[29] Lin T, Pan Y, Chen S, Zuo L. Modeling and field testing of an electromagnetic energy harvester for rail tracks with anchorless mounting. Applied Energy. 2018;213:219-26.
[30] Bernal E, Spiryagin M, Cole C. Onboard Condition Monitoring Sensors, Systems and Techniques for Freight Railway Vehicles: A Review. IEEE Sensors Journal. 2019;19:4-24.
[31] Li C, Luo S, Cole C, Spiryagin M. An overview: modern techniques for railway vehicle on-board health monitoring systems. Vehicle System Dynamics. 2017;55:1045-70.
[32] Vasisht MS, Vashista GA, Srinivasan J, Ramasesha SK. Rail coaches with rooftop solar photovoltaic systems: A feasibility study. Energy. 2017;118:684-91.
[33] Rohollahi E, Abdolzadeh M, Mehrabian MA. Prediction of the power generated by photovoltaic cells fixed on the roof of a moving passenger coach: A case study. Proceedings of the Institution of Mechanical Engineers, Part F: Journal of Rail Rapid Transit. 2015;229:830-7.

[34] Nagode C, Ahmadian M, Taheri S. Axle generator for freight car electric systems. ASME Joint Rail Conference 2012. p. 761-5.
[35] Ahn D, Choi K. Performance Evaluation of Thermoelectric Energy Harvesting System on Operating Rolling Stock. Micromachines. 2018;9:359.
[36] De Pasquale G, Somà A, Fraccarollo F. Piezoelectric energy harvesting for autonomous sensors network on safety-improved railway vehicles. Proceedings of the Institution of Mechanical Engineers, Part C: Journal of Mechanical Engineering Science. 2012;226:1107-17.
[37] Cho JY, Jeong S, Jabbar H, Song Y, Ahn JH, Kim JH, Jung HJ, Yoo HH, Sung TH. Piezoelectric energy harvesting system with magnetic pendulum movement for self-powered safety sensor of trains. Sensors and Actuators A: Physical. 2016;250:210-8.
[38] Erturk A, Hoffmann J, Inman DJ. A piezomagnetoelastic structure for broadband vibration energy harvesting. Applied Physics Letters. 2009;94:254102.
[39] Zhou S, Cao J, Erturk A, Lin J. Enhanced broadband piezoelectric energy harvesting using rotatable magnets. Applied Physics Letters. 2013;102:173901.
[40] Ung C, Moss SD, Chiu WK. Electromagnetic energy harvester using coupled oscillating system with 2-degree of freedom. Active and Passive Smart Structures and Integrated Systems 2015. p. 94312C.
[41] De Pasquale G, Soma A, Zampieri N. Design, simulation, and testing of energy harvesters with magnetic suspensions for the generation of electricity from freight train vibrations. Journal of Computational Nonlinear Dynamics. 2012;7:041011.
[42] Schaeffler. FAG Axlebox Generator. 2013.
[43] Nagode C. Electromechanical suspension-based energy harvesting systems for railroad applications [Ph.D Dissertation]: Virginia Tech; 2013.
[44] Matamoros-Sanchez AZ. The use of novel mechanical devices for enhancing the performance of railway vehicles [Doctoral Thesis]: © Loughborough University; 2013.
[45] Wang R, Crosbee D, Iwnicki S, Zhao Y, Bevan A. Power regeneration in the primary suspension of a railway vehicle. International Conference on Rail Transportation 2017.
[46] Wang R, Gu F, Cattley R, Ball A. Modelling, testing and analysis of a regenerative hydraulic shock absorber system. Energies. 2016;9:386.
[47] Abdelkareem MAA, Xu L, Ali MKA, Elagouz A, Mi J, Guo S, Liu Y, Zuo L. Vibration energy harvesting in automotive suspension system: A detailed review. Applied Energy. 2018; 229:672-99.
[48] Nagode C, Ahmadian M, Taheri S. Effective energy harvesting devices for railroad applications. Active and Passive Smart Structures and Integrated Systems 2010. p. 76430X.
[49] Nagode C, Ahmadian M, Taheri S. Motion-based energy harvesting devices for railroad applications. ASME 2010 Joint Rail Conference. p. 267-71.
[50] Li Z, Zuo L, Luhrs G, Lin L, Qin Y-x. Electromagnetic energy-harvesting shock absorbers: design, modeling, and road tests. IEEE Transactions on Vehicular Technology. 2013;62:1065-74.
[51] Liu Y, Xu L, Zuo L. Design, Modeling, Lab, and Field Tests of a Mechanical-Motion-Rectifier-Based Energy Harvester Using a Ball-Screw Mechanism. IEEE/ASME Transactions on Mechatronics. 2017;22:1933-43.
[52] Li Z, Zuo L, Kuang J, Luhrs G. Energy-harvesting shock absorber with a mechanical motion rectifier. Smart Materials and Structures. 2013;22:025008.

[53] Zhai W, Cai Z. Dynamic interaction between a lumped mass vehicle and a discretely supported continuous rail track. Computers & Structures. 1997;63:987-97.
[54] Zhai W. Vehicle-track coupling dynamics. China Railway Press, Beijing, People's Republic of China. 2007.
[55] Li D, Selig ET. Method for railroad track foundation design. II: Applications. Journal of Geotechnical and Geoenvironmental Engineering. 1998;124:323-9.
[56] Van Dyk BJ, Edwards JR, Dersch MS, Ruppert Jr CJ, Barkan CP. Evaluation of dynamic and impact wheel load factors and their application in design processes. Proceedings of the Institution of Mechanical Engineers, Part F: Journal of Rail and Rapid Transit. 2017;231:33-43.
[57] Nagode C, Ahmadian M, Taheri S. Vibration-based energy harvesting systems for on-board applications. ASME Joint Rail Conference 2011. p. 333-7.
[58] Pan Y, Liu F, Jiang R, Tu Z, Zuo L. Modeling and onboard test of an electromagnetic energy harvester for railway cars. Applied Energy. 2019;250:568-81.
[59] Peigney M, Siegert D. Piezoelectric energy harvesting from traffic-induced bridge vibrations. Smart Materials and Structures. 2013;22:095019.
[60] Wang H, Jasim A, Chen X. Energy harvesting technologies in roadway and bridge for different applications – A comprehensive review. Applied Energy. 2018;212:1083-94.
[61] Pan Y, Lin T, Qian F, Liu C, Yu J, Zuo J, Zuo L. Modeling and field-test of a compact electromagnetic energy harvester for railroad transportation. Applied Energy. 2019;247:309-21.
[62] Pan H, Li H, Zhang T, Laghari AA, Zhang Z, Yuan Y, Qian B. A portable renewable wind energy harvesting system integrated S-rotor and H-rotor for self-powered applications in high-speed railway tunnels. Energy Conversion and Management. 2019;196:56-68.
[63] Wang Y, Zhu X, Zhang T, Bano S, Pan H, Qi L, Zhang Z, Yuan Y. A renewable low-frequency acoustic energy harvesting noise barrier for high-speed railways using a Helmholtz resonator and a PVDF film. Applied Energy. 2018;230:52-61.
[64] Gao M, Su C, Cong J, Yang F, Wang Y, Wang P. Harvesting thermoelectric energy from railway track. Energy. 2019;180:315-29.
[65] Kalker JJ. Wheel-rail rolling contact theory. Wear. 1991;144:243-61.
[66] Shabana AA, Zaazaa KE, Escalona JL, Sany JR. Development of elastic force model for wheel/rail contact problems. Journal of Sound and Vibration. 2004;269:295-325.
[67] Wu Q, Sun Y, Spiryagin M, Cole C. Methodology to optimize wedge suspensions of three-piece bogies of railway vehicles. Journal of Vibration and Control. 2018;24:565-81.
[68] Wu Q, Cole C, Spiryagin M, Sun YQ. A review of dynamics modelling of friction wedge suspensions. Vehicle System Dynamics. 2014;52:1389-415.
[69] Podwórna M. Modelling of random vertical irregularities of railway tracks. International Journal of Applied Mechanics Engineering. 2015;20:647-55.
[70] Garg V. Dynamics of railway vehicle systems: Elsevier; 1984.
[71] Zhai W. Vehicle-track coupling dynamics. Beijing, China: Science Publishing House; 2007.
[72] Pan Y, Guo S, Jiang R, Xu Y, Tu Z, Zuo L. Performance Evaluation of Train Suspension Energy Harvesting Shock Absorber on Railway Vehicle Dynamics. ASME 2018 Dynamic Systems and Control Conference. p. V003T42A5.

[73] Marin A, Turner J, Ha DS, Priya S. Broadband electromagnetic vibration energy harvesting system for powering wireless sensor nodes. Smart Materials and Structures. 2013;22:075008.
[74] Erickson RW, Maksimovic D. Fundamentals of power electronics: Springer Science & Business Media; 2007.
[75] Simpson C. Battery charging. National semiconductor. 1995;18.
[76] Zhai W, Wang K, Cai C. Fundamentals of vehicle–track coupled dynamics. Vehicle System Dynamics. 2009;47:1349-76.
[77] Erickson RW, Maksimovic D. Fundamentals of power electronics: Springer Science & Business Media; 2007.
[78] Paing T, Shin J, Zane R, Popovic Z. Resistor emulation approach to low-power RF energy harvesting. IEEE Transactions on Power Electronics. 2008;23:1494-501.
[79] Kong N, Ha DS, Erturk A, Inman DJ. Resistive impedance matching circuit for piezoelectric energy harvesting. Journal of Intelligent Material Systems and Structures. 2010;21:1293-302.
[80] Jiang JZ, Matamoros-Sanchez AZ, Goodall RM, Smith MC. Passive suspensions incorporating inerters for railway vehicles. Vehicle System Dynamics. 2012;50:263-76.
[81] Jiang JZ, Matamoros-Sanchez AZ, Zolotas A, Goodall RM, Smith MC. Passive suspensions for ride quality improvement of two-axle railway vehicles. Proceedings of the Institution of Mechanical Engineers, Part F: Journal of Rail and Rapid Transit. 2015;229:315-29.
[82] Matamoros-Sanchez AZ, Goodall RM. Novel mechatronic solutions incorporating inerters for railway vehicle vertical secondary suspensions. Vehicle System Dynamics. 2015;53:113-36.
[83] Wang F-C, Hsieh M-R, Chen H-J. Stability and performance analysis of a full-train system with inerters. Vehicle System Dynamics. 2012;50:545-71.
[84] Wang F-C, Liao M-K. The lateral stability of train suspension systems employing inerters. Vehicle System Dynamics. 2010;48:619-43.
[85] Wang F-C, Liao M-K, Liao B-H, Su W-J, Chan H-A. The performance improvements of train suspension systems with mechanical networks employing inerters. Vehicle System Dynamics. 2009;47:805-30.

ACKNOWLEDGEMENT

The authors wish to thank and acknowledge the US Department of Transportation, University Transportation Center Program (RailTEAM UTC) for funding support for this research.

ABOUT THE AUTHORS

Mehdi Ahmadian, J. Bernard Jones Chair and Director

Dr. Mehdi Ahmadian is a Dan Pletta Professor of Mechanical Engineering at Virginia Tech, where he also holds the position of Director of Center for Vehicle Systems and Safety (CVeSS), and the Railway Technologies Laboratory (RLT). Dr. Ahmadian has authored more than 130 archival journal publications and more than 250 conference publications, including a number of keynote lectures. He has served as Editor or Editor-in-Chief for four journals on Vehicle System Dynamics, Vibration and Control, Shock and Vibration and Automobile Engineering. Dr. Ahmadian is Fellow of American Society of Mechanical Engineers of the American Institute for Aeronautics and Astronautics (AIAA). He has received many distinguished scholar awards.

Yu Pan

Mr. Yu Pan was a Graduate Research Assistant when he worked on this project. Yu Pan was a Postdoctoral Researcher at Center for Vehicle Systems and Safety (CVeSS) at Virginia Tech. He got his Ph.D. (2019) of Mechanical Engineering from Virginia Tech, and his bachelor's degree (2015) of Vehicle Engineering from Institute of Rail Transit at Tongji University, Shanghai, China. Dr. Pan's research interests include rail vehicle and track dynamics, wheel-rail contact mechanics and dynamics, rail lubricity detection and evaluation, as well as energy harvesting.